

# ***VULNERABILITY, STRENGTHENING AND MONITORING OF RC STRUCTURES***

**THEO DE SOUZA ROSARIO**

Dissertation submitted in partial fulfilment of the requirements for the degree of  
**MASTER'S IN CIVIL ENGINEERING – SPECIALIZATION IN STRUCTURES**

---

Supervisor: Professor Doutor Humberto Salazar Amorim Varum

---

Co-supervisor: Professor Doutor Guido Camata

JULHO DE 2023

## **MESTRADO EM ENGENHARIA CIVIL 2022/2023**

DEPARTAMENTO DE ENGENHARIA CIVIL

Tel. +351-22-508 1901

✉ [m.ec@fe.up.pt](mailto:m.ec@fe.up.pt)

*Editado por*

FACULDADE DE ENGENHARIA DA UNIVERSIDADE DO PORTO

Rua Dr. Roberto Frias

4200-465 PORTO

Portugal

Tel. +351-22-508 1400

✉ [feup@fe.up.pt](mailto:feup@fe.up.pt)

🌐 <http://www.fe.up.pt>

Reproduções parciais deste documento serão autorizadas na condição que seja mencionado o Autor e feita referência a *Mestrado em Engenharia Civil - 2021/2022 - Departamento de Engenharia Civil, Faculdade de Engenharia da Universidade do Porto, Porto, Portugal, 2022.*

As opiniões e informações incluídas neste documento representam unicamente o ponto de vista do respetivo Autor, não podendo o Editor aceitar qualquer responsabilidade legal ou outra em relação a erros ou omissões que possam existir.

Este documento foi produzido a partir de versão eletrónica fornecida pelo respetivo Autor.

A meus pais e amigos

*Se olhe, se valorize, e se permita errar.*

*Se dê de presente a chance de pelo menos tentar.*

*Se o “se” for bem usado, o impossível sonhado pode se realizar.*

*Bráulio Bessa*



## **AGRADECIMENTOS/ACKNOWLEDGEMENTS**

Ao atingir a etapa final desta longa jornada acadêmica que durou 5 anos, não seria possível deixar de agradecer e refletir acerca das pessoas que diretamente ou indiretamente foram pilares centrais para a conclusão deste trabalho.

Gostaria de começar agradecendo com profunda admiração ao meu orientador, Professor Doutor Humberto Varum, pela dedicação em me supervisionar e ajudar ao longo deste trabalho, e que sem o qual esta dissertação não estaria concluída, pelos conhecimentos que me transmitiu, mas, sobretudo pelas palavras de motivação e insuperável boa disposição. É uma grande honra ter realizado este trabalho sob a direção de tamanho profissional.

A Kerakoll e a toda equipa do ISAAC pela disponibilização dos dados dos ensaios sísmicos realizados no laboratório EUCENTRE.

Um agradecimento especial ao meu coorientador, Professor Doutor Guido Camata, pela oportunidade e confiança dedicada a mim para o estudo deste tema. Foi uma experiência enriquecedora ter realizado esta dissertação na Itália em uma empresa de tão relevante referência.

Aos engenheiros Nicola Germano e Massimo Petracca pelo incansável apoio em relação à modelação e ao uso do software.

Ao engenheiro Prabakaran Kesavan pela amizade desenvolvida, pela troca de experiências e por toda a disponibilidade prestada.

Um grande obrigado à Hannah Cartwright pela incrível pessoa que demonstrou ser ao me acolher de maneira tão genuína. Agradeço imensamente por todas as trocas de experiência, desabafos, mas, principalmente, pela amizade desenvolvida neste longo período de mobilidade que teve tanto seus pontos altos como seus pontos baixos.

A todos os meus amigos, em especial à Luma Vittorazzo, ao Bernardo Oliveira, ao Leonardo Ciampi, ao Lorenzo Matos e ao Tiago Ruiz os quais considero irmãos. Definitivamente, todo o apoio e carinho foram fundamentais para mim. A falta que vocês fizeram deixou meu coração apertado muitas vezes, mas, também, serviu de motivação extra para terminar com sucesso este trabalho.

Por fim, mas igualmente importante, à minha mãe, Aparecida Fátima, e ao meu pai, Paulo Cesar, dedico o meu eterno amor e agradeço por todo o suporte ao longo deste percurso até chegar ao fim desta etapa. Muito obrigado por nunca desistirem de mim e por toda a compreensão durante este período tão importante e ao mesmo tempo tão estressante. Foram inúmeras as vezes que me transferiram palavras de motivação que me ajudaram na finalização deste projeto. Tudo que já atingi e irei atingir é devido a vocês.



## RESUMO

Os recentes relatórios de campo pós-terremoto destacaram a extensão dos graves danos, enfatizando a necessidade da pesquisa em engenharia de terremotos se concentrar na avaliação da vulnerabilidade das construções existentes que não possuem características adequadas de resistência sísmica. Especificamente, a mitigação do risco sísmico em estruturas de BA com alvenarias de enchimento é de suma importância, principalmente nos países do sul da Europa.

Apesar dos inúmeros estudos sobre a contribuição estrutural das alvenarias de enchimento para o comportamento sísmico das estruturas, os códigos atuais de projeto sísmico ainda consideram essas alvenarias como membros "não estruturais". No entanto, o impacto delas depende em grande parte da sua distribuição no plano por piso, da rigidez relativa e da conexão com a estrutura ao redor.

Esta tese de mestrado tem como objetivo calibrar um complexo modelo numérico de um edifício real realizado em BA e com alvenarias de enchimento para simular e investigar com precisão sua resposta estrutural a movimentos do solo. Um edifício em escala real de três andares feito em BA e com alvenarias de enchimento foi construído e submetido a testes dinâmicos, servindo como validação para o modelo de elementos finitos adotado e apoiando as conclusões tiradas deste estudo.

Para ter embasamento, esta dissertação apresenta uma visão geral de campanhas experimentais anteriores que examinaram a resposta de estruturas de BA com alvenaria de enchimento a cargas cíclicas nas direções no plano e fora do plano. Atenção especial é dada à influência e ao posicionamento das aberturas na resposta dinâmica e estática dessas estruturas.

Além disso, foi demonstrado que a reabilitação sísmica de estruturas de BA com alvenarias de enchimento representa um desafio significativo na mitigação dos riscos sísmicos. As descobertas de vários autores apoiam os efeitos benéficos do uso de materiais de reforço como TRM, FRCM, FRP e ECC para melhorar a capacidade de suporte de carga, a dissipação de energia e a ductilidade das estruturas. Esses materiais de reforço ajudam a evitar ou a retardar o comportamento frágil e quase frágil dos materiais constitutivos das alvenarias de enchimento.

Além disso, esta dissertação apresenta uma revisão concisa das técnicas de modelagem não linear disponíveis para descrever o comportamento das alvenarias de enchimento e a sua interação com as estruturas porticadas de BA. O foco deste projeto está em uma abordagem simplificada de elementos finitos, combinando elementos de viga para pilares, elementos de casca grossa para paredes de enchimento e lajes, e elementos de treliça para barras de aço de contraventamento. Apesar das grandes dimensões do modelo numérico, essa abordagem reduz significativamente o esforço computacional. O modelo é calibrado usando os resultados de aceleração obtidos em testes de mesa vibratória em escala real.

A fim de avaliar as características dinâmicas e a validade do modelo de elementos finitos adotado para a estrutura do corpo de prova, é realizada uma análise de sensibilidade numérica (análise modal). Depois que as características modais são calibradas, são realizadas análises histórico-temporais.

Os resultados obtidos nesse estudo demonstram que o modelo numérico é capaz de prever com precisão a evolução experimental das acelerações ao longo do tempo para cada intensidade de terremoto a que a estrutura foi submetida, reproduzindo eficazmente sua resposta não linear.

**PALAVRAS-CHAVE:** Risco sísmico, estruturas de BA com alvenarias de enchimento, modelo numérico, ensaios em mesa vibratória, reabilitação sísmica.



## **ABSTRACT**

Recent post-earthquake field reports have highlighted the extent of severe damages, emphasizing the need for research in earthquake engineering to focus on assessing the vulnerability of existing constructions lacking appropriate seismic resistance characteristics. Specifically, the mitigation of seismic risk in masonry-infilled RC structures is of paramount importance, particularly in countries of southern Europe.

Despite numerous studies on the structural contribution of infills to the seismic behavior of structures, current seismic design codes still consider infills as 'non-structural' members. However, the impact of infills largely depends on their plan distribution per floor level, relative stiffness, and connection to the bounding frame.

This master's thesis aims to calibrate a complex numerical model of an existing infilled RC building to accurately simulate and investigate its structural response to ground motions. A full-scale three-storey infilled RC framed building was constructed and subjected to dynamic testing, serving as a validation for the adopted finite element model and supporting the conclusions drawn from this study.

As a background, this thesis presents an overview of previous experimental campaigns that examined the response of masonry-infilled RC frames to cyclic loads in both in-plane and out-of-plane directions. Special attention is given to the influence and positioning of openings on the dynamic and static response of these frames.

Additionally, it has been demonstrated that seismic retrofitting of existing masonry-infilled RC structures poses a significant challenge in earthquake risk mitigation. The findings of several authors support the beneficial effects of using reinforcing materials such as TRM, FRCM, FRP, and ECC to enhance the load-bearing capacity, energy dissipation, and ductility of infilled RC frames. These reinforcing materials help to prevent or delay the brittle and quasi-brittle behavior of the constitutive materials of masonry infills.

Furthermore, this thesis provides a concise review of the nonlinear modeling techniques available for describing the behavior of masonry infills and their interaction with RC framed structures. The focus of this project is on a simplified finite element approach, combining beam elements for columns, thick shell elements for infill panels and slabs, and truss elements for bracing steel rods. Despite the large dimensions of the numerical model, this approach significantly reduces computational effort. The model is calibrated using the acceleration results obtained from full-scale shaking table tests.

In order to assess the dynamic characteristics and validity of the adopted finite element model for the specimen structure, a numerical sensitivity analysis (eigenvalue analysis) is performed. Once the modal characteristics are calibrated, time-history analyses are conducted.

The results obtained from this study demonstrate that the numerical model is capable of accurately predicting the experimental evolution of accelerations over time for each earthquake intensity the infilled RC structure was subjected to, effectively reproducing their nonlinear response.

**KEYWORDS:** Seismic risk, masonry-infilled reinforced concrete structures, numerical model, shaking table tests, seismic retrofitting.



**GENERAL INDEX**

<b>AGRADECIMENTOS/ACKNOWLEDGEMENTS</b> .....	i
<b>RESUMO</b> .....	iii
<b>ABSTRACT</b> .....	v
<b>1. INTRODUCTION</b> .....	1
1.1. OVERVIEW.....	1
1.2. DISSERTATION OBJECTIVES .....	2
1.3. DISSERTATION STRUCTURE.....	2
<b>2. LITERATURE REVIEW</b> .....	5
2.1. SEISMIC VULNERABILITY OF REINFORCED CONCRETE STRUCTURES.....	5
2.1.1. FIELD EVIDENCE OF OBSERVED DAMAGE IN RC BUILDINGS DURING RECENT EARTHQUAKES.....	5
2.1.1.1. The April 6 <sup>th</sup> , 2009, L'Aquila earthquake, Italy.....	5
2.1.1.2. The November 26 <sup>th</sup> , 2019, Durrës earthquake, Albania.....	8
2.1.1.3. The October 30 <sup>th</sup> , 2020, Izmir earthquake, Turkey.....	11
2.1.2. TYPICAL FAILURE MECHANISMS OF NON-DUCTILE RC BUILDINGS.....	15
2.2. PREVIOUS EXPERIMENTAL RESEARCH ON INFILLS .....	16
2.2.1. IN-PLANE RESPONSE .....	17
2.2.1.1. Uniaxial Loading .....	17
2.2.1.2. Lateral Loading.....	17
2.2.2. OUT-OF-PLANE RESPONSE .....	24
2.2.2. CODE APPROACH FOR MASONRY INFILLS IN RC FRAMES.....	28
2.3. SEISMIC REHABILITATION OF EXISTING RC STRUCTURES .....	32
<b>3. BRIEF OVERVIEW OF THE EXPERIMENTAL CAMPAIGN</b> .....	35
3.1. INTRODUCTION.....	35
3.2. DESCRIPTION OF THE SPECIMEN STRUCTURE .....	36
3.3. INSTRUMENTATION: SENSORS AND LAYOUT .....	38
3.4. PRELIMINARY DYNAMIC ANALYSIS .....	41
3.5. THE NOVEMBER 23 <sup>RD</sup> , 1980, IRPINIA EARTHQUAKE, ITALY .....	43

<b>3.6. SHAKING-TABLE EXPERIMENTAL CAMPAIGN</b> .....	45
3.6.1. EARTHQUAKE WITH A PGA OF 0.24 G .....	47
3.6.2. EARTHQUAKE WITH A PGA OF 0.44 G .....	48
<b>4. NUMERICAL MODELING OF THE SPECIMEN STRUCTURE</b> .....	51
<b>4.1. FINITE ELEMENT MODELING REVIEW</b> .....	51
4.1.1. INTRODUCTION .....	51
4.1.2. MASONRY INFILLS MODELING APPROACHES .....	51
4.1.2.1. Micro-modeling .....	52
4.1.2.2. Macro-modeling .....	54
4.1.2.3. Meso-modeling .....	56
4.1.3. FRAME-INFILL MODELING APPROACHES .....	57
4.1.4. DISCRETIZATION METHODS FOR RC MEMBERS .....	58
<b>4.2. DESCRIPTION OF THE ADOPTED NUMERICAL MODEL</b> .....	58
4.2.1. INTRODUCTION .....	58
4.2.2. RC FRAME MODELING .....	59
4.2.2.1. Columns .....	59
4.2.2.2. Beam-Slabs .....	61
4.2.3. REINFORCEMENT MODELING .....	62
4.2.4. MASONRY INFILLS MODELING .....	63
4.2.4.1. Infill panel .....	64
4.2.4.2. Frame-infill contact surface .....	65
<b>5. METHODOLOGY AND VALIDATION OF THE NUMERICAL SIMULATION RESULTS</b> .....	67
<b>5.1. INTRODUCTION</b> .....	67
<b>5.2. EIGEN ANALYSIS</b> .....	68
<b>5.3. TIME-HISTORY ANALYSES</b> .....	70
5.3.1. RESULTS OF THE COMP_01 TRANSIENT ANALYSIS .....	72
5.3.2. RESULTS OF THE COMP_02 TRANSIENT ANALYSIS .....	75
5.3.3. RESULTS OF THE COMP_03 TRANSIENT ANALYSIS .....	77
5.3.4. RESULTS OF THE COMP_04 TRANSIENT ANALYSIS .....	80

5.3.5. RESULTS OF THE COMP_05 TRANSIENT ANALYSIS .....	82
<b>5.4. DISCUSSION OF THE NUMERICAL RESULTS .....</b>	<b>84</b>
<b>5.5. CONTRIBUTION OF MASONRY INFILL WALLS.....</b>	<b>87</b>
5.5.1. INTRODUCTION .....	87
5.5.2. MODAL PROPERTIES.....	87
5.5.3. DYNAMIC ANALYSIS .....	88
<b>6. CONCLUSION AND FUTURE WORKS.....</b>	<b>91</b>
6.1. INTRODUCTION.....	91
6.2. CONCLUDING REMARKS.....	91
6.3. FUTURE WORKS .....	92
<b>BIBLIOGRAPHIC REFERENCES .....</b>	<b>95</b>



**FIGURE INDEX**

Figure 2.1 – L’Aquila epicenter location and shake intensity distribution (Reuters) .....6

Figure 2.2 - Damage due to design flaw of buildings without coinciding floors (Marazzi et al., 2011) ....7

Figure 2.3 - Example of damage owing to frames arranged only in one direction (Marazzi et al., 2011) .....8

Figure 2.4 - Insufficient reinforcement resulting in buckling of vertical rebars (Marazzi et al., 2011).....8

Figure 2.5 - Durrës epicenter and affected areas (The Guardian Journal, Shaun Walker) .....9

Figure 2.6 - Liquefaction phenomena in the coastal part of southern Durrës (Andonov et al., 2022) .....9

Figure 2.7 - Damage on buildings in Durës (McKenney, 2019) .....10

Figure 2.8 – Damage due to soft-storey mechanism (McKenney, 2019).....11

Figure 2.9 - Damage due to short-column mechanism (McKenney, 2019) .....11

Figure 2.10 -The Alpine-Himalayan seismic belt in Turkey (Koçer and Ünal, 2022) .....12

Figure 2.11 – Izmir’s active fault map (adapted from Emre et al., 2013) .....12

Figure 2.12 - Typical RC building in the city of Izmir (Google Maps, June 2021) .....13

Figure 2.13 - Column damages (Koçer and Ünal, 2022) .....14

Figure 2.14 - Strong-beam and weak-column mechanisms (Koçer and Ünal, 2022) .....15

Figure 2.15 - Commonly used specimen .....18

Figure 2.16 – Load transferring mechanism from frame to truss action (Murty and Jain, 2000) .....18

Figure 2.17 - Panagiotakos and Fardis [1996] force-displacement envelope.....19

Figure 2.18 - Infilled frames’ force-displacement envelope (Verderame et al., 2016; De Risi et al., 2018) .....19

Figure 2.19 - Hysteresis loop for specimen “A-2” (Markulak et al., 2013).....20

Figure 2.20 – Base-shear versus top-displacement for Christiana et al. (2022) model.....21

Figure 2.21 - Typical strut approach for infill panels with central openings .....22

Figure 2.22 – Corner crushing and diagonal compression failures (Asteris et al., 2011) .....23

Figure 2.23 – Shear sliding, diagonal cracking and frame failures (Asteris et al., 2011).....23

Figure 2.24 – Masonry-infilled RC frames damage states (Cardone and Perrone, 2015).....24

Figure 2.25 – Evolution of damage (adapted from De Risi et al., 2018) .....24

Figure 2.26 – Double arching effect in a square masonry infill wall (De Risi et al., 2019) .....25

Figure 2.27 – Cracking pattern and experimental response for ‘80\_OOP\_2E’ specimen (Di Domenico, 2018) .....26

Figure 2.28 – Out-of-plane force-displacement of the top beam (Verdarame et al., 2019) .....26

Figure 2.29 – Out-of-plane force-displacement of the infill (Verdarame et al., 2019) .....26

Figure 2.30 – Cracking pattern and experimental response for ‘80_OOP_4E’ specimen (Di Domenico, 2018) .....	27
Figure 2.31 - Out-of-plane crack pattern for ‘TA1’ specimen (Hak et al., 2014) .....	27
Figure 2.32 - Out-of-plane deformed shape for ‘TA1’ specimen at 75 mm target displacement (Hak et al., 2014).....	27
Figure 2.33 – Lisbon’s Palace of Justice constructed in 1970 (FCG/Biblioteca de Arte).....	30
Figure 2.34 - Three-storey RC structure in Italy that failed due to soft-storey mechanism (Verderame, G.).....	30
Figure 2.35 - Short-column due to beams (Pokharel and Goldsworthy, 2015).....	31
Figure 2.36 - Short-column due to slopped terrain (Pokharel and Goldsworthy, 2015).....	31
Figure 2.37 - Elastic response spectrum for type 1 earthquake (EC8, 2004).....	31
Figure 2.38 - Elastic response spectrum for type 2 earthquake (EC8, 2004).....	31
Figure 2.39 – Fabric strengthening system applications (Drizoro construction products) .....	33
Figure 2.41 - Fabric application: (a) direct; (b) sandwich (Salgar et al., 2019) .....	34
Figure 3.1 - Active Seismic Damping System (ISAAC technical report, 2020).....	36
Figure 3.2 – Specimen RC frame building (ISAAC technical report, 2020) .....	37
Figure 3.3 - Structure Plan Configuration [mm].....	38
Figure 3.4 - Columns’ Cross-Section [cm] .....	38
Figure 3.5 - Brick unit .....	38
Figure 3.6 - Accelerometers placed at the shaking table and building base: (4) Uniaxial; (5) Biaxial (ISAAC technical report, 2020).....	39
Figure 3.7 - Accelerometers in the structures under study (9, 11, 15, 17, 21, 23 – Triaxial / 10, 16, 22 – Biaxial): (a) 1 <sup>st</sup> Floor; (b) 2 <sup>nd</sup> Floor; (c) 3 <sup>rd</sup> Floor (ISAAC technical report, 2020) .....	40
Figure 3.8 - Accelerometers installed at the floors (Extradados and Intrados) (ISAAC technical report, 2020) .....	40
Figure 3.9 - Wired Displacement Sensor at the 1 <sup>st</sup> Floor (ISAAC technical report, 2020).....	41
Figure 3.10 - Wired Displacement Sensor at the 2 <sup>nd</sup> Floor (ISAAC technical report, 2020) .....	41
Figure 3.11 - Piezoelectric accelerometer to measure the floors’ acceleration (ISAAC technical report, 2020) .....	42
Figure 3.12 - The 1.5 kg vibrator at the highest floor (ISAAC technical report, 2020).....	42
Figure 3.13 - Experimentally obtained modes of vibration (ISAAC technical report, 2020).....	43
Figure 3.14 - Recent seismic events in Italy (Del Gaudio et al., 2020) .....	44
Figure 3.15 - One of the cities after the earthquake, 1980 (Di Fabiana Bianchi).....	45
Figure 3.16 - Reference acceleration time history: Irpinia, 1980 (ISAAC technical report, 2020) .....	46
Figure 3.17 – Complete time history of input earthquakes (ISAAC technical report, 2020) .....	47

Figure 3.18 - Acceleration measured at the shaking table along the y direction .....	47
Figure 3.19 - Cracks along the infill wall main diagonal (ISAAC technical report, 2020).....	48
Figure 3.20 - Crushing at the infill wall corner (ISAAC technical report, 2020).....	48
Figure 3.21 - Acceleration measured at the shaking table along the y direction .....	49
Figure 3.22 - Partial collapse of the infill opening (ISAAC technical report, 2020) .....	49
Figure 3.23 - Observed cracks at the slab joints (ISAAC technical report, 2020).....	49
Figure 4.1 - Micro-modeling techniques .....	54
Figure 4.2 - Single strut approach (Holmes, 1961) .....	55
Figure 4.3 - Double strut with shear spring (Crisafulli, 1997) .....	55
Figure 4.4 - Triple strut approach (Chrysostomou et al., 2002) .....	55
Figure 4.5 - Rigid strut with nonlinear central element (Furtado et al., 2015).....	55
Figure 4.6 - Homogenization process (adapted from Bouarroudj and Boudaoud, 2022) .....	56
Figure 4.7 - Homogenization for shell elements (Petracca et al., 2017) .....	57
Figure 4.8 - Frame-infill interaction model (Stavridis and Shing, 2009).....	58
Figure 4.9 – ASDShellQ4 representation (ASDShellQ4 user manual) .....	60
Figure 4.10 – Example of a fiber beam-column section (Morteza Razi).....	60
Figure 4.11 – Concrete material stress-strain relationship .....	61
Figure 4.12 – 1 <sup>st</sup> floor slab model .....	62
Figure 4.13 – 2 <sup>nd</sup> floor slab model .....	62
Figure 4.14 – Hysteretic behavior with kinematic hardening .....	62
Figure 4.15 – Steel material stress-strain envelope.....	62
Figure 4.16 – Damage surfaces (Petracca et al., 2017) .....	64
Figure 4.17 – Tensile hardening (Petracca et al., 2017) .....	64
Figure 4.18 – Compressive hardening (Petracca et al., 2017) .....	64
Figure 5.1 – Computed natural modes of vibration .....	69
Figure 5.2 – Maximum acceleration at storey levels .....	72
Figure 5.3 – COMP_01 storey acceleration time histories and Fourier transform (3 <sup>rd</sup> , 2 <sup>nd</sup> and 1 <sup>st</sup> storeys) .....	73
Figure 5.4 – COMP_01 displacement vs acceleration envelope (3 <sup>rd</sup> , 2 <sup>nd</sup> and 1 <sup>st</sup> storeys) .....	74
Figure 5.5 – COMP_01 drift vs acceleration envelope (3 <sup>rd</sup> , 2 <sup>nd</sup> and 1 <sup>st</sup> storeys).....	74
Figure 5.6 – COMP_01 maximum displacement profile .....	74
Figure 5.7 – COMP_01 maximum drift profile.....	74
Figure 5.8 – COMP_02 storey acceleration time histories and Fourier transform (3 <sup>rd</sup> , 2 <sup>nd</sup> and 1 <sup>st</sup> storeys) .....	75

Figure 5.9 – COMP_02 displacement vs acceleration envelope (3 <sup>rd</sup> , 2 <sup>nd</sup> and 1 <sup>st</sup> storeys) .....	76
Figure 5.10 – COMP_02 drift vs acceleration envelope (3 <sup>rd</sup> , 2 <sup>nd</sup> and 1 <sup>st</sup> storeys).....	76
Figure 5.11 – COMP_02 maximum displacement profile .....	77
Figure 5.12 – COMP_02 maximum drift profile.....	77
Figure 5.13 – COMP_03 storey acceleration time histories and Fourier transform (3 <sup>rd</sup> , 2 <sup>nd</sup> and 1 <sup>st</sup> storeys) .....	78
Figure 5.14 – COMP_03 displacement vs acceleration envelope (3 <sup>rd</sup> , 2 <sup>nd</sup> and 1 <sup>st</sup> storeys) .....	79
Figure 5.15 – COMP_03 drift vs acceleration envelope (3 <sup>rd</sup> , 2 <sup>nd</sup> and 1 <sup>st</sup> storeys).....	79
Figure 5.16 – COMP_03 maximum displacement profile .....	79
Figure 5.17 – COMP_03 maximum drift profile.....	79
Figure 5.18 – COMP_04 storey acceleration time histories and Fourier transform (3 <sup>rd</sup> , 2 <sup>nd</sup> and 1 <sup>st</sup> storeys) .....	80
Figure 5.19 – COMP_04 displacement vs acceleration envelope (3 <sup>rd</sup> , 2 <sup>nd</sup> and 1 <sup>st</sup> storeys) .....	81
Figure 5.20 – COMP_04 drift vs acceleration envelope (3 <sup>rd</sup> , 2 <sup>nd</sup> and 1 <sup>st</sup> storeys).....	81
Figure 5.21 – COMP_04 maximum displacement profile .....	82
Figure 5.22 – COMP_04 maximum drift profile.....	82
Figure 5.23 – COMP_05 storey acceleration time histories and Fourier transform (3 <sup>rd</sup> , 2 <sup>nd</sup> and 1 <sup>st</sup> storeys) .....	83
Figure 5.24 – COMP_05 displacement vs acceleration envelope (3 <sup>rd</sup> , 2 <sup>nd</sup> and 1 <sup>st</sup> storeys) .....	84
Figure 5.25 – COMP_05 drift vs acceleration envelope (3 <sup>rd</sup> , 2 <sup>nd</sup> and 1 <sup>st</sup> storeys).....	84
Figure 5.26 – COMP_05 maximum displacement profile .....	84
Figure 5.27 – COMP_05 maximum drift profile.....	84
Figure 5.28 – Evolution of the maximum drift at each storey along the y-direction .....	86
Figure 5.29 – Displacement versus acceleration at storey levels for the IN model .....	88
Figure 5.30 – Displacement versus acceleration at storey levels for the BF model .....	88
Figure 5.31 – Drift-acceleration hysteresis diagram at storey levels for the IN model.....	89
Figure 5.32 – Drift-acceleration hysteresis diagram at storey levels for the BF model.....	89

**TABLE INDEX**

Table 3.1 – Italian RC structures categorization (adapted from Gesualdi et al., 2020) .....35

Table 3.2 – Experimental modal parameters obtained .....42

Table 3.3 – Ground motions .....45

Table 3.4 – PGA 0.24 g Results: Maximum storey lateral displacement and maximum inter-storey drift  
.....48

Table 3.5 – PGA 0.44 g Results: Maximum storey lateral displacement and maximum inter-storey drift  
.....48

Table 4.1 – Concrete model mechanical parameters .....61

Table 4.2 – Slab plate section parameters.....62

Table 4.3 – Steel model mechanical parameters.....63

Table 4.4 – Material parameters for the infill panels .....65

Table 5.1 – Natural frequencies numerically evaluated .....68

Table 5.2 – Cumulative modal participation mass ratios numerically evaluated .....68

Table 5.3 – Numerical results of maximum displacement and maximum storey drift.....86

Table 5.4 – Computed modal properties for the IN and BF models.....87



## SYMBOLS, ACRONYMS AND ABBREVIATIONS

DOF – Degree of Freedom

EC – Eurocode

ECC – Engineered Cementitious Composites

FE – Finite Element

FEM – Finite Element Modeling

FRCM - Fiber-Reinforced Cementitious Matrix

FRP – Fiber-Reinforced Polymer

OpenSees - Open System for Earthquake Engineering Simulation

PGA – Peak Ground Acceleration

RC – Reinforced Concrete

STKO – Scientific ToolKit for OpenSees

TRM – Textile-Reinforced Mortar

URM – Unreinforced Masonry

$E_0$  – Steel Initial Elastic Tangent

$E_{pm}$  – Ratio of Flexural to Membrane Stiffness

$E_{ts}$  – Concrete Tensile Softening Stiffness

$E_x$  – Young's Modulus along x-direction

$E_y$  – Young's Modulus along y-direction

$E_z$  – Young's Modulus along z-direction

$F_y$  – Steel Yield Strength

$G_c$  – Compressive Fracture Energy

$G_t$  – Tensile Fracture Energy

$f_c$  – Concrete Compressive Strength

$f_{cu}$  – Concrete Crushing Strength

$f_{mc}$  – Masonry Infill Panel Compressive Strength

$f_{mt}$  – Masonry Infill Panel Tensile Strength

$f_t$  – Concrete Tensile Strength

$\varepsilon_c$  – Concrete Strain at Maximum Compressive Strength

$\varepsilon_{cu}$  – Concrete Strain at Maximum Crushing Strength

E – Modulus of Elasticity

$g$  – Gravity acceleration

$G$  – Shear Modulus

$\Delta t$  – Time Step

$b$  – Steel Strain-Hardening Ratio

$\lambda$  – Concrete Ratio Between Unloading Slope at  $\varepsilon_{cu}$  and Initial Slope

$\nu$  – Poisson's Ratio





# 1

## INTRODUCTION

### 1.1. OVERVIEW

Earthquakes are undoubtedly one of the greatest sources of risk for the humanity. Due to their unpredictable nature and high destructive power, earthquakes represent a huge challenge to be overcome by civil engineers in the design of structures that should be adequately resistant, stiff, and ductile. These structures need to be capable of dissipating energy, yet ensuring minimal damage in order to maintain the functioning of vital services and, above all, to safeguard the lives of its occupants.

Masonry materials has been used in the construction industry for centuries, specially to satisfy accessibility, economics and aesthetics demands (Angel, 1994). For several years, structural engineers and design codes have neglected the important influence of masonry infill walls in the structural response of buildings, especially when under strong earthquake motions. This has led to inadequate design practices that evaluate the integrity and the overall response of structures without considering the infill walls as part of the load resisting system. These design practices are commonly present in many existing RC structures. Therefore, these structures were designed without taking into account the strength, stiffness and ductility introduction by the masonry infills. The reluctance in not considering the infills' contribution might be due to the brittle behavior exhibited by masonry materials, and to the lack of specific methods to evaluate their stiffness and strength (Mehrabi et al., 1996).

Fortunately, owing to the extensive amount of research and experimental campaigns on the behavior of masonry infills, nowadays the scientific and technical communities widely acknowledge for their significant role in the structural system. Their positive and negative effects for the seismic performance of structures depends on several aspects, such as their positioning thorough the storeys, boundary conditions, the effectiveness of their connection to the bounding frame, among others (Furtado and De Risi, 2020).

Recent earthquakes that have occurred around the world keep remembering the society that research in this area should be directed for the analysis and eventual strengthening of existing buildings. In many regions, the structural conception and design strategy options adopted until the 1970's did not give the adequate attention to the seismic risk, eventually disregarding the seismic demands in detriment of other actions (Gesualdi et al., 2020). This is proved by recent post-earthquake damage reports present in this study, which highlight the severe state of damage in some regions following seismic ground motions. According to these reports, these structures present certain vulnerabilities that compromise their capacity to resist earthquakes, which may result in potential large economic and human losses. These vulnerabilities are mainly due to the use of low-strength materials, the deterioration of elements and deficiencies in the design and construction stages (Furtado et al., 2021).

A significant number of the structures in seismic-prone areas were erected prior to the implementation of modern seismic regulations. Particularly, in multi-use buildings, while upper storeys are dedicated to housing, ground storeys are typically reserved for commercial use, where large openings and slender vertical elements are employed. This configuration tends to create a dangerous difference in the lateral stiffness between adjacent storeys, specially due to the presence and positioning of masonry infill walls, which may induce the collapse of the building.

The importance of seismic vulnerability assessment and structural health monitoring of the existing structures is clear, particularly from the perspective of the observed effects of the latest earthquake that struck high populated regions of Turkey and Syria in February 2023, leaving tens of thousands injured and dead (UNOCHA, 2023). This is not only due to the fact these regions are located close to geological faults, but it also might be due to deficient detailing of structural members, irregularities in the structural systems, which induce the formation of well-known failure mechanisms (especially soft-storeys and short-columns mechanisms) related to irregular distribution (in plan and/or in elevation) of the structural elements or masonry infill walls.

The above observations evidence that these structures lack adequate seismic resisting characteristics. Consequently, they are the main source of risk and are the cause of most casualties (Varum, 2003). Therefore, the strengthening of existing structures against seismic demands is a subject of high importance. The retrofiting strategies for these buildings should be focused in guaranteeing a harmony of strength, stiffness, and ductility between their members, making sure to not prejudice the safety and load capacity of the others (Fardis, 1998).

In the current context of seismic design of structures, there is an increasing demand for the use of software based on FE models, which are essential and powerful computing tools that professionals and researchers use daily to reproduce and investigate the non-linear response of structures. These numerical analyses are crucial for evaluating the seismic risk and supporting mitigation policies. For this reason, many numerical strategies have been developed in the last decade. The modeling of masonry infill panels is particularly complex and, therefore, different models have been implemented in commercial software packages, ranging from one or more equivalent diagonal struts, to detailed linear and nonlinear FE models.

Reliable numerical estimates, in addition to the reliability of the adopted model itself, depends on the adoption of accurate mechanical properties for the materials employed (Petracca et al., 2017). Moreover, the accuracy of such numerical models is strongly impacted by the modeling approach and material uncertainties. However, the precise knowledge of these materials characteristics is a challenging and economically demanding task, specially for brittle materials as masonry (Petracca et al., 2017).

## **1.2. DISSERTATION OBJECTIVES**

To achieve the objectives of this study, an extensive literature review is conducted in order to increase the knowledge about the behavior of masonry infills and how the frame-infill interface interacts under earthquake motions. Therefore, the load-bearing capacity of infill walls on the in-plane and out-of-plane directions was assessed based on previous works. However, as infill walls are very stiff elements, the theoretical work also give emphasis to the investigation of their impact on the structural response of buildings.

In order to complement the analytical work, the results of the experimental campaign conducted at the EUCENTRE laboratory are used to confirm the parameters adopted in the modeling stage of the specimen structure. The experimental program consisted of twelve full-scale shake table tests of

increasing intensity. The specimen consisted of a three-storey, single-bay RC frame with masonry infill walls arranged in only one direction (y-direction).

The primary scope of the theoretical and analytical work subject of this master's thesis is to fine-tune the numerical model in the STKO software of a three-storey masonry-infilled RC frame in order to be able to accurately reproduce its structural behavior under seismic motions. The numerical results were validated with the results of the experimental campaign. Thus, the calibrated model can be used in the vulnerability assessment of the specimen structure and of structures with similar structural system.

### **1.3. DISSERTATION STRUCTURE**

The present master's thesis is organized in 6 chapters, where the topics inherent for the comprehensive understanding of the research subject of this study are described.

The second chapter presents an overview of the most relevant findings in recent post-earthquake field mission reports. Next, it is presented a review of the work done in relation to the in-plane and out-of-plane behavior of masonry-infilled RC frames. Special attention is given to the well-known contribution of infill masonry walls to the global structural response of buildings, particularly in the event of an earthquake. Finally, the retrofitting strategies which are typically applied in existing RC structures are briefly described.

In the third chapter, the experimental campaign conducted at the shaking table facility of EUCENTER research center is presented. The chapter focus on a brief description of some key aspects of the laboratory tests, namely: (i) the specimen dimensions, materials and details; (ii) the instrumentation layout; (iii) the results of the dynamic identification; (iv) the seismic input signals adopted; and (v) a brief description of the structural response.

The fourth chapter presents a thorough assessment of the most used numerical modeling techniques for the simulation of masonry-infilled RC frames. Next, the modeling methodology adopted in this work, as well as the material models and element models used are described in more detail.

The fifth chapter, "Methodology and Validation of the Numerical Simulation Results" aims in evaluating the numerical results obtained from the eigenvalue and time-history analyses. In addition, it is presented the strategy adopted and the parameters adopted on each numerical analysis in order to reproduce the experimental results.

The sixth chapter is reserved to draw general conclusions derived from this study and to list some proposals for eventual future investigations.



# 2

## LITERATURE REVIEW

### 2.1. SEISMIC VULNERABILITY OF REINFORCED CONCRETE STRUCTURES

#### 2.1.1. FIELD EVIDENCE OF OBSERVED DAMAGE IN RC BUILDINGS DURING RECENT EARTHQUAKES

In regions with frequent ground shaking of significant magnitude, structural design has become more sophisticated and led to improvements in the performance of engineered structures. Engineers and researchers have understood a lot about the appropriate and inappropriate methods of construction of earthquake load-resisting systems by observing how structures behave during low, medium, and severe earthquakes. Due to local differences regarding building materials and techniques, some design methodologies might not be globally applicable, but structural engineers can still learn a lot by studying them. The design and building of earthquake-resistant structures in other areas can be influenced by such information, which will also enhance the overall efficacy of structures when subjected to seismic loading (Varum, 2003).

Merhabi et al. (1996) pointed out that the masonry infill walls, which are frequently referred to as "non-structural" elements in structural design codes, as they are mostly designed to contribute to façade's functions (e.g., thermal and acoustic insulation), are responsible for significant losses (material, economic and human) and, therefore, have a crucial role in the seismic performance RC framed structures. Thus, the investigation of the behavior of structures during earthquakes and post-earthquake damage reconnaissance reports, highlights the significant importance of learning lessons from such events in order to improve seismic design practices.

RC buildings are known for their extreme redundancy nature, which is valuable for preserving their integrity in the event of a local element failure. However, despite being constructed with a high degree of hyperstaticity, they can still collapse when a single element fails, owing to load redistribution effects that cause additional stresses on the remaining elements which lack additional strength to withstand it (Furtado et al., 2021).

This section aims to provide a comprehensive understanding of the response of RC buildings during past earthquake events in Europe, as per to post-earthquake field reports from various authors. Particularly, the assessment will focus on the seismic behavior and properties of various components of RC buildings, namely: infills, columns, and beams. The behavior and vulnerability of these elements are believed to be the primary contributing factors to the seismic deficiency of RC buildings, resulting in their poor response and, consequently, damage or collapse.

##### 2.1.1.1. The April 6<sup>th</sup>, 2009, L'Aquila earthquake, Italy

The capital of the Italian region of Abruzzo, L'Aquila, as well as some of its nearby towns were severely damaged by a disastrous 6.3 moment magnitude earthquake that occurred on the night of April 6, 2009, at 3:33 a.m. local time. As depicted in Figure 2.1, the epicenter depth was about 10 km, and the highest intensity was estimated to be 8.5 MCS. As a result, many buildings, especially historical buildings, suffered severe damage and collapsed. The disaster's aftermath resulted in 309 fatalities and over 1600 injuries (Benessia and De Marchi, 2017). Tens of thousands of people were forced to evacuate, and tens of billions of euros were estimated in damage, due to the destruction of several buildings. The two most devastating earthquakes to strike the city of L'Aquila were the ones that happened in 1461 and 1703 (Pondrelli et al., 2009). The 2009 earthquake, in particular, had similarities to the 1461 seismic event. Accelerometric stations located throughout and around the city of L'Aquila captured motions with peak values between 0.4 and 0.6 g, which were characterized by short durations of less than 10 seconds (Marazzi et al., 2011).

Despite not being an exceptionally strong earthquake, owing to the seismic vulnerability of historical buildings at the old center and to some recently constructed buildings, the material and human losses were significant (Benessia and De Marchi, 2017). Additionally, a portion of the residents did not take safety actions, such as evacuating their homes and seeking shelter outside, after the occurrence of two strong foreshocks in the late evening (Benessia and De Marchi, 2017). This negligence led to a higher number of casualties and fatalities.

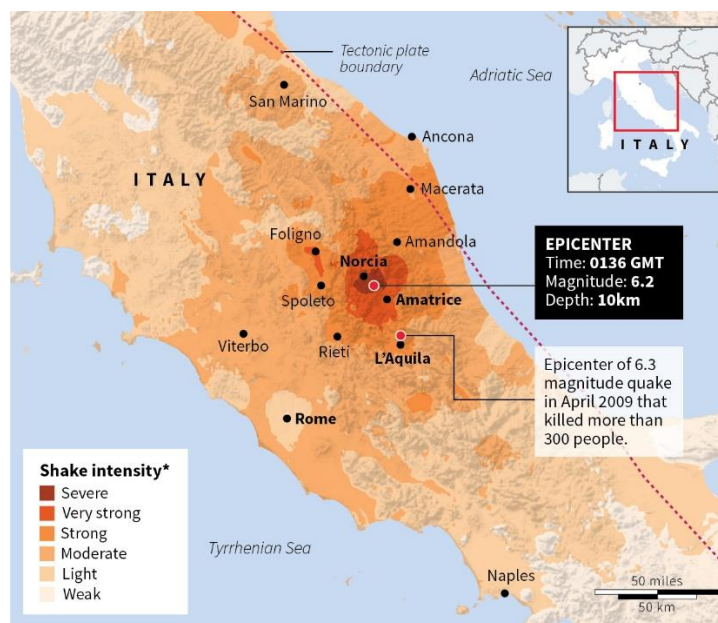


Fig. 2.1 – L'Aquila epicenter location and shake intensity distribution (Reuters)

The field report done in 2011 by the Joint Research Centre European Commission summarizes the damage assessment on public, military, hospital, and school buildings. In summary, a considerable proportion of the buildings, specifically over 29%, were deemed unusable in the aftermath of the earthquake. This percentage increases significantly when considering solely the old heritage buildings, of which more than 50% fall under the unusable category. According to Liel and Lynch (2012), the building stock of the city was represented by a majority of 66% of RC buildings being characterized by single-family residential use and 7% being characterized by residential with commercial use.

Certain RC framed buildings had to be located on slopes due to the topographic profile of the region, which inherently contrived to some vertical members being shorter than others. This, in turn, contributed to further shear demand on shorter elements of the ground floor, which developed a short-column mechanism and failed. Further, during the earthquake, it was observed that most of the older RC structures suffered serious damage, with a considerable number of them collapsing entirely or being reduced to rubble. The damage was substantial and varied in nature, including partial or total collapse owing to soft-storeys mechanisms, shear damage caused by short-column mechanisms, damage of beam-column joints, diagonal cracking, and out-of-plane collapse of masonry-infilled walls (Marazzi et al., 2011).

For instance, Marazzi et al. (2011) emphasize some seismic deficiencies, as shown in Figure 2.2. which is an illustration of inadequate conceptual design, in which two adjacent buildings have floor levels that do not coincide in elevation. The masonry building is naturally stiffer than the RC one, and as a result, the RC framed structure suffered severe damage as a consequence of pounding at that floor level. Also, as observed by the authors, the structures used to be frequently constructed with a frame configuration in which only one of the primary directions were braced by the infill panels, as shown in Figure 2.3. The adoption of this arrangement leads to poor strength and stiffness of the RC frame in the other direction. The lack of consideration for seismic effects during the design and construction of these buildings contributed to their vulnerability to seismic actions.

In addition to the design flaws, some structures had their vertical elements varying dimensions in elevation, as they were constructed with slabs at different heights to follow the natural slope of the terrain, and, thus, creating an irregularity in elevation that amplified their vulnerability to the earthquake motion (Marazzi et al., 2011). 70% of regular buildings showed negligible damage, while 30% exhibited moderate or higher damage. On the other hand, among irregular buildings, 40% displayed negligible damage, while 60% suffered from moderate or higher damage (Liel and Lynch, 2012). From the post-earthquake field report (Marazzi et al., 2011), as expected, it was concluded that in general buildings with regular construction received less damage in comparison to those exhibiting some sort of irregularity. Other detailing flaws, such as the longitudinal and transversal reinforcement, did not provide sufficient anchoring for the horizontal rebars and intensified local ductility of structural elements, in some cases, leading to the rebars being pulled out of the concrete (Figure 2.4).



Fig. 2.2 – Damage due to design flaw of buildings without coinciding floors (Marazzi et al., 2011)



Fig. 2.3 - Example of damage owing to frames arranged only in one direction (Marazzi et al., 2011)



Fig. 2.4 - Insufficient reinforcement resulting in buckling of vertical rebars (Marazzi et al., 2011)

#### 2.1.1.2. The November 26<sup>th</sup>, 2019, Durrës earthquake, Albania

Albania has been many times the epicenter of massive earthquakes in the last century. On November 26<sup>th</sup>, 2019, a powerful earthquake measuring 6.4 on the Richter scale happened. This earthquake was the deadliest one in Albania since the Shkoder earthquake in 1979 and although it had its epicenter 22 km from the city center of Durrës, as shown in Figure 2.5, the nearby areas of the city also suffered (Leti and Bilgin, 2021). The epicenter of the earthquake coincides with the boundary between the Adriatic and Eurasian plates. The city of Durrës and the town of Thumanë, located in the central western region of Albania, were identified as the most heavily impacted areas (Leti and Bilgin, 2021). Northwestern Albania is known to be highly susceptible to geotechnical effects, including liquefaction and slope movement, which were triggered by the mainshock in several sites. The liquefaction phenomena in the affected sites led to individual sand boils, the ejection of liquified material (comprising: sand, silt, and water) from ground cracks (Figure 2.6), and sand fountains in still waters that affected the local road network (Andonov et al., 2022). The earthquake's consequences caused 51 people to be reported dead, and more than 200000 were affected (IFRC, 2021).



Fig. 2.5 - Durrës epicenter and affected areas (The Guardian Journal, Shaun Walker)



Fig. 2.6 - Liquefaction phenomena in the coastal part of southern Durrës (Andonov et.al., 2022)

According to Leti and Bilgin (2021) survey, old masonry structures were observed to be the dominant building typology in the region. The studies indicated that the preferred building systems in the region were characterized by either unreinforced masonry (URM) or RC structures with hollow clay tile infill partition. The structures relied primarily on well-known materials such as stone, rubble, brick, and hollow clay tile. Moreover, the authors observed that due to the poor capacity in dissipating the earthquake's energy, the majority of the reported damage at Durrës was restricted to obsolete masonry

structures and non-ductile RC buildings, mostly presenting shear cracks along the entire thickness of the wall (Figure 2.7). Furthermore, it was found that due to inadequate anchorage, and in extreme cases, the absence of any anchoring system, many masonry infills experienced out-of-plane or shear failure.

The site investigations following the earthquake revealed that many buildings in the region did not comply with the Albanian building code norms, as they had been constructed with various irregularities (Andonov et al., 2022). The primary reason for this was the rapid development of the country after the 1990's, which placed an enormous burden on the local government. Consequently, the government was unable to properly monitor the construction of buildings, which resulted in the prevalence of irregularities in many of these structures. This highlights the importance of strict adherence to building codes and the need for effective government monitoring during construction to ensure the safety and resilience of buildings against seismic events.



Fig. 2.7 – Damage on buildings in Durrës (McKenney, 2019)

The majority of masonry buildings that were exposed to the earthquake were low-rise, single-family buildings, or old masonry structures, which constitute a significant portion of the building stock in Albania (Andonov et al., 2022). These were mostly two-story, non-engineered, unreinforced masonry buildings designed and constructed by builders accordingly to older earthquake-resistant design codes. In many cases, the damage was caused by building extensions (construction of additional floors), irregular plan shapes, and use of low-strength masonry units (usually fired clay bricks). Great part of the seismic vulnerability of the region owes to the fact that the older buildings, especially masonry ones, suffer from poor material quality, deficient detailing and aging (Andonov et al., 2022).

The severe damage or collapse of RC buildings in the November 2019 earthquake was due to the presence of one or more flaws related to detailing for local ductility of RC frame elements, such as stirrups with 90° hooks and insufficient anchorage length (as opposed to 135° hooks prescribed by EC8), stirrup diameter as small as 6 mm, excessively large stirrup spacing in the top and bottom of columns, and rebar corrosion due to the poor concrete cover (Leti and Bilgin, 2021; Andonov et al., 2022; Marinkovic et al., 2022). Relatively large inter-storey drifts demand at the lower levels, which were mostly open and flexible, caused significant damage on the infills.

Marinkovic et al. (2022) observed that in low- and mid-rise buildings, masonry infills completely changed the structural behavior and contributed to significant overall damage or collapse. The development of soft-storey and short-column mechanisms were the reason behind the failure of these structures (Leti and Bilgin, 2021). Typically, these failure were caused by continuous window openings at the top of infill walls between columns (Figures 2.8 and 2.9), along with an asymmetrical stiffness distribution of elements in plan. Furthermore, out-of-plane failures were commonly observed in both URM and RC buildings, causing partial or total collapse of masonry walls. These failures can be attributed to the insufficient fastening of the wall to the rigid diaphragm (storey slab). This indicates the need for better fastening systems and adequate building codes for URM and RC buildings to improve the seismic resilience.



Fig. 2.8 – Damage due to soft-storey mechanism (McKenney, 2019)



Fig. 2.9 – Damage due to short-column mechanism (Leti and Bilgin, 2021)

#### 2.1.1.3. The October 30th, 2020, Izmir earthquake, Turkey

Turkey, a country located in the Alpine-Himalayan seismic belt (Figure 2.10), is known to have one of the highest seismic activity rates globally, with around 20% of earthquakes around the world occurring in this region (Koçer and Ünal, 2022). Every five years, Turkey consistently experiences devastating earthquakes, leading to substantial loss of both life and property. As indicated by the authors, approximately 95% of Turkey's population resides in earthquake-prone areas. Over the past three decades, Turkey has witnessed a series of destructive earthquakes, including the 6.3 magnitude Adana-Ceyhan Earthquake in 1996 and the 7.4 magnitude Adapazari-Izmit Earthquake in 1999 (Koçer and Ünal, 2022).

On October 30<sup>th</sup>, 2020, at 11:51 GMT, a powerful earthquake measuring 7.0 on the Richter scale occurred in the proximity of the Samos Island (Greece) and Izmir, the third most populous city in Turkey with an estimated population of 4.5 million (Karakale and İpek, 2020). This earthquake impacted the largest urban complex within the affected region (Figure 2.11). The epicenter was situated in the eastern Aegean Sea, approximately 17.26 km off the coast of Seferihisar (Izmir) (Koçer and Ünal, 2022). Moreover, 116 lives were lost, over thousand injured and about 5% of the city's buildings were affected. Immediately, when the ground shake started, 6 buildings collapse completely, and later 14 buildings were demolished (Karakale and İpek, 2020).

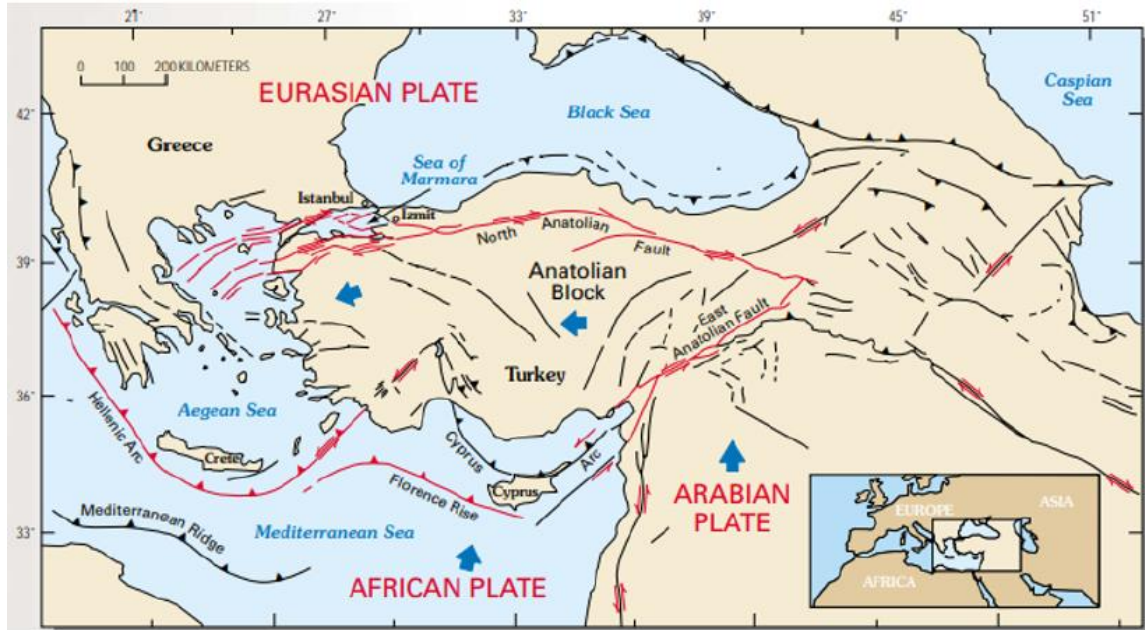


Fig. 2.10 – The Alpine-Himalayan seismic belt in Turkey (Koçer and Ünal, 2022)

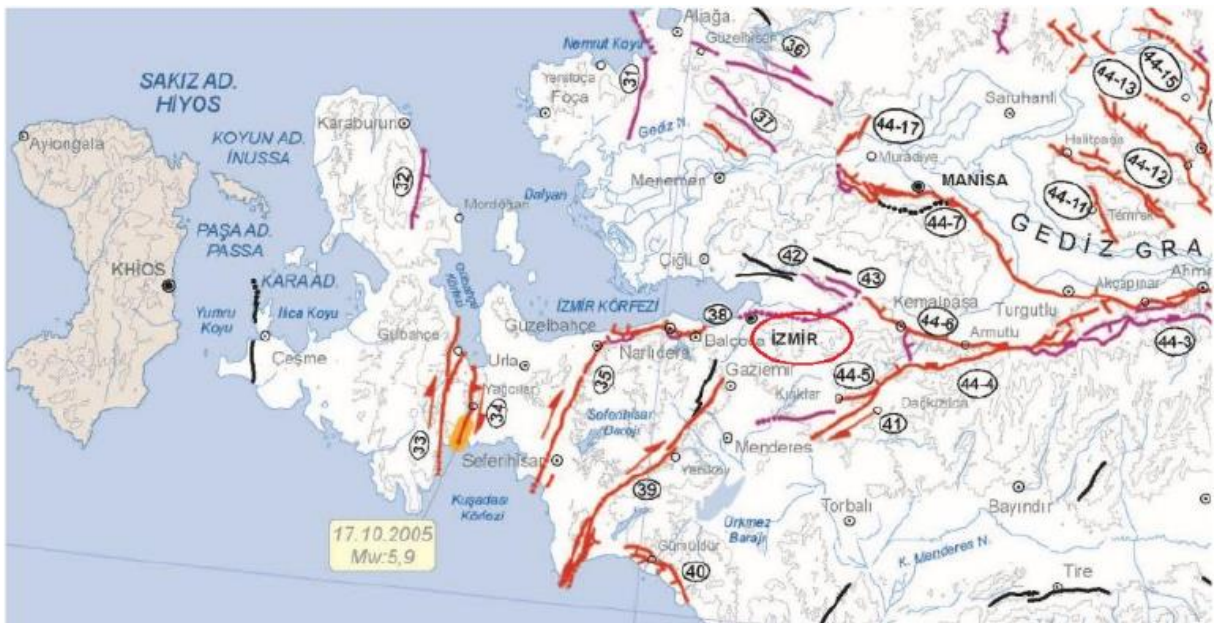


Fig. 2.11 – Izmir’s active fault map (adapted from Emre et al., 2013)

As highlighted by Koçer and Ünal (2022), a better understanding of the building stock and seismic performance is necessary to improve the safety of the built environment in Turkey. The construction industry in Turkey has undergone significant changes in the past two decades. Before the year 2000, the predominant construction practice involved the utilization of cast-in-situ concrete for structures. These structures often were ribless and featured poor quality concrete, employing weak reinforcements for load-bearing structural elements. However, with the rapid economic and technological advancements, the utilization of “ready to use” concrete has experienced widespread adaption (Koçer and Ünal, 2022).

The predominant buildings in Turkey are usually multi-story RC commercial and residential structures with non-structural masonry-infilled walls. A notable consequence of this trend is observed in numerous buildings, wherein the ground floors are predominantly designated for commercial purposes. Unfortunately, these floors often exhibit soft behavior, due to the lack of adequate bracing, compromising their structural integrity. Moreover, in an effort to expand the building area on higher floors, overhangs have been incorporated into many of structures within the region. These changes on the structure have a significant impact on the seismic performance of the building. Figure 2.12 provides an example of a building located in Izmir, illustrating the characteristics of the building stock in the region.



Fig. 2.12 – Typical RC building in the city of Izmir (Google Maps, June 2021)

According to Karakale and İpek (2020), based on different sources, the city of Izmir recorded a total of 9444 damaged buildings following the earthquake. Taking into account the estimated total number of buildings in the area at the time, which was approximately 700000, the percentage of damaged buildings in Izmir amounts to approximately 1.3%. Further examination by the authors revealed that among the affected buildings, 8% (795) were classified as heavily damaged, including those that collapsed. Additionally, 9% (804) were categorized as moderately damaged, while the majority of the structures, totaling 83% (7845), were deemed slightly damaged (Karakale and İpek, 2020).

The severity of the earthquake-induced damage in certain districts of Izmir, notably Karsiyaka and Bayrakli, was remarkably extensive (Koçer and Ünal, 2022). This can be attributed, at least in part, to the presence of soft sediments in these areas, which could have amplified the frequencies of the ground motion, and consequently intensifying the level of damage on buildings. Karakale and İpek (2020) analysis of the distribution of structural damage as a function of construction period indicates that a substantial proportion of the damaged buildings were built between 1990 and 2000. In contrast, buildings constructed after 2010 exhibit significantly less structural damage.

After the Izmir Earthquake, Koçer and Ünal (2022) conducted site investigations, revealing a notable pattern among the collapsed or massively damaged buildings. Surprisingly, it was discovered that a significant portion of these structures had been designed in compliance with the Turkish Earthquake Code 1975 regulation, which outlines minimum dimensions and reinforcement specifications for RC elements, such as beams and columns (as depicted in Figure 2.13), as well as principles for calculating shear in column-beam connections (as illustrated in Figure 2.14). However, on construction sites, it was observed that some details in the regulation were not followed, namely: inadequate anchorage in longitudinal beam reinforcement and large stirrup spacings. This clearly indicates the insufficiency of on-site inspections. These deficiencies resulted in non-ductile frames, which completely or partially collapsed during the earthquake. Despite this, both Karakale and İpek (2020) and Koçer and Ünal (2022) revealed that even some recently constructed high-rise buildings suffer significant damages on partition walls, demonstrating poor performance, mostly attributed to the repetition of well-known design mistakes of the past.

Post-earthquake reports, by the authors, Karakale and İpek (2020) and Koçer and Ünal (2022), highlight the following main causes for the observed damages or collapses in buildings:

- Column-Shear wall failure due to the lack of stirrup confinement on the columns;
- No employment of desirable shear walls or bracing elements, especially at the ground floor where, instead, was used glass walls since the buildings were used as workplaces;
- Strong-beam weak-column mechanism;
- Structural alterations;
- In-plane irregularities.



Fig. 2.13 – Column damages (Koçer and Ünal, 2022)



Fig. 2.14 – Strong-beam and weak-column mechanisms (Koçer and Ünal, 2022)

### 2.1.2. TYPICAL FAILURE MECHANISMS OF NON-DUCTILE RC BUILDINGS

The review above indicates that seismic risk in urban areas is still an important concern, particularly in RC structures, which are widely used in construction due to their strength, durability, and versatility. Moreover, the frame type RC structures were the primary structural system used in buildings in southern European countries until the late 1970's. Many of them were constructed following old earthquake-resistant building codes, making them obsolete. Thus, in terms of ductility, they lack the ability to deform plastically under extreme loads and are especially vulnerable to earthquake events.

The disastrous consequences from seismic activity have been evident in many recent past earthquakes, resulting in extensive damage on RC buildings, and in human casualties all around the world. This reveals that research on the assessment and strengthening of existing structures is urgently needed. In spite of the current rather strict seismic code requirements, serious weaknesses still take place in the design and construction of most structures (Varum, 2003). The review in the previous section proves that the heavily damaged or collapsed buildings analyzed are a result of structural deficiencies and a failure to implement prescribed seismic demands from modern building codes. Thereby, it is crucial for an earthquake-resistant building to be provided with balanced characteristics, i.e., the strength, ductility and stiffness between its elements and connections must be in harmony (Varum, 2003).

Finally, understanding the mechanisms of failure allows engineers and builders to take a step forward in mitigating damage and improving the seismic resilience of structures. From the literature and past research, it can be pointed out major sources of seismic weakness in RC structures, as follow:

- Design deficiencies, such as insufficient lateral stiffness and strength, in plan irregularities, short-columns, soft-story, and weak-column strong-beam mechanisms;
- Construction deficiencies, such as poor material quality, poor workmanship and structures not following detailing demands;
- Detailing deficiencies, such as insufficient and improper anchorage of the longitudinal reinforcement at the joints, especially at beam-column and column-foundation joints;
- Structural modifications and structural elements deterioration.

Ultimately, the observed damage in the various post-earthquake investigations reveal that the contribution of masonry infills to the overall seismic response of buildings cannot be underestimated. While the presence of infilled walls can enhance the strength and global stiffness of the building, their impact on the seismic response can be detrimental, depending on the extent and placement in the building's earthquake-resistant design. Therefore, it is crucial to consider the influence of infilled walls

in the seismic performance of structures and acknowledge that they cannot be regarded as non-structural or secondary elements (Furtado and De Risi, 2020).

## **2.2. PREVIOUS EXPERIMENTAL RESEARCH ON INFILLS**

Extensive research has been dedicated to investigating the load-bearing capacity and behavior of URM infill walls, subjected to both in-plane and out-of-plane forces (Angel, 1994). These studies have presented significant findings, highlighting the positive impact of infill walls within RC frames. Specifically, it has been concluded that the inclusion of masonry infills enhances the lateral capacity and the initial stiffness of the frame (when compared to the bare frame solution) by attracting a major portion of the lateral seismic shear forces, consequently reducing the stress exerted on the RC frame itself. This highlights that URM infill walls play an important role in enhancing the dynamic performance and overall resilience of RC structures.

The coupling of strong frames with weak infills has been found to contribute to the shear failure of columns (Mehrabi et al., 1994). Furthermore, the authors' observations suggest that when strong frames are paired with strong infills, there is a substantial increase in the load-bearing capacity and energy dissipation of the wall compared to configurations in which both the frame and the infill have low strength and stiffness. Moreover, local brittle shear failure mechanisms of structural element or global failure mechanisms may be introduced by the frame-infill interaction (Mehrabi et al., 1994).

Past studies reveal that around 80% of stiffness and strength loss in buildings are due to damage in non-structural elements, such as masonry infills and internal partition walls (Cardone and Perrone, 2016). However, accurately assessing the seismic performance of URM infills is challenging, primarily due to the inherent variability in the mechanical properties and the lack of performance criteria for some masonry typologies in design codes. Consequently, infill walls are usually accounted as non-structural elements in the design of buildings, disregarding their contribution to the global structural behavior.

Current seismic design codes, for example the European seismic code EC8 (2004): part 1 and the Italian code NTC18 (2018), lack specific rules in respect to the typology and structural configuration of infill panels. The existing regulations regarding the verification of strength, control of damage, and assessment of seismic induced forces have a general nature, rather than being individual for each type of masonry. The lack of well-defined testing protocols, when conducting both in-plane and out-of-plane experiments, have led to a wide variety of experimental setups and specimens, from monotonic loading arrangements to a few shaking-table tests (Angel, 1994). In fact, past experimental campaigns have barely focused on dynamically testing masonry infills in the out-of-plane direction. Moreover, more rigorous sustainability requirements have led to the enhancement of the global performance of façades in general, especially the ones made of masonry materials. Hence, an actual socio-economic and environmental need has been the improvement of structural seismic safety and energy efficiency.

It is obvious that there are several determining parameters when modeling infilled walls in order to properly recreate and better understand their behavior. These parameters usually have a large range of possible values, that have a significant impact on the behavior of infills. In particular, uncertainties related to the material heterogeneous properties, construction techniques, and panel geometrical characteristics must be taken into account (Petracca et al., 2017).

This section aims to provide a summary of previous experimental studies conducted on masonry infills. Its purpose is to gain insight into the type of work that has already been accomplished, and to identify the effects of infills in the dynamic behavior of RC framed structures. The section is divided into two

parts based on the two main directions of study (in-plane and out-of-plane response) and a third part dedicated to the seismic contribution of infills in the buildings' structural response.

## 2.2.1. IN-PLANE RESPONSE

### 2.2.1.1. Uniaxial Loading

Even though masonry infills are not expected to bear vertical loads apart from its own self-weight, it is valuable to comprehend its behavior under vertical compression. Under compressive loads, the brick-mortar interface introduces a stress state that leads to the mortar joints experiencing triaxial compression, whereas the bricks undergo a state of biaxial compression (Zahra and Dhanasekar, 2016). This loading transfer phenomena through the constitutive materials have been studied by (Anthoine, 1995) in a generalized two-dimensional media assuming plane stress and by (Zucchini and Lourenço, 2007) considering a three-dimensional thick media, both authors used homogenization theory. This state of stress demonstrates linear behavior at low levels of force, but as compressive stress increases the material's response becomes extremely nonlinear and vertical splitting cracks on the bricks starts at levels of force lower than the compressive capacity (Anthoine, 1995). Therefore, the comprising materials (brick and mortar) should be regarded as being subject to a multiaxial state of stress (Zahra and Dhanasekar, 2016). Moreover, crushing of the mortar joint is rarely reported.

In their homogenized model, Zucchini and Lourenço (2007) synthesize how the brick masonry response is characterized when under compression. They incorporated compression failure theories from previous research and several analytical relations suggested by former researchers. The authors concluded that the use of poor quality (weak) mortar leads to the mortar prematurely exhibiting nonlinear behavior, whereas the bricks plasticity is introduced at a later stage (Zucchini and Lourenço, 2007). Finally, they concluded that the compressive behavior of masonry is dependent on the characteristics of the constitutive materials (brick and mortar) under tension and compression (Zucchini and Lourenço, 2007).

Typically, when the perforations of hollow bricks are placed vertically, it becomes challenging to construct walls with horizontal mortar joints of simple execution. This is owing to the fact that the holes in the bottom course need to be covered to prevent the mortar from dripping, which might increase the manufacturing cost of the infill wall due to additional work requirements.

### 2.2.1.2. Lateral Loading

Experimental assessment of the response of masonry infill walls loaded within their plane is extensive (Angel, 1994). Multiple hypothesis on the modeling and behavior of infills have previously been presented in the literature, but yet a large set of experimental tests should be gathered in order to demonstrate the efficacy and reliability of such models.

Nowadays the design of RC frames aim at achieving flexural behavior in order to withstand seismic actions (Basha and Kaushik, 2016). It is well known that the use of masonry infill walls enhance the in-plane strength, energy dissipation capacity, and stiffness of the infill frame. However, the column's shear behavior still dominates the lateral load resistance (Basha and Kaushik, 2016). Moreover, if the infill walls are strong enough it might cause the columns to fail in shear. This has been shown by authors when numerically investigating the behavior and influence of masonry infill walls on the global response of RC frames (Asteris and Cotsovos, 2012a; Asteris et al., 2013a).

The most commonly used specimen in past studies is comprised by a single-span and single-story infilled frame (Figure 2.15). The introduction of infills into RC frames, replaces the predominant frame

action for the predominant truss action as the mechanism for transferring lateral loads, as illustrated in Figure 2.16. This effect is responsible for the increase of axial forces and decrease of bending moments demand in the RC frame (Murty and Jain, 2000).

In an initial stage, the frame and infills are responsible for the energy dissipation of the system. However, the stiffness of the frame decreases gradually if numerous loading cycles are applied (Angel, 1994). This is an important factor that should be considered when analyzing the behavior of infilled RC frames subjected to seismic actions. Therefore, after the load-bearing capacity of the infills is compromised due to damage, the energy dissipation of the system is established by the development of plastic hinges in the columns. According to Basha and Kaushik (2016), the energy dissipated by ductile infilled frames is about 50% higher than of bare frames, with the potential of reaching even greater values when considering non-ductile frames.

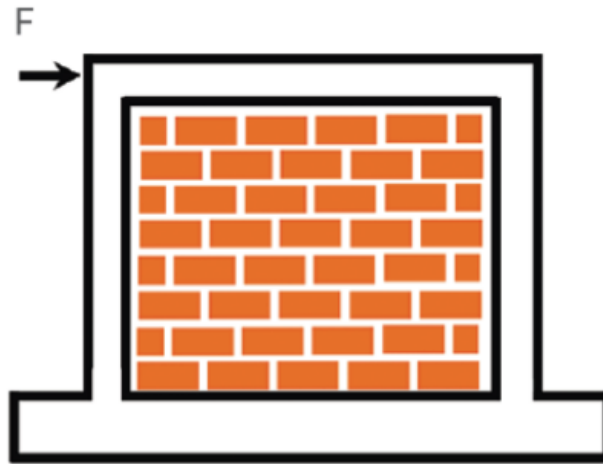


Fig. 2.15 – Commonly used specimen

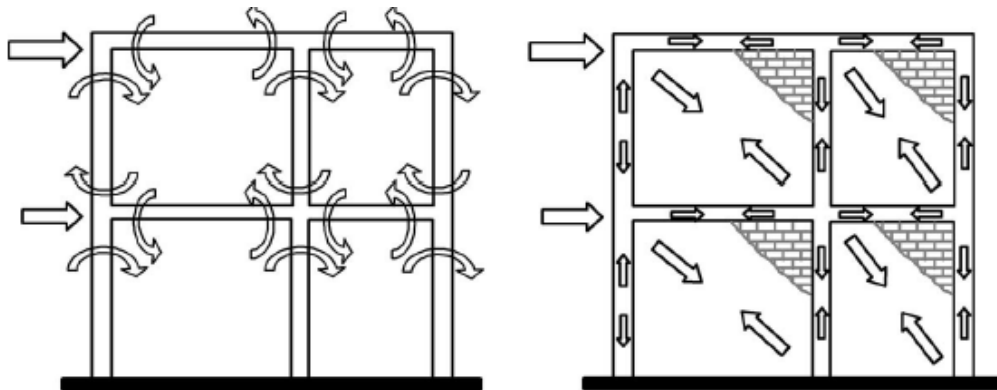


Fig. 2.16 – Load transferring mechanism from frame to truss action (Murty and Jain, 2000)

It has been experimentally proved by several authors (Panagiotakos and Fardis, 1996; Verdarama et al., 2016; De Risi et al., 2018) that the in-plane behavior of masonry infill walls is typically characterized by a clear high initial lateral stiffness with limited deformability (linear branch). However, when cracks start to develop at the panel, it introduces degradation of the stiffness until a maximum loads is reached. Subsequently, a decreasing branch occurs until complete failure of the panel.

Panagiotakos and Fardis (1996) pioneer infill model described the in-plane response of masonry infills based on four branches, as depicted in Figure 2.17. In the initial branch the infill behaves elastically, as there is no occurrence of cracks yet. The subsequent branch (cracked) extends to a peak load, though in a less pronounced manner as the cracks cause the stiffness to decrease. Thus, this branch is dependent on the cracking strength. The third branch continues up to a residual strength and its slope is controlled by a scalar factor that multiplies the initial elastic stiffness. This factor is ranged between 0.5-10%. The final branch (full plasticity) is equivalent to 1-2% of the peak load and is horizontal.

In Figure 2.18 an average horizontal force versus displacement envelope (Verdarama et al., 2016) is presented to demonstrate the infill’s envelope under in-plane lateral load. This envelope is also comprised by four branches. De Risi et al. (2018) analyzed a comprehensive database of in-plane loading tests on infilled RC frames. Particularly, only experimental tests on masonry infill panels with hollow clay tile bricks were considered, in which 60% of masonry infill walls were characterized by bricks with holes horizontally orientated and 90% were comprised by bricks with at least 45% of void percentage. The authors observed that, on average, the ratio between cracking strength and peak lateral load was equal to about 0.67. Moreover, the authors state that due to the wide range of values among the collected data, softening and cracking stiffness were the most difficult parameters to be obtained. De Risi et al. (2018) identified some key parameters, namely: peak load ( $F_{peak}$ ); cracking strength ( $F_{cr}$ ); secant-to-cracking stiffness ( $K_{cr}$ ); secant-to-maximum stiffness ( $K_{peak}$ ); softening stiffness ( $K_{soft}$ ).

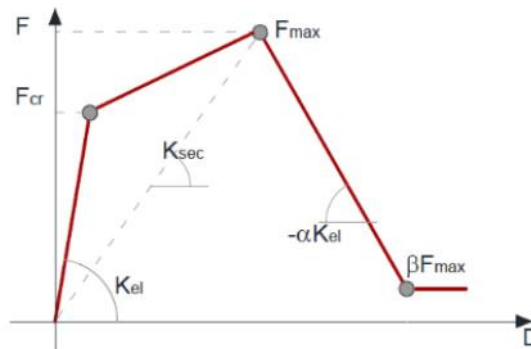


Fig. 2.17 – Panagiotakos and Fardis (1996) force-displacement envelope

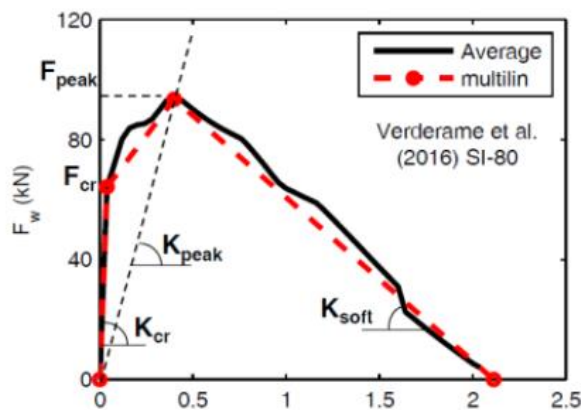


Fig. 2.18 – Infilled frames' force-displacement envelope (Verdarama et al., 2016; De Risi et al., 2018)

Experimental studies carried out by Fardis (2009) and Markulak et al. (2016) have highlighted some key aspects that significantly influence the failure mechanisms exhibited by infilled frames, such as the shear/tensile mortar resistance, opening percentage, aspect ratio, amount of compressive forces on the columns, beam-column stiffness ratio, type of brick used and workmanship. In fact, Markulak et al. (2016) analyzed infilled steel frames and observed that when the infill's compression strength is exceeded, diagonal cracking can be observed followed by notorious shattering and spalling of the masonry units in the outer layer of the panel. Although in a less significant level as the brick, the mortar resilience in compression is also a key aspect that contributes to the shear load strength of masonry-infilled RC frames (Chiou and Hwang, 2015). Similarly, Angel (1994) observed that for the particular case of infills constructed with type N mortar the shear stresses levels were on average 50% higher than those constructed with lime mortar. Thus, it can be concluded that the maximum infill shear stress varies with the type of mortar used. Hence, it can be deduced that any enhancement in bond strength possesses the potential to demonstrate greater in-plane shear capacity, which could prove to be beneficial in withstanding higher lateral loads resulting from earthquakes.

According to Angel's study (1994) on the behavior of infills under in-plane loads, any damage to the infill specimen in one direction had no effect on the specimens' in-plane behavior when loaded in the opposite way. Furthermore, for loading in both directions, the lateral force-displacement behavior is symmetrical. When examining the hysteresis loop graph (Figure 2.19) from the cyclic lateral loading experiments in steel infilled frames carried out by Markulak et al. (2016), it is clear that this is the case.

Mehrabi et al. (1996) and Fardis (2009) have shown that the configuration of weak and non-ductile columns with relative stiff infills might be the primarily cause of shear failure in columns. On the contrary, although low strength infills coupled with high strength frames was used in Basha and Kaushik (2016) experimental tests, columns failed in shear mode. Such brittle behavior can be associated to the weakening of the frame-infill interface, which decrease the effective contact length between the column and infill (Basha and Kaushik, 2016).

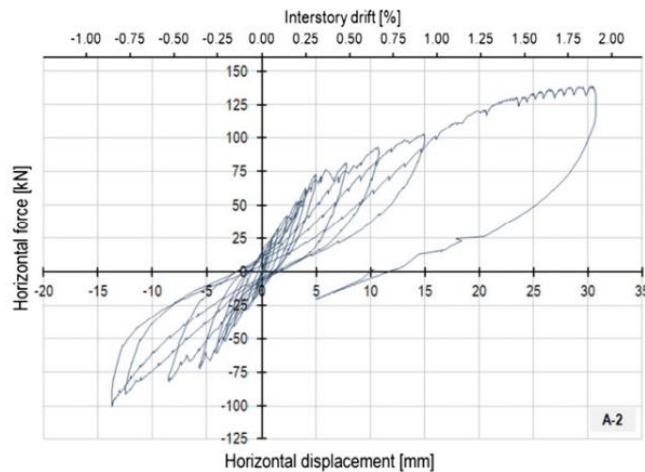


Fig. 2.19 – Hysteresis loop for specimen “A-2” (Markulak et al., 2013)

In relation to the impact of openings on the in-plane behavior of masonry-infilled RC frames, experimental campaigns dedicated to infills with openings generally analyze the correspondence with a solid panel, used as a reference. The findings from numerous studies indicate that when masonry infills have door or window openings, it leads to a more flexible structural system, resulting in reduced lateral

strength and stiffness compared to a solid infilled RC frame. However, it is important to note that the increase of the opening's area is not directly proportional to this issue (Christiana et al., 2022).

Kakaletsis and Karayannis (2007 and 2008) conducted an experimental study to find the effect of windows and doors positioning on the hysteretic characteristics of infilled RC frames. The observations made by the authors regarding specimens with window openings indicate that the first significant diagonal cracks appeared at a drift of 3-4%. This was followed by the formation of plastic hinges at the top and bottom of the columns at a drift range of 3-9%. These failures were primarily attributed to sliding along the bed joints. In all cases of infilled specimens, whether with door or window openings, beam cracking was observed far from the column face, closer to the middle. Plastic hinges in the beams were observed to form at drifts higher than 9% (Kakaletsis and Karayannis, 2008). Furthermore, according to Mansouri et al. (2018), in the case of infilled RC frames with central openings, the primary load-bearing mechanism is the development of a compression strut and diagonal cracking in the RC frame column that surround the masonry infill. This results in the lateral strength of the infill panel being determined as the minimum value between the resistance to diagonal tension and the resistance to corner crushing of the column (Mansouri et al., 2018).

Infilled frames experience a reduction of 75% in their lateral strength and a decrease of 85-90% in their lateral stiffness if the masonry infill panel has an opening on its compressed diagonal (Mallick and Garg, 1971). Moreover, the authors indicate that, for central square openings with a cross-section equal to 20% of the masonry infill panel area, the infilled frame can experience a reduction of 25% up to 50% in its stiffness and strength. Kakaletsis and Karayannis (2007 and 2008) observed that the strength of infilled RC frames is reduced by 19% and 32% for central openings percentages of 12.5% and 25% respectively. Later, Christiana et al. (2022) assessed and compared the effect of different central openings dimensions on the lateral capacity of masonry-infilled RC frames, as shown in Figure 2.20. The authors pointed out that for infilled RC frames with 12% and 27% opening percentages, the maximum lateral strength of the wall decreases about 15% and 31%, respectively.

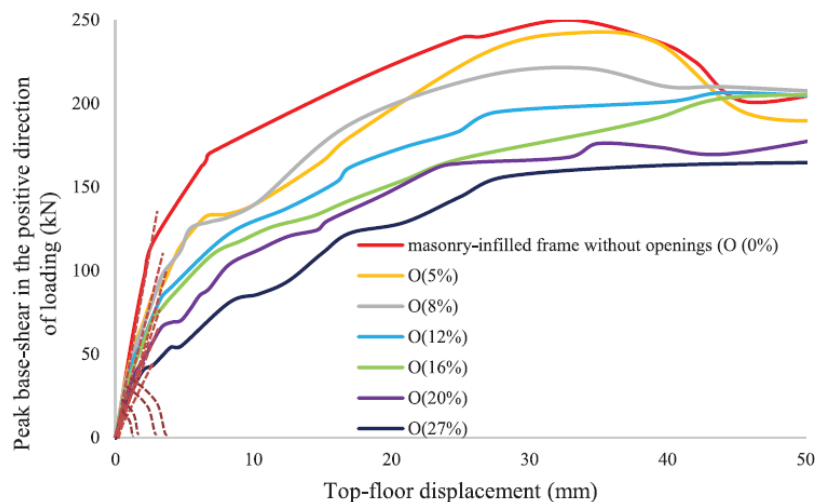


Fig. 2.20 – Base-shear versus top-displacement for Christiana et al. (2022) model

According to the authors results herein presented, there is a clear confirmation of the formation of a multi-diagonal strut mechanism by infilled frames with openings, as illustrated in Figure 2.21. The majority of authors agree that the increase of the openings' eccentricity, in the masonry infill panel, provides an improvement to the performance of infilled RC frames. It can be concluded that the increase

in the opening's eccentricity is followed by an increase in masonry strength and energy dissipation when in comparison to the infilled frame with central openings (Kakaletsis and Karayannis, 2007). However, this does not mean that masonry infill walls with openings can dissipate energy more effectively than solid masonry infill walls, as masonry infills fail earlier due to the openings (Mallick and Garg, 1971). In fact, owing to the effect of openings on masonry infill walls, cracking and detachment of infill panels from the bounding RC frame occur at an early stage, before the yielding in the column's reinforcement starts (Kakaletsis and Karayannis, 2007). Moreover, the authors indicate that the energy dissipation mechanism by friction across the bounding frame and mainly across the cracks of the infill panel seems to be more active in the case of the larger columns. This is evidenced by the development of a well-distributed crack pattern in the masonry infill wall.

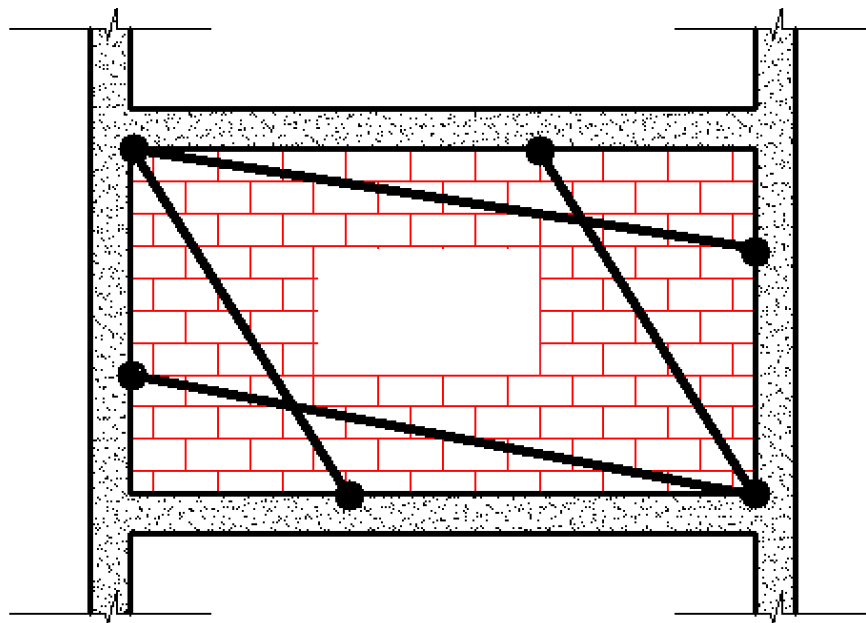


Fig. 2.21 – Typical strut approach for infill panels with central openings

The mechanism of failure developed by infilled RC frames is largely influenced by the frame and its connection to the infill. If the system is composed by weak infills coupled with a strong frames, the masonry infill wall cracks in order to adapt to the new deformed shape of the RC frame (Angel, 1994). On the contrary, the configuration of brittle frames and infills with sufficiently large strength and stiffness, lead to the failure being controlled by the masonry infill panel. Therefore, the flexibility and strength of the confining frame play a significant role in governing the mode of failure developed in masonry-infilled RC frames (Angel, 1994).

The type of failure mechanism observed in masonry-infilled RC frame specimens varies accordingly to the frame-infill interaction. This has been substantiated by several researchers (Asteris et al., 2011a; Asteris et al., 2011b; Asteris et al., 2012b; Cardone and Perrone, 2015; De Risi et al., 2018), through experimental studies, who observed that the in-plane behavior of a generic infill panel can exhibit five main failure modes:

- Failure caused by diagonal compression, in which the infill's middle portion is crushed. Characteristic of a slender infill panel, which fail owing to out-of-plane buckling (Figure 2.22);

- Failure caused by diagonal crack, which happens simultaneously with sliding shear failure and involves cracks extending across the compressed diagonal of the infill panel. Characteristic of weak frames or frames with weak mortar joints and stiff infills (Figure 2.23);
- Sliding shear failure, as an example of bed joint horizontal sliding. Characteristic of strong frame with weak mortar joints (Figure 2.23);
- Failure due to corner crushing, which occurs when at least one of the infill's comers is crushed. It is characteristic of weak infills bounded by a strong frame but with weak joints (Figure 2.22);
- Failure of the frame, in which there is the development of plastic hinges in the frame columns or at the beam-column joints (Figure 2.23).

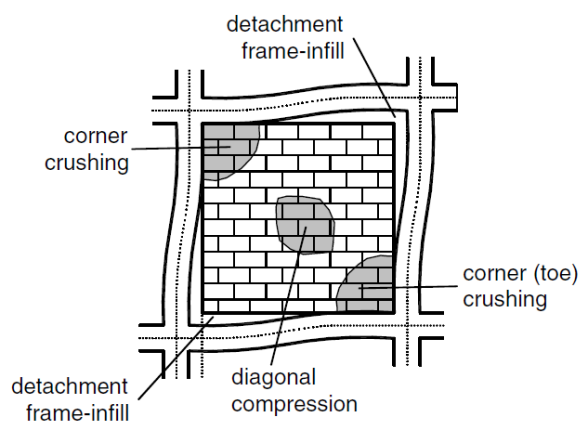


Fig. 2.22 – Corner crushing and diagonal compression failures (Asteris et al., 2011a)

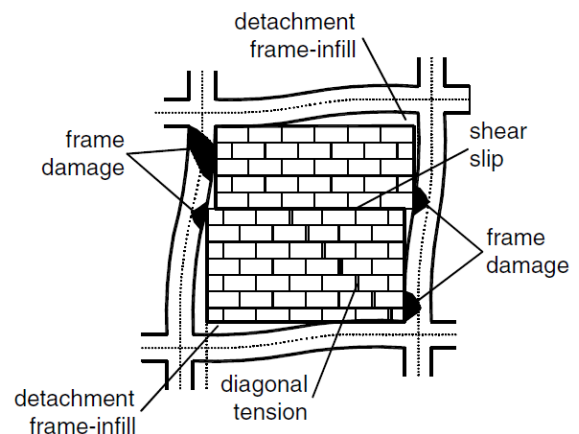


Fig. 2.23 – Shear sliding, diagonal cracking and frame failures (Asteris et al., 2011a)

Some authors have addressed the definition of displacement thresholds corresponding to specific damage levels on masonry infill walls by analyzing the severity of crack patterns on infill panels, they define different damage states (DS). Cardone and Perrone (2015) proposed a classification system consisting of four DS, which explicitly relates the displacement capacity of the infill to its in-plane response, i.e., the equivalent drift ratio between floors. The four DS (DS1-DS4) are illustrated in Figure 2.24.

From a phenomenological point of view, the damage progression resulting from to in-plane lateral loading tests on masonry infill walls can be described as follows (Cardone and Perrone, 2015; De Risi et al., 2018): (i) it begins with small cracks developing (along the mortar bed joints or in the bricks) in the middle portion of the masonry infill panel (Slight Damage or DS1); (ii) the damage advances to more severe diagonal cracking (principal direction of tensile stress) and crushing of bricks, typically in the corners, where there is the development of a biaxial compression stress state and where portion of the panel around the compressed diagonal acts as a bracing element (Moderate Damage or DS2); (iii) as the lateral load increases, the shear and flexural deformation in the masonry infill wall and RC frame, respectively, causes the detachment of the masonry infill panel from the frame along part of its height (Severe Damage or DS3); (iv) eventually, the masonry infill panel becomes heavily damaged and completely fail, transferring all the load demand to the bounding frame (Collapse or DS4). This process is better illustrated in Figure 2.25 by De Risi et al. (2018) experimental campaign. It is important to note that the above failure sequence occurs unless the columns fail at an earlier stage than the infills due to shear. The shear failure of the columns happens primarily when non-ductile columns are coupled with stiff and strong infills.

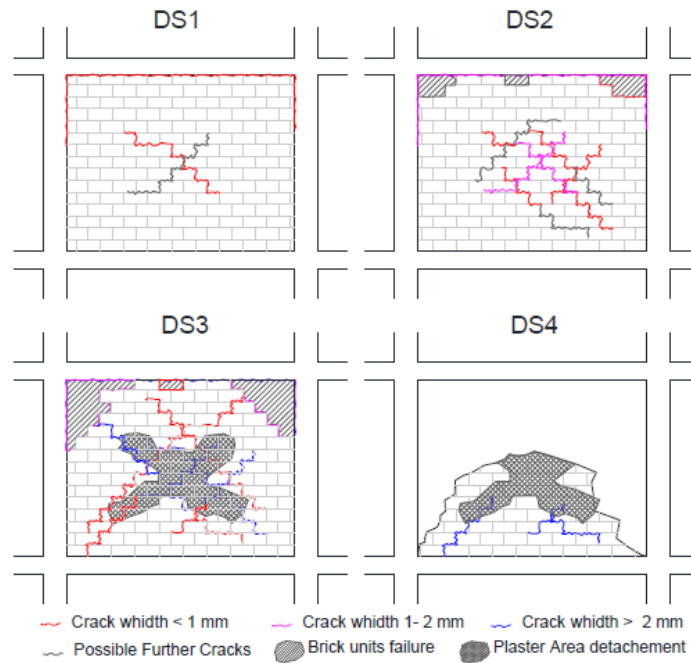


Fig. 2.24 – Masonry-infilled RC frames damage states (Cardone and Perrone, 2015)

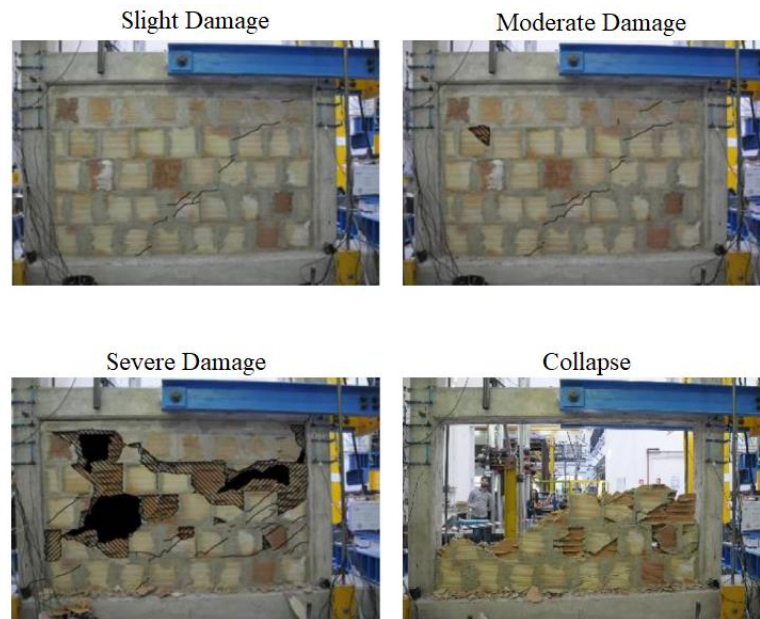


Fig. 2.25 – Evolution of damage (adapted from De Risi et al. (2018))

### 2.2.2. OUT-OF-PLANE RESPONSE

With respect to the amount of studies done for the in-plane direction, much less effort has been addressed to study the out-of-plane behavior of masonry infills. In fact, in the literature, very often articles highlight the limitation of the existing research works. For instance, there is a lack of understanding of the influence of the type of brick and mortar used on the out-of-plane response of masonry-infilled walls,

and the existing research work is mostly limited to two-dimensional models that do not fully capture the complex three-dimensional behavior of infill walls (Angel, 1994).

Past research on the out-of-plane strength, under static and dynamic actions, of URM infill walls has demonstrated that the out-of-plane damage in masonry infills is greatly influenced by arching effects. Panels that are restrained along all their perimeter by relatively stiff frames develop double arching resisting mechanisms (vertical and horizontal) (Figure 2.26). This has been observed by many authors (Di Domenico, 2018; De Risi et al., 2019; Verderame et al., 2019) using acceleration and displacement profiles along the vertical and horizontal direction. Therefore, this leads to an important observation that the distribution of accelerations, and consequently out-of-plane forces, are not uniform along the masonry infill panel surface but close to triangular, with the maximum load acting at the central part of the panel.

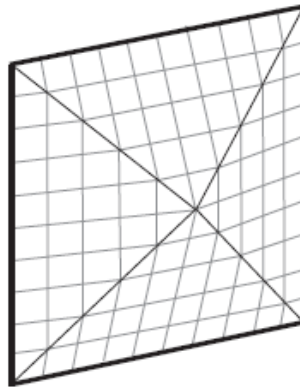


Fig. 2.26 – Double arching effect in a square masonry infill wall (De Risi et al., 2019)

Di Domenico (2018) conducted experimental tests on masonry-infilled RC frames with different boundary conditions and widths (80 and 120 mm), in which the specimens were bonded along two, three or four edges to the surrounding RC frame. The first observation made by the author is that specimens bonded along the top and bottom edges exhibited spreading horizontal cracks at mid-height in the mortar layers between bricks, extending from the central portion of the masonry infill panel until the free lateral edges (Figure 2.27). This corresponds to the formation of a one-way arching effect in the vertical direction. Moreover, the author indicates that after the peak load is reached, the load resistance capacity of the specimen has a noticeable drop, mainly due to the crushing of masonry, as the wall loses its capacity to redistribute the stresses to the restrained edges. Verderame et al. (2019) experimental campaign on masonry infills bonded along the top and bottom edges, also indicated this arching effect. Specifically, upon the initial occurrence of cracking, a noticeable deflection of the upper beam can be observed. This is evident by the sudden decrease in the tangent stiffness of the out-of-plane force-deflection of the beam, as depicted in Figure 2.28. According to the authors, these are indications that after the development of cracks, a slight increase in the out-of-plane force acting on the infill wall leads to a substantial increase in the force acting on the top RC beam. Consequently, arching thrusts were formed within the infill thickness, which were then transmitted to the RC beam, thereby inducing deflection in the beam. Therefore, phase I (illustrated in Figure 2.29) corresponds to the flexural strength mechanism of the infill wall panel, whereas phase II is characterized by the development of the arching effect (Verderame et al., 2019). Finally, for specimens bonded only along two edges of the frame, detachment of the masonry infill wall from the RC frame occurs mainly at the restrained edges.

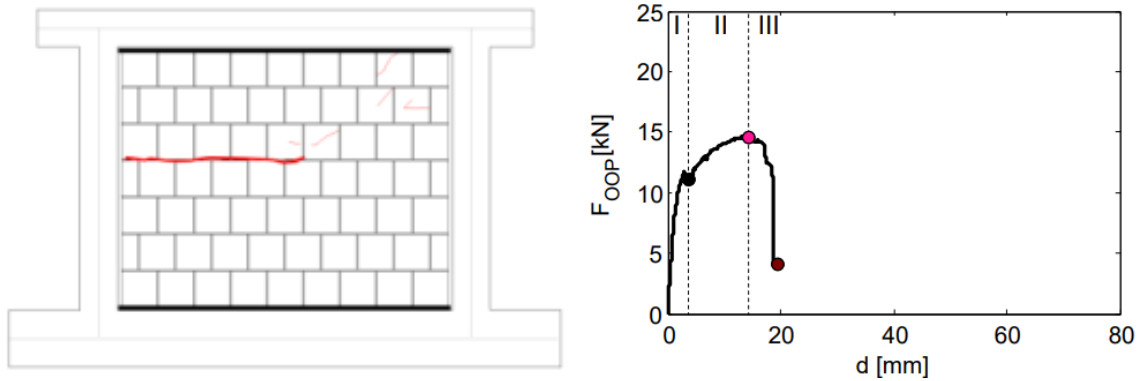


Fig. 2.27 – Cracking pattern and experimental response for ‘80\_OOP\_2E’ specimen (Di Domenico, 2018)

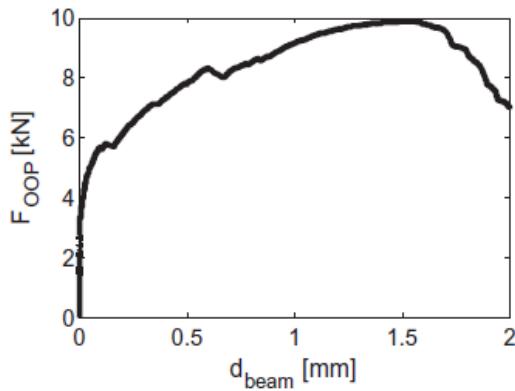


Fig. 2.28 – Out-of-plane force-displacement of the top beam (Verderame et al., 2019)

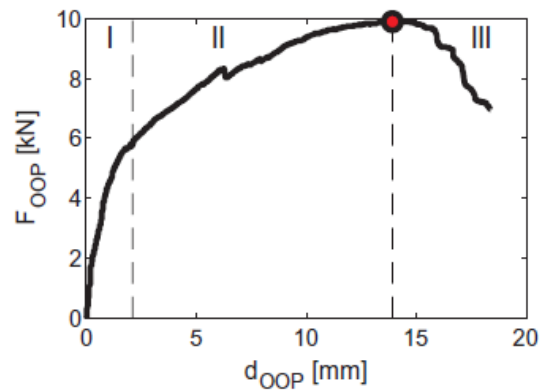


Fig. 2.29 – Out-of-plane force-displacement of the infill (Verderame et al., 2019)

The behavior of masonry infill walls bonded along all their perimeter to the surrounding RC frame is very similar to the previous specimens described (bonded along two edges). The major difference is that due to all edges being restrained to the frame, the loading transfer is accomplished more easily. Thus, according to Di Domenico (2018), for the ‘80\_OOP\_4E’ specimen no detachment from the frame was observed and no significant out-of-plane displacement on the top RC beam was registered. Owing to the double arching effect, the masonry infill panel cracked in a “X” shape (Figure 2.30). As a result, the specimen was able to reach a much higher out-of-plane load when in comparison to the ‘80\_OOP\_2E’ specimen. The attainment of the maximum load was not followed by a noticeable drop (softening branch), as it was reported for the ‘80\_OOP\_2E’ specimen. In Dawe and Seah (1989) study it was observed that the presence of gaps or slippage of the panels at the edges affects the cracking pattern and deformed shape of the infill, which consequently affects their out-of-plane stiffness and strength. For instance, the ‘WE2’ specimen, which was confined at four edges, exhibited 1.8 times the out-of-plane strength of the ‘WE6’ specimen, which was confined at three edges.

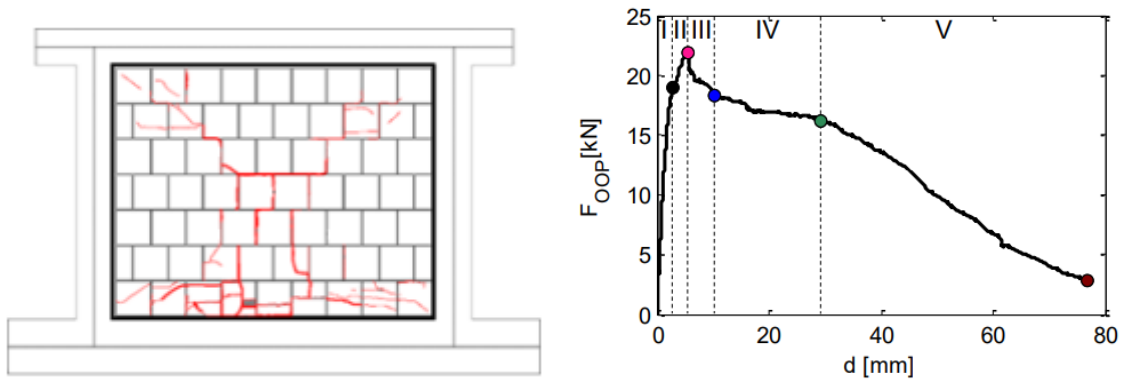


Fig. 2.30 – Cracking pattern and experimental response for '80\_OOP\_4E' specimen (Di Domenico, 2018)

Experimental studies carried out by Hak et al. (2014) on infills bonded to the confining frame along four edges (totally restrained), demonstrated that there is a significant decrease in both stiffness and strength in the out-of-plane direction as the previous in-plane drift and related damage increased, especially at high levels of drift and extensive pre-damage. For specimens 'TA3' and 'TA1', which were subjected to lower in-plane drifts of 1.0% and 1.5% respectively, comparable peak strength values were obtained. However, the stiffness decreased significantly, approximately 40%. The findings suggested that for specimen 'TA1' (shown in Fig. 2.31), a primary horizontal crack developed at the central joint of the infill, which was then followed by the occurrence of diagonal stepwise cracks spreading towards the corners. Figure 2.32 depicts the 'TA1' fully infilled specimen's deflected shape during the cycle of the 75 mm target displacement. On the other hand, specimen 'TA2', which had previously experienced a higher in-plane drift of 2.5%, showed a significant decrease in stiffness, around 75%, when in comparison to the stiffness of specimen 'TA3'. This is in accordance with many authors (Ricci et al., 2018a; Ricci et al., 2018b; De Risi et al., 2019), whose observations indicate that the less damage the specimens had from previous in-plane loading test, they would exhibit lower displacements and higher accelerations, especially in comparison with heavily damaged infills. The latter would reach higher displacement values at an earlier stage than the less damaged walls.

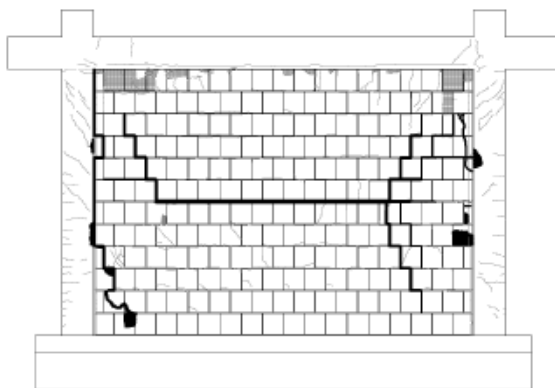


Fig. 2.31 – Out-of-plane crack pattern for 'TA1' specimen (Hak et al., 2014)

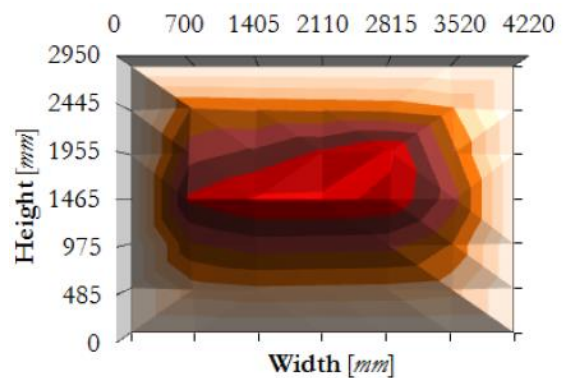


Fig. 2.32 – Out-of-plane crack deformed shape for 'TA1' specimen at 75 mm target displacement (Hak et al., 2014)

Dawe and Seah (1989) pointed out that the effectiveness of arching effects are not affected by the presence of openings in the masonry infill walls. Moreover, the authors observed that the masonry infill

wall thickness significantly impacts their out-of-plane strength. In fact, they suggested the relation that the square of the infill's thickness is directly proportional to the out-of-plane strength. Similarly, in order to investigate the impact of infill panels with different aspect ratios (1.28 and 1) on their out-of-plane direction, De Risi et al. (2019) conducted a testing campaign and observed that the DS of square and rectangular infills were proved to be considerably different. For instance, the square walls had less damage than the rectangle-shaped ones (De Risi et al., 2019). Additionally, for panels that had previously been subjected to low in-plane drift ratios of around 0.30%, the square panels were reported with a 24% strength decrease while the rectangle-shaped ones were reported with a 52% strength reduction. Therefore, the in-plane damage of the infill panel significantly reduces its out-of-plane strength. As a result, it is frequently assumed that the out-of-plane strength of a cracked masonry-infilled walls is fairly low.

The frame-infill connection is typically executed with weak mortar and during seismic events, infills may get detached from the bounding RC frame and become vulnerable to collapse in the out-of-plane direction. Such out-of-plane failure, however, is uncommon on infill walls with low slenderness value (Kaushik et al., 2006). This is in agreement with Ricci et al. (2018a), who have also observed that the out-of-plane strength of masonry infills decreases simultaneously with the increase of their slenderness.

### 2.2.3. CODE APPROACH FOR MASONRY INFILLS IN RC FRAMES

For many years, seismic design codes have been reluctant to incorporate the contribution of infills to the structural behavior of buildings. The primary reason is the lack of complete understanding of the various variables and uncertainties involved (Kaushik et al., 2006). Furthermore, the behavior of infills and their interaction with the frame is highly dependent on the type of brick unit and the frame geometry, which can significantly differ in various seismic-prone areas (concrete blocks, hollow clay bricks, solid clay bricks, single or double leaf infills, etc.). In fact, modern design codes, such as EC8 (2004), have introduced design principles for infilled RC frames in new construction projects. For instance, in order to account for irregularities caused by infills on the structure's plan or elevation, certain penalty factors are applied to the structure (EC8, 2004). However, despite these modifications, design verifications for the complete structure remain the same as those for the bare frame (Fardis, 2009).

In EC8 (2004) there are two performance requirements that the structure must follow in order to ensure good behavior in the case of an earthquake: the requirement of no occurrence of collapse and the requirement of damage limitation.

The non-collapse requirement mandates that the structure maintain its structural integrity without exhausting its resistant capacity, both locally and globally, even after an earthquake event. The ultimate limit states compliance is directly related to this requirement, ensuring the safety of occupants and property associated with the structure.

On the other hand, the damage limitation requirement mandates that the structure be designed and built to resist a seismic action that has a higher probability of occurrence than the design seismic action, without damage or limitations on use. The costs associated with the damage or limitations on use should not be disproportionately high compared to the costs of the structure itself (Kaushik et al., 2006). This requirement presupposes the fulfillment of damage limitation states, associated with damage beyond which the structure will not meet certain utilization requirements.

As previously mentioned, masonry-infilled RC frames are considerably stiffer than bare RC frames. Thus, it is expected that in an event of an earthquake, a portion of the total lateral load is resisted by the infill walls in proportion to their lateral stiffness. Therefore, masonry infills, which have a very high

initial stiffness, attract most of the design seismic forces in the cost of prematurely failing as a result of the brittle characteristics of its materials (Kaushik et al., 2006). To address this issue and to maintain the structure's integrity, EC8 (2004) requires that the RC frames are at least capable of resisting 25% of the total design seismic forces in addition to the lateral loads due to vertical loads on the structure.

Infills have doors and windows openings as a result of the buildings' needs, such as ventilation and functionality. Because of a decrease in lateral strength and stiffness, the presence of holes in infills alters the actual behavior of RC frames. In masonry-infilled walls with large openings, it is required that all the edges of the infill panel be bounded to the RC frame. Particularly, if an opening has an area larger than 1.5 m<sup>2</sup>, it is mandatory that the infill wall has vertical RC elements of at least 150 mm in dimension on both sides (EC8, 2004).

To provide a satisfactory performance against any type of loading action, an adequate structural conception is vital. For horizontal loading demands, simple, regular, and redundant resistant systems typically exhibit better response (Furtado et al., 2021). When achieving dynamic independence between structures is not feasible, alternative solutions should be considered, such as incorporating expansion joints. It is crucial to ensure a ductile dissipative behavior that prevents brittle fractures and premature formation of unstable mechanisms. Therefore, EC8 (2004) recognizes that careful placement of infills is important for the effective seismic performance of buildings. Simple and regular geometries are recommended for better seismic performance. However, the use of infills can introduce additional stiffness to the framed structure, and therefore, the location of the infills must be selected with caution to prevent introducing irregularities in the plan of the structure. In contrast, complex structures often present some sort of seismic deficiency related to the detailing and dimensioning of structural members. In buildings, any abrupt changes (whether in plan or in elevation) in stiffness, strength, and mass of elements may lead to greatly different horizontal loading distributions and deformations from those seen in regular structures (Furtado et al., 2021).

In plan irregularities are introduced to the building owing to the asymmetric placement of infills, which increases the shear demand on the structural components, particularly at the columns (Kaushik et al., 2006). According to EC8 (2004), minor in plan irregularities can be accounted by considering accidental eccentricities of the center of mass, which leads to further torsional effects on the structure. Additionally, in modern seismic design, implementing a ductile behavior for the structural components (such as columns and beams) is crucial. Because of this, seismically resistant structures must avoid the brittle failure states. That requires either limiting the shear demand or enhancing the shear strength capacity of the structural elements. Increasing the cross-sectional area of RC components, utilizing high quality concrete, and maintaining a sufficient confinement, all contribute to a better ductile behavior. The major objective is to stop the brittle concrete from crushing before the yielding in the tensile reinforcement begins (Furtado et al., 2021).

Achieving vertical regularity is also crucial as it helps to prevent the formation of sensitive zones that are prone to high stress concentrations and ductility demands, leading to potential structural collapse. Such irregularities may result from the absence of shear walls in certain storeys, which increases the susceptibility in developing soft-story mechanisms. Thus, it is important to avoid big stiffness difference between floors, columns discontinuity, and height variations among the storeys. In the city of Lisbon, particularly, a significant portion of the RC buildings constructed in the 1950's were designed supported by slender columns in order to allow the free circulation of people, garage and commerce at ground storeys, which makes them highly susceptible to soft-storey mechanisms, as depicted in Figure 2.33 (Furtado et al., 2021).

The common mode of failure in buildings susceptible to soft-storey mechanisms is the columns' failure (in shear or in bending), leading to the storey collapse. In some cases, the damage caused by the soft-storey effect can be observed only in specific storeys while the remaining floors of the building remained undamaged (Furtado et al., 2021). For example, Figure 2.34 shows the aftermath of the 2009 L'Aquila earthquake, where the ground floor of the house suffered considerable damage while the upper floors remained intact. Furthermore, short-column mechanisms are also frequently reported as the main cause of RC structures collapses. This failure mode may be mobilized in two circumstances: (i) the existence of columns that are shorter than the rest of the columns in a moment-resistant frame system, as shown in Figure 2.35, either because of the presence of a beam or because the infill panels do not fill the entire column height; (ii) structures built on slopped terrain, which create columns of different lengths at the same storey level, as seen in Figure 2.36.



Fig. 2.33 – Lisbon's Palace of Justice constructed in 1970 (FCG/Biblioteca de Arte)



Fig. 2.34 – Three-storey RC structure in Italy that failed due to soft-storey mechanism (Verdarama, G.)

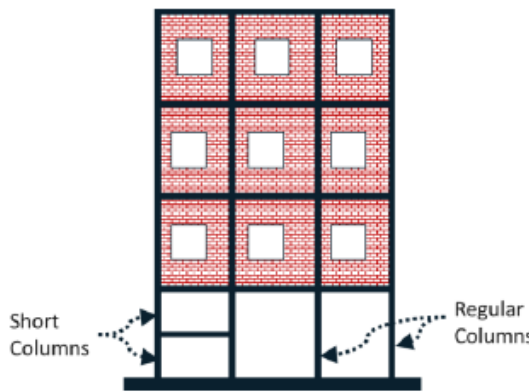


Fig. 2.35 – Short-columns due to beams (Pokharel and Goldsworthy, 2015)

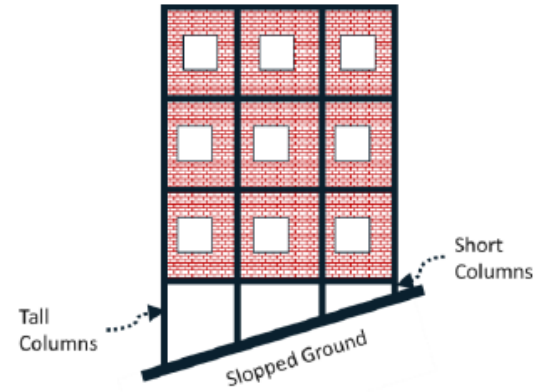


Fig. 2.36 – Short-columns due to sloped terrain (Pokharel and Goldsworthy, 2015)

The building’s natural frequencies depend mainly upon their mass and lateral stiffness, and therefore the stiffness increment due to infills is very significant in the seismic design. This is because the response spectrum, and consequently the design seismic forces, are prescribed in EC8 (2004) in relation to the structure’s natural period of oscillation (Figures 2.37 and 2.38). The amount of infill walls in the first story greatly influences the natural period of the building while their placement in upper stories simply adds mass. Particularly, EC8 (2004) recommends estimating the natural period of the building based on the combined effective area of masonry infills at the first floor.

As previous discussed in subsection 2.2.2. the opening size in infill walls affects the stiffness, and consequently the fundamental period of the whole structure. However, the variation in periods cannot be accurately determined using the formulas provided by seismic design codes (Kaushik et al., 2006). While there is no clear evidence of relationship between opening percentage and fundamental period, studies have shown that the opening does indeed have an influence on the structure's fundamental period (Asteris et al., 2012b; Christiana et al., 2022).

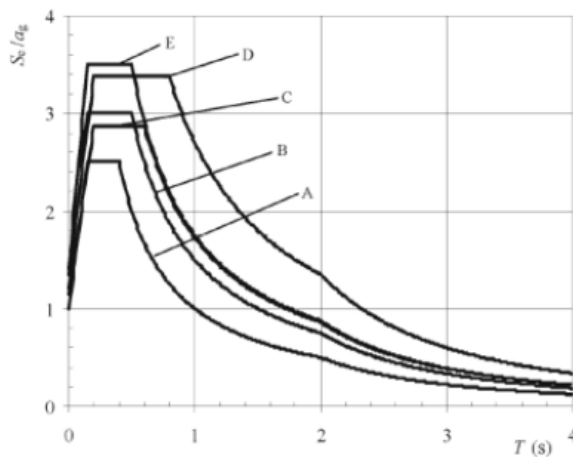


Fig. 2.37 – Elastic response spectrum for type 1 earthquake (EC8, 2004)

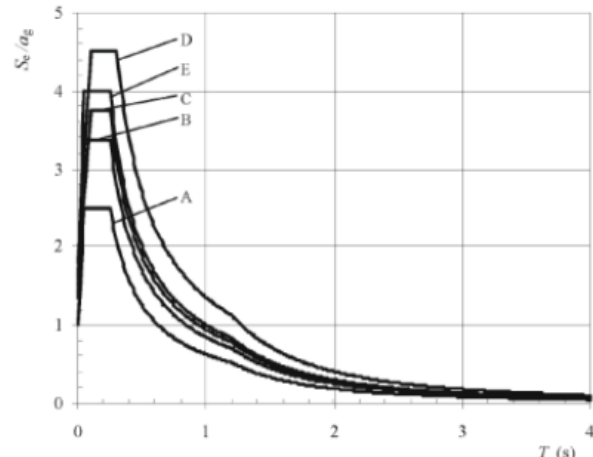


Fig. 2.37 – Elastic response spectrum for type 2 earthquake (EC8, 2004)

The relationship between masonry infill walls and the infilled RC structures behavior during seismic events has been clearly demonstrated by the damage and destruction discussed previously (subsection 2.1.). As a result, it might be assumed that their traditional designation as "non-structural" components is inappropriate. Furthermore, shown by the cracking along the panel edges, the infill panels generally

sustain severe damage during large earthquakes, whereas in minor seismic events the masonry-infilled walls tend to separate from the bounding RC frame. This has been demonstrated by the economic losses and fatalities in recent earthquakes. The high frequency of out-of-plane collapses reported is also one of the primary concerns with masonry infill walls. Since there are no mechanical connections between the infill panels and the RC frame, the walls susceptibility to collapse is higher. In fact, due to the typical high slenderness of infills in existing RC structures, the issue becomes more significant (Furtado et al... 2021).

### **2.3. SEISMIC REHABILITATION OF EXISTING RC STRUCTURES**

Numerous numerical studies and experimental campaigns have been conducted mainly to develop efficient methods for improving the structural response of infilled RC structures, especially in the case of an earthquake event. Owing to the brittle behavior exhibited by masonry materials, the effort put in these methods are mainly focused in improving the behavior of masonry infill walls. Particularly, in the case of external masonry walls, new bricks and new construction techniques are mainly focused in increasing the thermal comfort, owing to concerns regarding cooling costs and heating losses.

Retrofitting and structural behavior enhancement are topics interrelated. It is crucial to take into account this correlated behavior when retrofitting a structure. The primary strategy is the proper integration of masonry infill walls into the superstructure and reinforcement of the wall surface.

It is not feasible to fully assess the building's seismic vulnerability and any potential damage on its components (structural or non-structural) utilizing exclusively the guidelines from seismic codes. Therefore, the process of seismic retrofitting an existing RC structure, typically includes the following three steps (Varum, 2003):

- Complete vulnerability assessment of the structure;
- Seismic retrofitting plan;
- Management and execution of the seismic retrofitting plan.

According to Bertero (1997), buildings can achieve an efficient resistant behavior by carefully selecting their configuration and structural arrangement, and by properly proportioning and detailing their structural and non-structural members. For instance, Fardis (1998) conducted shaking table tests in order to investigate the behavior of a single-bay two-storey square RC framed structure with an irregular configuration of masonry infills. In his study, the input ground motion was applied in both plan directions. The results clearly indicated that the not adequate positioning of the stiff masonry infill walls introduced torsional effects in the structure.

Retrofitting strategies and its implementation should be based on a detailed evaluation of the structure's seismic performance (Varum, 2003). Despite years of extensive research, seismic retrofitting of masonry-infilled RC structures remains a challenging engineering problem that requires unique approaches (Christiana et al., 2022). Fardis (1998) emphasizes that these interventions in the structure should not compromise the safety or strength capacity of any of its components. Therefore, the rehabilitation plan is a crucial stage to take into account by engineers. There is the need of responsibility by the engineers that strengthening a beam does not shift the plastic hinging to the columns, that improving the flexural capacity of an element does not make it critical in shear, and that consequences of retrofitting (improvement of columns' strength capacity and addition of masonry walls or bracing elements) do not concentrate damage in storeys above the retrofitted level (Varum, 2003).

In order to meet modern seismic design codes requirements, a variety of strengthening techniques have been proposed in the literature and have been tested on structures over the years. Therefore, the most

common approaches include: (i) fiber-reinforced polymers (FRP); (ii) fiber-reinforced cementitious matrixes (FRCM); (iii) engineered cementitious composites (ECC); (iv) textile-reinforced mortar (TRM); and (v) bed joint reinforcement. It is important to note that these retrofitting methods integrate the masonry infill wall in the structure, improve its associated behavior, and reduce the out-of-plane vulnerability of the infill. The use of TRM composite materials has gained a lot of attention lately, this is due to the fact that it introduces innovative sustainable materials. TRM is a combination of inorganic matrix, either cement- or lime-based, with non-corrosive multi-axial textile fabrics (Christiana et al., 2022).

According to the National Research Council (CNR-DT 215/2018) (2018), the application of these reinforcing materials on RC structures can be done by several ways: (i) flexural strengthening of beams and columns; (ii) shear strengthening of beams and columns; (iii) confinement of columns; (iv) strengthening of beam-column joints; (v) shear strengthening of infill walls; and (vi) strengthening of infill walls against overturning. Figure 2.40 depicts most of the fabric-reinforced materials applications herein listed.

The reinforcement methods which use fabric materials can be continuous (with each fabric sheet being applied adjacent to the prior one) or discontinuous (with the strengthening strips spaced out between empty spaces). Structural elements (columns and beams) can also be strengthened by being entirely wrapped across their cross-section. On the other hand, the connection of infills to the bounding frame by using reinforcing grids along with anchors, can securely fasten the infill panel to the structure (CNR, 2018).



Fig. 2.40 – Fabric strengthening system applications (Drizoro construction products)

Sagar et al. (2019) evaluated the in-plane (statically) and the out-of-plane (dynamically) behavior of URM and FRCM reinforced masonry infill walls. Two different anchorage systems were used (A – anchored or U – unanchored), along with two methods of applying the fiber-reinforced material (D – direct or S – sandwich). The ‘direct’ application consists of applying the FRCM directly to the infill’s surface and coating it with an external cement-based mortar layer (Figure 2.41a). On the contrary, in the ‘sandwich’ method, the FRCM is placed between two cement-based mortar layers of 2 mm and 4 mm thickness (Figure 2.41b). From the testing campaign, the authors concluded that the ‘direct’ method was more effective than the ‘sandwich’ one, owing mainly to the efficiency in reinforcing the panel rather

than adding strength to the mortar layer. Oblique fabric orientation (in relation to bed joints) was found to be less efficient than orthogonal orientation, mainly because it caused the fabric to overstress at an earlier stage, resulting in fabric tearing. Moreover, the authors observed that the ‘direct’ method permitted the specimen to withstand higher in-plane drift levels (drifts up to 2.75%), without major degradation of its in-plane strength. Further, the tensile capacity of the FRCM system was better exploited due to the presence of anchors, which limited the frame-infill separation, resulting in a cracking pattern uniformly distributed and a better out-of-plane behavior. Thus, the anchored specimens exhibited a strength degradation factor of up to 90% higher than the unanchored counterparts, indicating greater residual strength at the final stage of the bi-directional test. Particularly, the anchored FRCM specimens dissipated energy at a rate that was approximately three times that of the infills in unanchored specimens. As expected, the strengthened specimens had enhanced in-plane behavior than the unreinforced ones, leading to late formation of shear-sliding cracks at drift levels approximately 50% higher. The FRCM strengthened specimens exhibited better load distribution between the infill and the bounding RC frame, thereby avoiding the frame-infill separation and the concentration of stress in the corners of the infill panels and columns ends. The URM infills developed shear cracks at the corners of the infill panels and at the ends of the columns, leading to an abrupt drop in the in-plane strength. In contrast, the FRCM strengthened infill panels developed shear cracks halfway up the columns and the infills remained in contact with the RC frame. As a result, the FRCM reinforced specimens showed better out-of-plane stability and structural integrity, because of their better connection at the frame-infill interface.

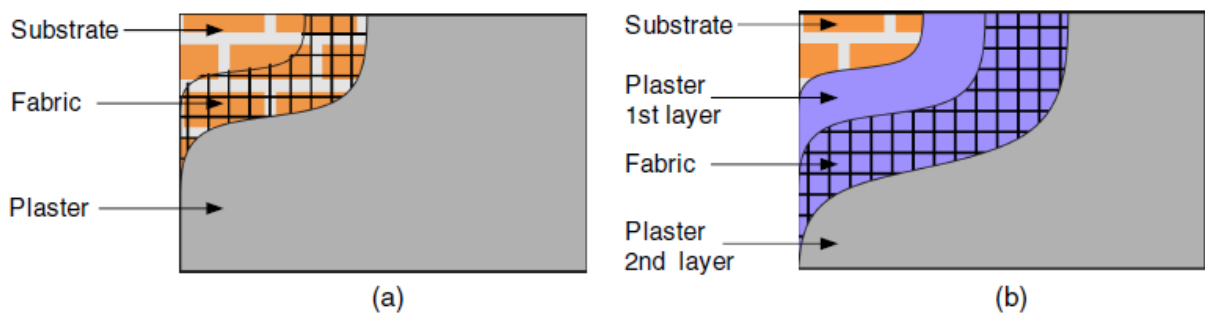


Fig. 2.41 – Fabric application: (a) direct; (b) sandwich (Sagar et al., 2019)

## 3

## BRIEF OVERVIEW OF THE EXPERIMENTAL CAMPAIGN

### 3.1. INTRODUCTION

The contents of this chapter detail the experimental campaign conducted at the EUROCENTRE research center, which were primarily derived from the technical report developed by Bussini et al. (2020) and provided by ISAAC, serving as the foundation for the information presented after.

The design standards and building techniques that are applicable to RC buildings have changed significantly during the past few decades. Within the building stock of Italian RC structures, Table 3.1 categorizes RC framed buildings into five different groups based on the date of construction, design strategy, and some construction characteristics (Gesualdi et al., 2020). According to the authors, they can be classified accordingly to the following:

- Buildings designed only for vertical loads (DVL);
- Buildings with deficient structural design (DSD);
- Buildings with poor earthquake design (PED);
- Buildings with good earthquake design (GED)
- Buildings with contemporary earthquake design (CED).

In many other countries and regions, it can be found similarities in terms of the evolution of design strategies and construction practices.

Table 3.1 – Italian RC structures categorization (adapted from Gesualdi et al., 2020)

Class	Date of Construction	Design Strategy	Characteristics
DVL	Before 1971	Only vertical loads	Double leaf infills
			Poor quality concrete Plain rebars
DSD	1971 – 1980	Equivalent loads	Double leaf infills Poor quality concrete Ribbed rebars
PED	1981 – 1995	Equivalent loads	Single leaf infills

			Poor quality concrete
			Ribbed rebars
			Single leaf infills
GED	1995 – 2003	Response Spectrum	Ribbed rebars
			Not mandatory ductile detailing
			Single leaf infills
CED	After 2003	Response Spectrum	Ribbed rebars
			Mandatory ductile detailing

This chapter is dedicated to presenting the case study of a three-story RC building with masonry infills, classified as CED, representative of the design and constructions practices in southern European regions, and covers a reasonable range of the current new building stock in Italy. As discussed in Chapter 2, it is recognized that masonry infill walls constitute a crucial factor for the building's seismic response and, in certain conditions, they can contribute to the development of well-known fragile mechanisms, as the soft-storey and the short-column mechanisms, which may result on the collapse of buildings.

In the next section are, described the experimental campaign developed at the shaking table facility of EUCENTRE in Pavia, Italy, namely it is presented: (i) the specimen dimensions, materials and details; (ii) the instrumentation layout; (iii) the results of the dynamic identification; (iv) the seismic input signals adopted; and (v) a brief description of the response.

### 3.2. DESCRIPTION OF THE SPECIMEN STRUCTURE

The unidirectional shaking table tests were conducted on two identical full-scale RC frames, constructed with the same materials, detailing and methods. The need of two specimens is due to the fact that the experimental campaign was focused on the performance assessment of an active seismic damping system (Figure 3.1). Simultaneous simulation of both specimens allowed the researchers to precisely evaluate the efficiency of the active seismic damping system. This complex hydraulic system was installed on the top storey of one of the RC specimens. Both structures were mounted on the shaking table allowing to impose the same base excitation on both structures. To ensure accurate measurements, a safety steel frame was constructed inside of each structure, and being independent of the RC structure.



Fig. 3.1 – Active Seismic Damping System (ISAAC technical report, (2020))

For the purpose of this master's thesis, in accordance with its objectives, in the next sections will only be represented the aspects related to the building without the active seismic control system.

The specimen consists of two parallel single-bay three-storey masonry-infilled RC frames, connected by transversal beams and slabs, as shown in Figure 3.2. The total height of the building is 8.7 m, with a useful inter-storey height of 2.5 m. In the construction, standard materials commonly employed were used, namely: concrete, steel reinforcement, hollow clay brick units, and mortar in the bed joint and plasters. Additionally, in the transversal direction ( $x$ ), "X" type bracing systems are installed at each storey and extremity of the structure, with cylindrical steel rods of 10 mm diameter.



Fig. 3.2 – Specimen RC frame building (ISAAC technical report, (2020))

The C30/37 class of concrete, accordingly to EC2, along with B450C steel reinforcement were used in the construction of all RC members, columns, beams and slabs.

The structure has a rectangular plan shape with dimensions at columns axes  $2.1 \times 5.0 \text{ m}^2$ , see Figure 3.3. Four uninterrupted square columns from the base to the top of the structure were built, with a cross-section with  $200 \times 200 \text{ mm}^2$ . These columns were reinforced with four longitudinal steel rebars, one on each corner, with a diameter of 16 mm (Figure 3.4). Stirrups spaced 10 mm apart were adopted along all the column's length, except on critical regions (1<sup>st</sup> floor slab joints), where up to a distance of 350 mm of the joint, 5 mm spacing was adopted in order to ensure the required ductility and to prevent local buckling of the longitudinal bars.

The slabs are 400 mm thick and have top- and bottom-reinforcement done with steel rebars of 14 mm in diameter, in both horizontal directions. Thus, it can be considered that the slabs work as rigid diaphragms, because they comply with the requirements of EC8 (2004) (having a thickness greater than 70 mm and being reinforced in both directions with at least the minimum reinforcement specified in EC2 (2004)).

The masonry infill panels were built in the bays oriented in the y-direction, after the curing of the concrete of the RC frame. The masonry infills have a thickness equal to 80 mm and are constructed using 250 x 250 mm<sup>2</sup> hollow clay bricks placed with holes horizontally oriented (approximately 55% of void percentage), as illustrated in Figure 3.5. The brick units are connected using 10 mm thick joints made of class M5 mortar.

To ensure the stability and integrity of the infilled RC structures during testing and transportation, a stiff foundation was constructed. This foundation, made of a thick continuous slab with a width of 400 mm, was connected to the shaking table.

For more detailed information regarding the specific detailing of the RC members and other dimensions of the structure, readers are encouraged to refer to ISAAC technical report (2020) and Appendix A1.

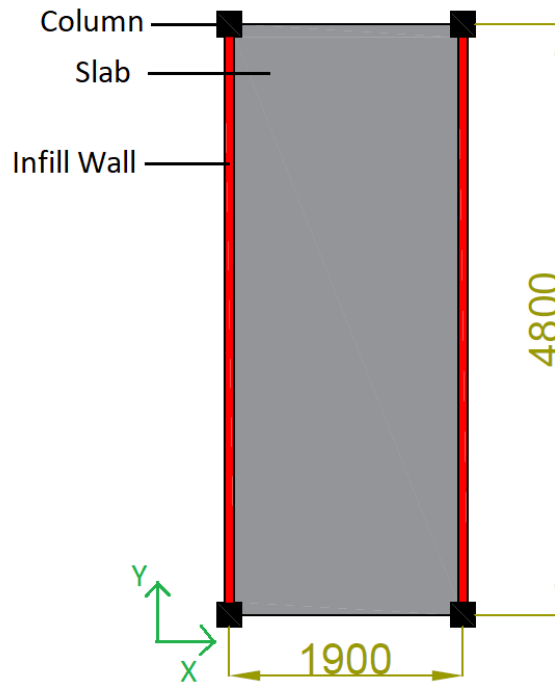


Fig. 3.3 – Structure Plan Configuration [mm]

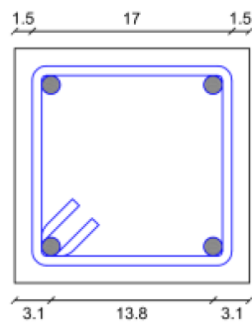


Fig. 3.4 – Columns' Cross-Section [cm]



Fig. 3.5 –Brick units

### 3.3. INSTRUMENTATION: SENSORS AND LAYOUT

Both infilled RC structures were extensively instrumented. For the shaking table test conducted at the EUCENTRE research center in Pavia, Italy, the following sensors were employed to monitor the dynamic behavior of the masonry-infilled RC frame and the shaking table:

- 2 accelerometers in the shaking table: one uniaxial in the y direction and the other biaxial (x and y);
- 18 accelerometers, 9 on each of buildings (three per floor).

The first group of sensors corresponds to the accelerometers installed in the shaking table and in the foundation (building base) to record the input as well as excitation at the building base (Figure 3.6). The remaining accelerometers were placed in opposite corners (triaxial sensors) and at the center (biaxial sensors) of each slab. The location of the accelerometers at each floor level is shown in Figure 3.7. This arrangement intended for monitoring the global response of the building, capturing the translational and torsional behavior.

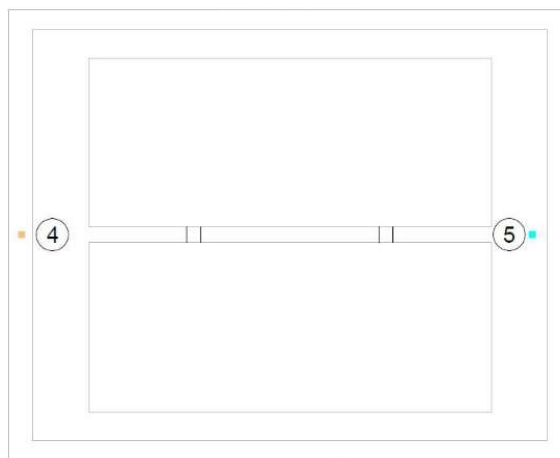
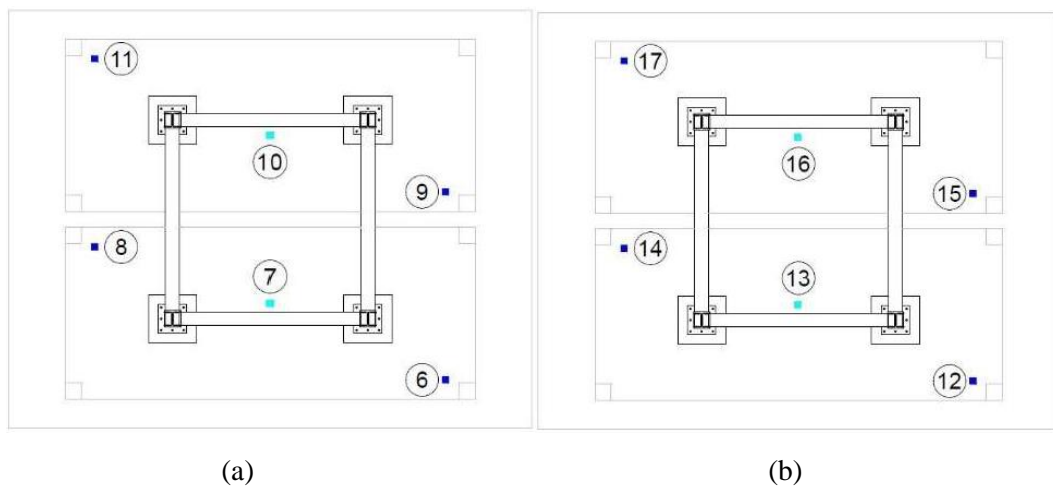
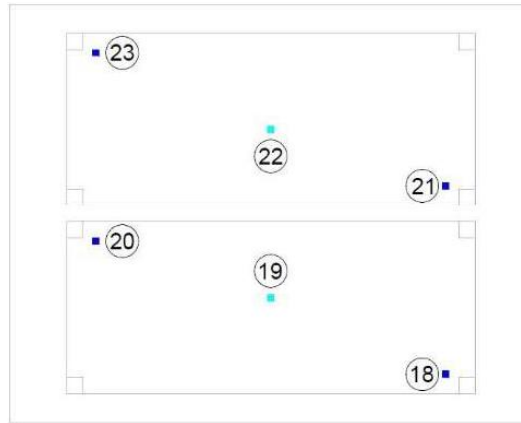


Fig. 3.6 – Accelerometers placed at the shaking table and building base: (4) Uniaxial; (5) Biaxial (ISAAC technical report, (2020))





(c)

Fig. 3.7 – Accelerometers in the structures under study (9, 11, 15, 17, 21, 23 – Triaxial / 10, 16, 22 – Biaxial): (a) 1<sup>st</sup> Floor; (b) 2<sup>nd</sup> Floor; (c) 3<sup>rd</sup> Floor (ISAAC technical report, (2020))

The measurements obtained by these low electrical noise analog accelerometric sensors are essential to the continuous acquisition and processing in real time of the data for monitoring the building seismic response.

Figure 3.8 illustrate an installation example of the accelerometers utilized to monitor the structural behavior under seismic actions and to monitor the integrity of the building.



Fig. 3.8 – Accelerometers installed at the floors (Extrados and Intrados) (ISAAC technical report, (2020))

Moreover, the structure was also equipped with wired displacement sensors to measure the relative displacements on each floor in real time. However, this data is not used in the work conducted in this thesis. Those sensors measure the relative displacement between the safety steel frame structure (idealized as infinitely rigid) and the floor slabs, as illustrated in Figures 3.9 and 3.10. It is important to emphasize that the steel frame does not interact with the RC building, and it was conceived as a control structure.



Fig. 3.9 – Wired Displacement Sensor at the 1<sup>st</sup> Floor (ISAAC technical report, (2020))



Fig. 3.10 – Wired Displacement Sensors at the 2<sup>nd</sup> Floor (ISAAC technical report, (2020))

### 3.4. PRELIMINARY DYNAMIC ANALYSIS

Once the construction of the three-story masonry-infilled RC building was concluded, it was subjected to a preliminary dynamic analysis (Modal Analysis) to identify modal parameters of interest, such as natural frequencies, damping coefficients and modes of vibration. It is essential to have a comprehensive understanding of these parameters as they play a crucial role in the calibration of the analytical structural model that will be to predict the non-linear dynamic response of the building, via simulations. This sequence of tests provide valuable insights into understanding of the behavior of this type of structures under different seismic conditions, allowing engineers to identify most likely failure mechanisms and to support the definition of strengthening measures to retrofit them. Therefore, a thorough knowledge of these parameters is critical for ensuring the safety and resilience of the RC buildings.

The modal analysis was executed by installing piezoelectric accelerometers at the nodes of the structure (Figure 3.11) and exciting it by a 1.5 kilograms vibrator at the top floor (Figure 3.12). The output results are summarized in Table 3.2, and the mode shapes are illustrated in Figure 3.13.



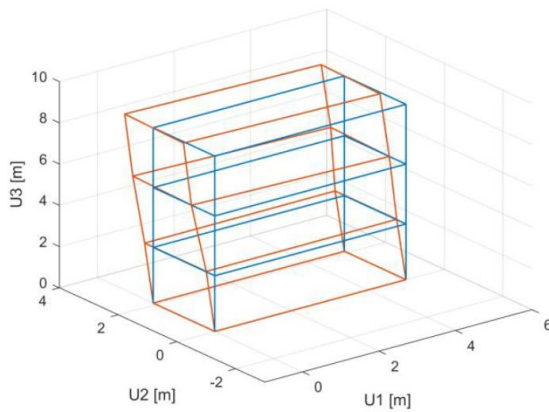
Fig. 3.11 – Piezoelectric accelerometer to measure the floors' acceleration (ISAAC technical report,



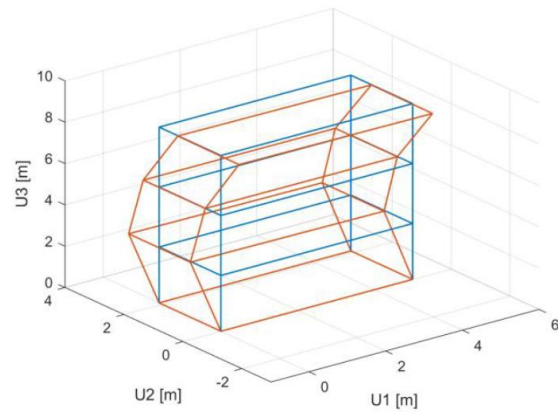
Fig. 3.12 – The 1.5 kg Vibrator at the highest floor (ISAAC technical report, (2020))

Table 3.2 – Experimental modal parameters obtained

Mode of Vibration	Frequency [Hz]	Damping [%]
1	1.84	0.68
2	5.84	0.66
3	6.68	0.71
4	8.39	0.91
5	9.09	0.56
6	29.91	0.73



Modo frequenza 1,84 Hz



Modo frequenza 5,84 Hz

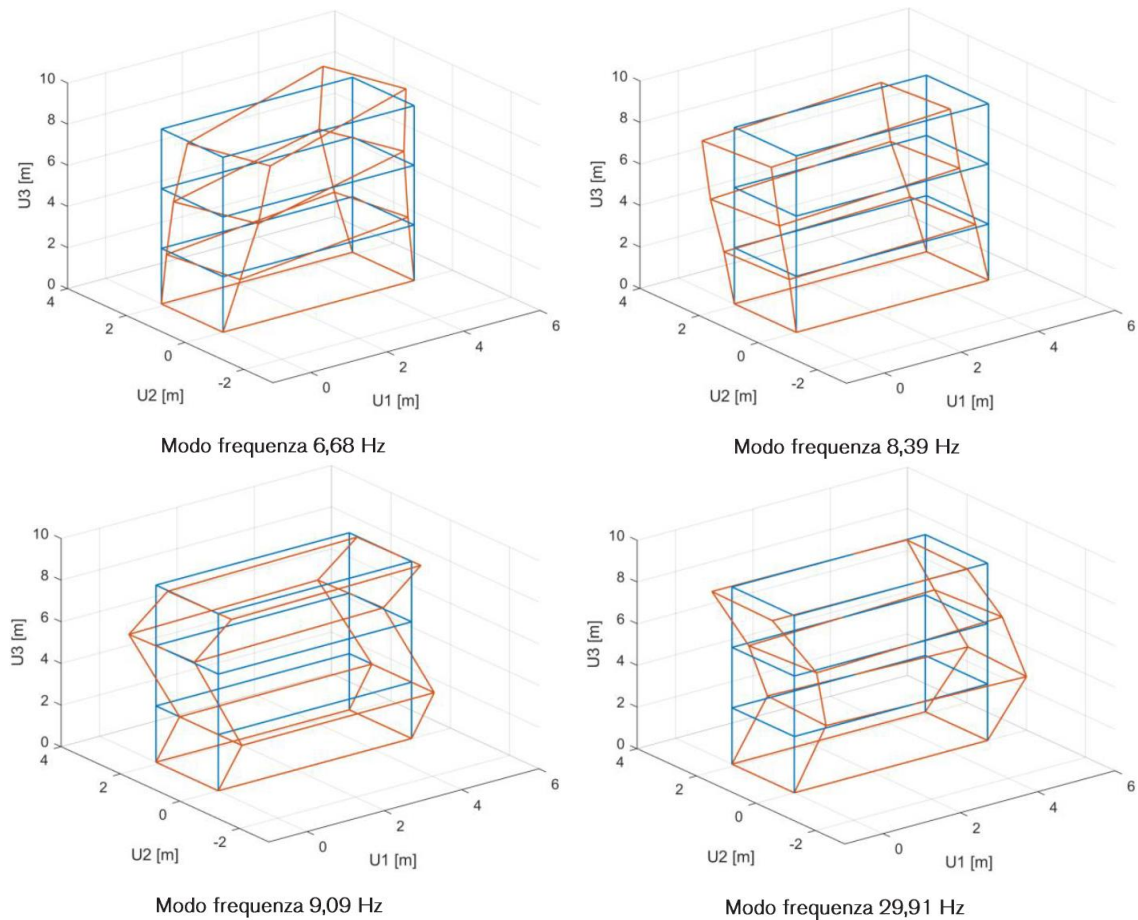


Fig. 3.13 – Experimentally obtained modes of vibration (ISAAC technical report, (2020))

It is noteworthy that indeed the 1<sup>st</sup> and 2<sup>nd</sup> modes, which correspond to two translational modes in the  $x$  direction (corresponding to the direction of the building without masonry infill walls), demonstrate substantially lower natural frequencies in comparison to the 4<sup>th</sup> and 6<sup>th</sup> modes, respectively, which represent the translational modes in the  $y$  direction (direction of the masonry infill walls). It is recalled that the  $y$  direction corresponds to the direction of the ground motion input, therefore it constitutes the direction of particular interest for this study. The 3<sup>rd</sup> mode corresponds to a torsional mode.

### 3.5. THE NOVEMBER 23<sup>RD</sup>, 1980, IRPINIA EARTHQUAKE, ITALY

The Irpinia earthquake, named by the region in Southern Italy where it occurred, took place on November 23, 1980, with the main shock striking at 18:34 UTC (19:34 local time). The epicenter was located near the village of Castelnuovo di Conza in Campania (Del Gaudio et al., 2020). Following the initial earthquake, a total of 90 aftershocks were recorded, three of which reached a significant intensity of 9<sup>th</sup> degree on the Mercalli scale. These aftershocks had epicenters located in distinct regions. The largest shock during the sequence recorded a peak ground acceleration (PGA) of 0.32g (ISAAC technical report, (2020)). Figure 3.14 shows the Italian map in terms of moments of magnitude of the recent earthquake events striking the country. It is evident that the Irpinia was undoubtedly the most devastating one.

The impact of the earthquake on buildings in the affected area varied depending on their construction type. Only a small percentage of the affected buildings (10%, or 3953) were constructed using RC

systems, primarily built before the 1970s. The majority of the affected buildings (79%, or 30033) were constructed using masonry (Del Gaudio et al., 2020). Among the 3953 RC buildings, only 2626 were located in municipalities with a PGA of 0.06 g or higher. Buildings constructed prior to the introduction of seismic classification were designed only for vertical loads (DVL), while buildings constructed after the introduction of seismic classification were designed considering seismic actions (DSD). Figure 3.15 shows the severity level of destruction caused by the earthquake. The Irpinia database reveals that most of the 41 affected municipalities were not classified as seismic regions until the 1980 earthquake. Consequently, out of the 2626 RC buildings, 2163 were categorized as DVL, while the remaining 463 were situated in one of the nine municipalities classified as seismic areas in 1915 or 1935 (Del Gaudio et al., 2020). Unfortunately, further information regarding the construction period and type of structural system adopted for the buildings in Irpinia is not available.

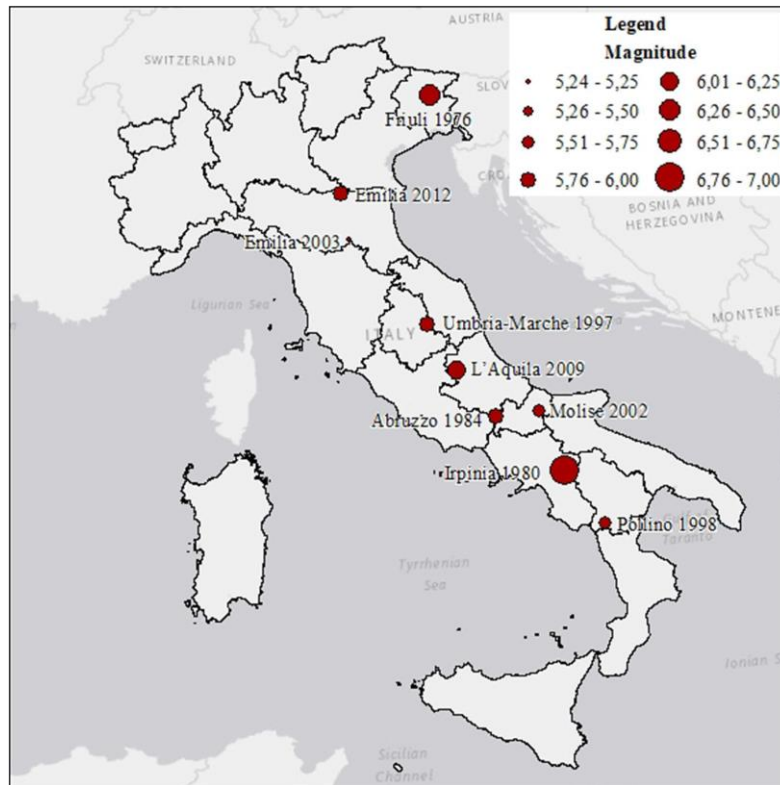


Fig. 3.14 – Recent seismic events in Italy (Del Gaudio et al., 2020)



Fig. 3.15 – One of the cities after the earthquake, 1980 (Di Fabiana Bianchi)

In the case of the building under study, assuming that it is located in Irpinia, it is worth noting that the region is mountainous, with most villages situated on stiff soil categorized as soil type B according to the current Italian code and EC8 classification. Following the strong earthquake of 1980, Castelnuovo di Conza and, therefore, the Irpinia region were designated as seismic-prone areas for the first time. The region falls under seismic class 1, indicating a high level of seismic hazard, with earthquakes having PGA values above 0.25 g. In contrast, the city of L'Aquila has an intermediate level of seismic hazard and, for the first time in 1915, L'Aquila was categorized as seismic class 2. Currently, Italy's seismic risk map identifies Castelnuovo di Conza as one of the most active cities in terms of earthquakes and the design earthquake intensity level is 0.35 g with a 475-year return period, and 0.47 g for a 2475-year return period, according to EC8 for ground type C.

### 3.6. SHAKING-TABLE EXPERIMENTAL CAMPAIGN

The input seismic motions were carefully selected to closely represent the characteristics of the 1980 Irpinia earthquake scenario. The infilled RC frame was subjected to increasing intensity seismic excitations applied at its base, along the y direction (longitudinal) only. These input ground motions are scaled representations of the original earthquake event ground acceleration and are labelled as presented in Table 3.3. The seismic inputs comprise a set of acceleration time series, with a duration of approximately 32 seconds each. A total of twelve acceleration time histories (accelerograms) were artificially generated with a time step of 0.01 seconds.

Figure 3.16 shows the accelerogram which was scaled and used as a reference to the ground motion inputs. The seismic excitations performed at the laboratory were generated by multiplying the earthquake time history by a scale factor, each earthquake intensity was successively applied, ranging from 10% of the original seismic event to over 100%.

Table 3.3 – Input ground motions

Name	PGA [g]
COMP_01	0.04

COMP_02	0.06
COMP_03	0.09
COMP_04	0.08
COMP_05	0.12
COMP_06	0.14
COMP_07	0.21
COMP_08	0.18
COMP_09	0.24
COMP_10	0.30
COMP_11	0.32
COMP_19	0.44

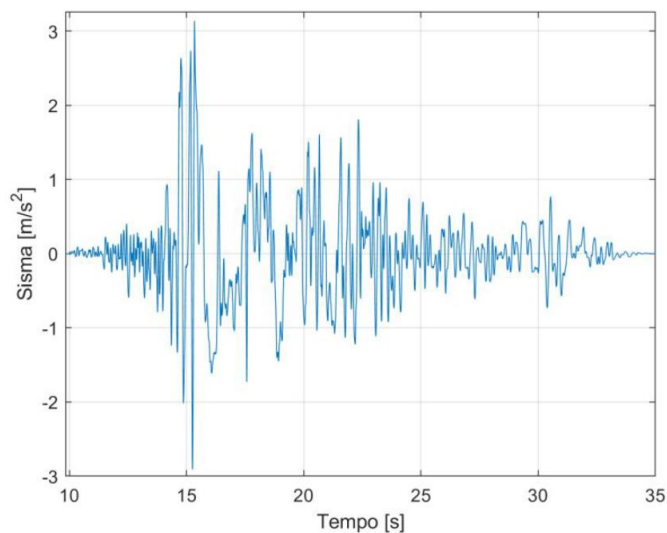


Fig. 3.16 – Reference acceleration time history: Irpinia, 1980 (ISAAC technical report (2020))

The complete time history of input ground motion generated in the shaking table is best illustrated in Figure 3.17. The series of tests was stopped when the RC structure started evidencing the development of potential failure mechanism, avoiding the full collapse and therefore potential damages in the laboratory equipment.

The ISAAC technical report (2020) describes only the significant tests for the assessment of the active seismic damping system effectiveness. Therefore, in the next, only the most relevant seismic excitations will be described.

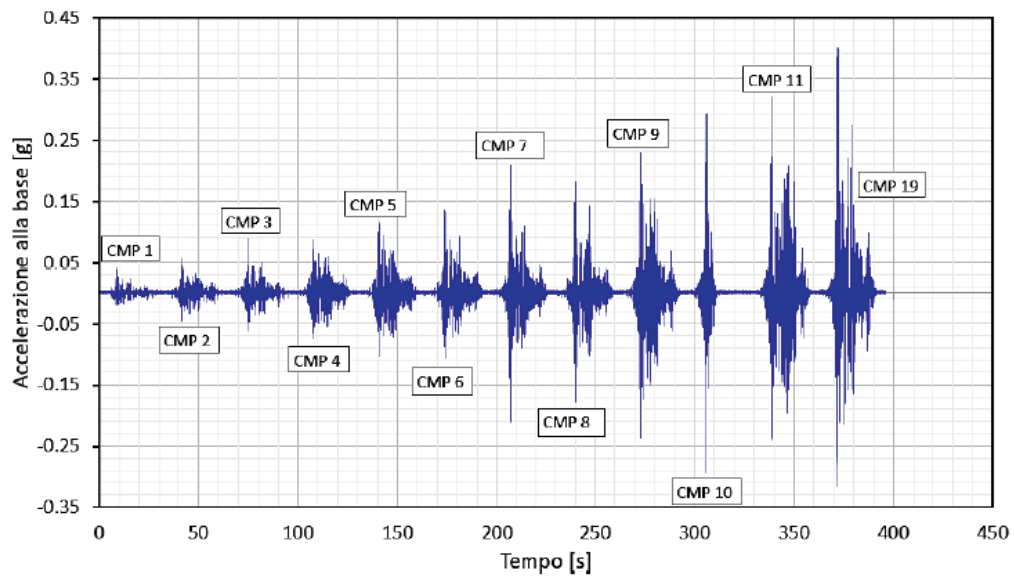


Fig. 3.17 – Complete time history of input earthquakes (ISAAC technical report (2020))

### 3.6.1. EARTHQUAKE WITH A PGA OF 0.24 G

Figure 3.18 illustrate the time history of the acceleration measured at the base of the structure during the PGA 0.24 g test. Figures 3.19 and 3.20 show the damages in the masonry-infilled RC structure, exposing the significant cracks on the non-structural elements (e.g., infills) along the compressed diagonal. Moreover, the detachment of a portion of the masonry plaster and crushing of the masonry at the infill corner, associated to the compression, can be observed. In Table 3.4 it is reported the global results in terms of maximum horizontal displacement (relatively to the base of the structure) per floor, as well as the corresponding maximum inter-storey drifts.

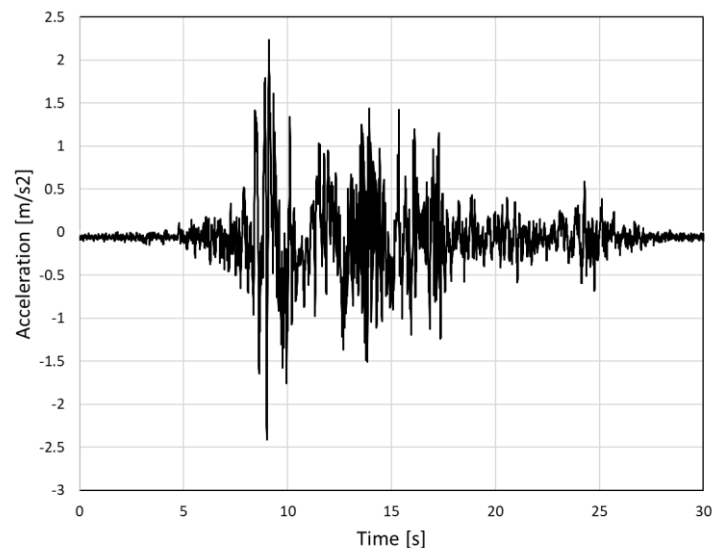


Fig. 3.18 – Acceleration measured at the shaking table along the y direction



Fig. 3.19 – Cracks along the infill wall main diagonal (ISAAC technical report, 2020)



Fig. 3.20 – Crushing at the infill wall corner (ISAAC technical report, 2020)

Table 3.4 – PGA 0.24 g Results: Maximum storey lateral displacement and maximum inter-storey drift

Storey	Maximum lateral displacement [mm]	Maximum inter-storey drift [mm]
1 <sup>st</sup> Storey	6.04	6.04
2 <sup>nd</sup> Storey	10.58	4.54
3 <sup>rd</sup> Storey	13.36	2.80

### 3.6.2. EARTHQUAKE WITH A PGA OF 0.44 G

In this earthquake intensity several portions of the non-structural elements that were already damaged by previous seismic excitation experienced partial collapses. In Table 3.5 it is reported the global results in terms of maximum horizontal displacement (relatively to the base of the structure) per floor, as well as the corresponding inter-storey drifts. Particularly, the severely affected areas were the corners of the openings that intersect either the main diagonal or the corner of the infill wall. The partial collapse of these bottom and upper wall portions was dominated by sliding along the bed joints. At the same time, shear cracks appear at the top of columns in the region which comes into contact with the compressed diagonal. Then plastic hinges can be seen developing at the top and the bottom of the columns, while flexural cracks appear in the external phases of the columns, because the tensile columns were braced by the bottom segment of the wall. Therefore, the building exhibited minor yet noteworthy cracks on the structural elements, especially at the intersections of the columns and the slabs on the 1<sup>st</sup> storey, this is best illustrated in Figure 3.23.

Table 3.5 – PGA 0.44 g Results: Maximum storey lateral displacement and maximum inter-storey drift

Storey	Maximum lateral displacement [mm]	Maximum inter-storey drift [mm]
1 <sup>st</sup> Storey	22.48	22.48

2 <sup>nd</sup> Storey	29.13	7.90
3 <sup>rd</sup> Storey	31.64	3.44

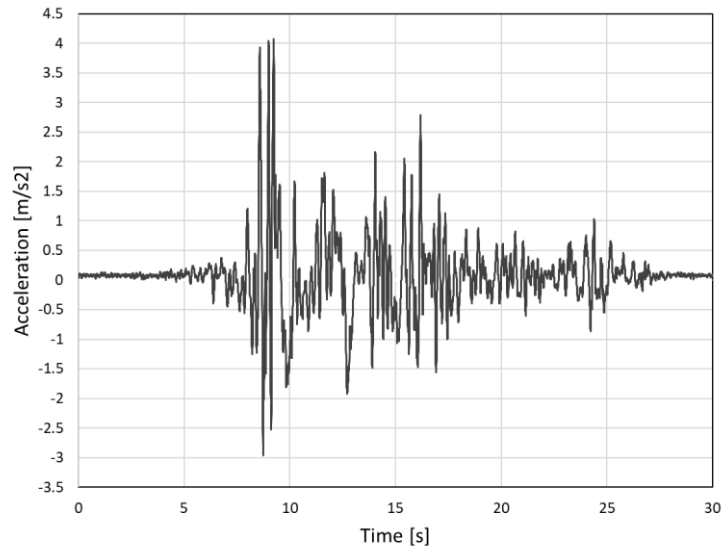


Fig. 3.21 – Acceleration measured at the shaking table along the y direction



Fig. 3.22 – Partial collapse of the infill opening (ISAAC technical report, 2020)



Fig. 3.23 – Observed cracks at the slab joints (ISAAC technical report, 2020)



# 4

## NUMERICAL MODELLING OF THE SPECIMEN STRUCTURE

### 4.1. FINITE ELEMENT MODELING REVIEW

#### 4.1.1. INTRODUCTION

Due to the complexities, limitations, uncertainties, and high expenses associated with experimental testing of full-scale RC structural forms, nonlinear finite element analysis has emerged as a popular and practical alternative. This numerical method offers a detailed description of the effects of various structural and non-structural elements, including infill walls, on the seismic response of masonry-infilled RC structures. In addition, it enables researchers to investigate complex structural forms beyond the simplistic case study framed structure.

Nonlinear finite element analysis is a powerful numerical technique that can simulate and analyze complex structural behavior under different loading conditions. By dividing the structure into a finite number of elements and solving the equations that describe the mechanical response of each element, it provides a better understanding of the global behavior of the structure. Furthermore, the FE method allows for the examination of various parameters that cannot be easily controlled in experimental testing, such as boundary conditions, material properties, and loading conditions. Therefore, the use of a finite element modeling (FEM) has significantly contributed to the development of safer and more efficient structural designs.

The major factors that influence the nonlinear response of infilled RC frames is due to the nonlinearity of the material. Specifically, nonlinearities related to the masonry infill panel (cracking, strength and stiffness degradation), to the frame-infill contact surface (variation of the contact length) and to the RC frame (yielding of reinforcement bars and development plastic hinges in the columns) (Crisafulli, 1997).

Thus, the aim of this section is to provide a thorough analysis of the most used numerical modeling approaches for the different comprising materials of masonry-infilled RC framed structures. In order to idealize this structural type, different modelling techniques in the literature are here presented, compared and discussed.

#### 4.1.2. MASONRY INFILLS MODELLING APPROACHES

Masonry-infilled panels have received significant attention in recent decades due to their widespread applications. This heterogeneous material provides thermal and acoustic isolation and is commonly used as internal and external partitions. However, developing phenomenological constitutive equations for such materials remains a challenge.

During seismic events, infill panels experience in-plane and out-of-plane lateral forces that are transmitted through the frame-infill interface (Bouarroudj and Boudaoud, 2022). Additionally, these forces play a crucial role in determining different failure modes of masonry infill panels. The consideration of the infill wall during analysis and design stages presents a modeling challenge due to the presence of numerous interacting parameters. This challenge is due to the fact that there are different possible failure modes that need to be evaluated with a high degree of uncertainty (Astari et al., 2013b).

Mehrabi et al. (1996) identified five different modes of failure that can be observed in infills. The failure modes mentioned by the author are primarily related to the in-plane behavior. It is crucial for the infill walls to withstand the out-of-plane seismic forces to ensure their load-carrying capacity. The collapse of infill walls under out-of-plane loads is a critical limit state for the safety of the building occupants. Approximately 80% of the human and property losses on the aftermath of an earthquake in RC buildings are directly related to damage in masonry infills (Cardone and Perrone, 2016). Moreover, the effect of masonry infills on the structure is strongly influenced by various factors, such as the presence of openings, frame-infill interaction, the type of mortar and brick units, among others (Fardis, 2009; Bouarroudj and Boudaoud, 2022). The infill panel aspect ratio, in particular, has the greatest impact on the global behavior of the infill wall, because it impacts the contact surface length between the confining RC frame and the infill wall, as well as the angle of inclination of the strut mechanism.

In modern constructions, RC frames are designed to ensure an overall dissipative and ductile behavior, and the infills are typically thick and comprised by a single-leaf, making it easier to control the out-of-plane loads. According to Angel (1994), infill panels with high slenderness ratios can experience up to a 50% reduction in their out-of-plane strength due to previous in-plane damage.

Since the mid-1950's, several experimental and numerical studies have been conducted for the analysis and model development of infilled RC frames to study and better understand their effect on the global behavior of RC framed structures. These structures notably exhibit a highly nonlinear inelastic behavior, introducing analytical complexities due to nonlinear effects (Crisafulli, 1997). Owing to the fact that these experimental campaigns have inherent high costs, as a result, a variety of numerical methods have been developed. These numerical methods are crucial for the seismic evaluation and rehabilitation of existing RC buildings.

Choosing the most appropriate numerical models for the design and evaluation of masonry infill panels presents considerable challenges. Typically, these models are developed and calibrated based on a specific set of experimental pseudo-static tests, however, the specimens are rarely comparable (Mucedero et al., 2020).

To better understand the approach and capabilities of each model, it may be useful to divide them into three categories: macro-, micro- and meso-modeling approaches (Bouarroudj and Boudaoud, 2022), based on their complexity, the level of detail by which they model an infill wall, and the information they provide the engineer about the behavior of the structure.

#### 4.1.2.1. Micro-modelling

According to Petracca et al. (2017), microstructural effects (localization of deformation and damage-induced anisotropy in the micro-structure), have a significant influence on the evolving response of the structure. However, accounting for the way in which the microstructure affects the overall macroscopic behavior can be challenging, especially when strain localization leads to complex dissipative mechanisms at the structural scale.

The fracturing of masonry infills under tension or shear mainly occurs at the brick-mortar interface, as observed in prior experimental findings discussed in Chapter 2. Micro-modeling methods aim to capture the localized behavior of infills, including crack patterns, failure mechanisms, and ultimate loads, providing accurate characterizations of their structural response. This is achieved by dividing the infills into multiple components and modelling them as separate elements.

In the study conducted by Liauw and Kwan (1984), triangular plane stress elements were employed to effectively model the infill panel. The material characteristics were idealized as follows: linear elastic brittleness in tension, isotropy before cracking, and anisotropy after cracking. The panel's response to compression was assumed to exhibit significant non-linearity in the stress-strain relationship. In a more recent development, Asteris (2003) utilized a four-node isoparametric rectangular FE model with eight DOFs to model and analyze the influence of openings on the behavior of infill walls. The anisotropic finite element stiffness matrix was derived analytically through integration over the element's area, providing a comprehensive representation of the panel's behavior. Later, Stavridis and Shing (2009) employed a smeared-crack model initially developed by Lotfi and Shing (1991). They employed two rectangular continuum elements to represent the brick units, interconnected by a vertical interface element. This approach ensured the capability of describing the tensile splitting of the masonry unit and its relative sliding upon cracking.

Two strategies can be employed, see Figure 4.1: (i) detailed micro-modelling, in which the units, mortar joints, and unit-mortar interfaces are modeled separately; and (ii) simplified micro-modeling, in which the units are modeled using continuum FEs and the mortar characteristics along with its interaction to the units are lumped into a single element (Bouarroudj and Boudaoud, 2022). However, a smeared-crack model cannot capture the shear sliding failure of the mortar joint due to the kinematic constraint introduced by the continuum approach, leading to a stress-locking issue (Lotfi and Shing, 1991). Thus, in detailed micro-modeling, the brick units and mortar joints are discretized using smeared-crack (continuum) elements and the brick-mortar interaction is represented by cohesive discontinuum interface elements, which is required for accurately simulating the failure behavior of infills (Mucedero et al., 2020). Moreover, in the simplified case, the mortar joints can be significantly simplified, by being represented by zero-thickness cohesive interface elements (Lotfi and Shing, 1994). On the other hand, this simplification implies that the tensile splitting of the brick and its interface to the mortar cannot be simulated.

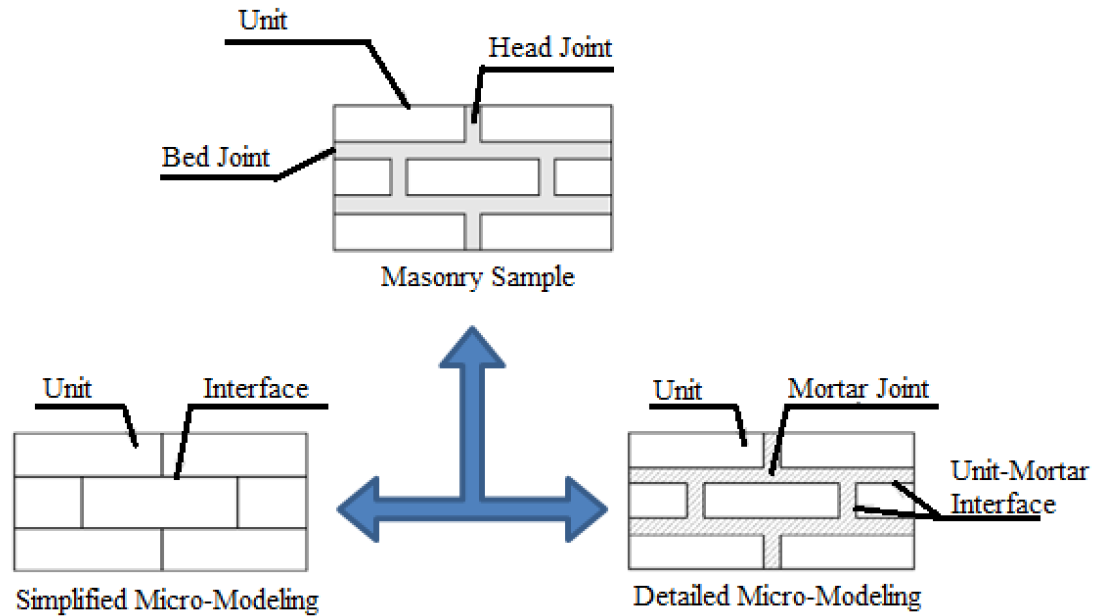


Fig. 4.1 - Micro-modeling techniques

The implementation of these micro-modeling techniques is challenging, as it demands an extensive amount of parameter calibration and a high computational resource, rendering it time-consuming (Petracca et al., 2017). Therefore, micro-modeling is typically reserved for specific research purposes.

#### 4.1.2.2. Macro-modelling

Since the first attempts to model the global response of composite materials, such as infilled RC frames. Past experimental campaigns have consistently indicated that infills acts as a compressive strut in the diagonal direction when the frame is subjected to in-plane shear loads (Bouarroudj and Boudaoud, 2022). Hence, the modeling of the global response of composite materials like masonry infills could be solved by using a diagonal strut with appropriate geometrical and mechanical characteristics (Asteris et al., 2013b). In fact, Holmes (1961) was the first to take up and further elaborate this idea, later proposing that the diagonal strut should be conceived with a width equal to  $1/3$  of the infill panel length, as illustrated in Figure 4.2. Nowadays, the equivalent strut model is the most commonly used macro-modeling approach, mostly due to its simplicity and easy applicability (Mucedero et al., 2020).

On the basis of examined data from previous seismic events and the findings of experimental tests, macro-models have been developed based on the physical understanding of the infills' behavior. Various numerical strategies can be used in macro-modeling, including simple equivalent single-strut models or more complex models incorporating multiple struts. Moreover, due to its low computational resource requirement, the macro-modeling strategy is recommended to evaluate the global behavior of infilled RC structures, specially of large-scale, while the micro- and meso-modelling approaches are suggested to explore local effects resulting from the frame-infill interaction. Recently, several macro-models have been proposed in the literature.

For instance, Holmes (1961) and Panagiotakos and Fardis (1996) suggest that representing masonry infills with a single diagonal strut is appropriate for capturing the global behavior of infilled frames. However, according to Crisafulli (1997), although single-strut models can predict the global behavior

of masonry-infilled frames fairly well, they cannot account for the frame-infill interaction, leading to inaccuracies in the distribution of induced moment and shear in the surrounding frame and not adequately predicting the location of plastic hinges. To address this issue, more complex macro-models using multiple diagonal struts had to be developed. In order to accurately capture the behavior of infilled frames subjected to earthquake loading and consider both stiffness and strength degradation, Crisafulli (1997) proposed a four-node panel element. This clever element addressed the shear and compressive behavior, separately, by employing a shear spring and a two-strut mechanism, respectively, in each direction, as depicted in Figure 4.3. In order to accurately replicate the local effects caused by the frame-infill interaction, as an example, Chrysostomou et al. (2002) suggested a six-strut strategy, with three struts in each direction, as shown in Figure 4.4.

It is worth noting that the previously discussed models have limitations when it comes to capturing the shear sliding failure of masonry walls. However, Furtado et al. (2015) upgraded the corresponding bi-diagonal compression strut model. They introduced a central element that concentrated the nonlinear hysteretic behavior, along with four diagonal truss components that exhibited rigid behavior, connected to the beam-column joints (see Figure 4.5).

During an earthquake, the contact between the infill panel and the surrounding frame is prone to cracks, leading to disconnection, primarily due to the discrepancy in lateral stiffness between the two members (Mucedero et al., 2020). Hence, a more realistic strut model should consider the reduction in contact length of the panel, adjusting the strut width based on the increase in lateral displacement. Crisafulli (1997) incorporated this phenomenon into their model, where the strut width varies as a function of the axial displacement.

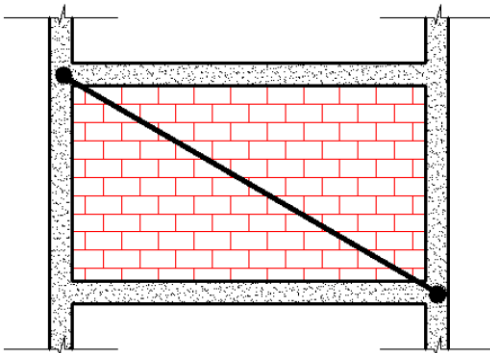


Fig. 4.2 – Single strut approach  
(Holmes, 1961)

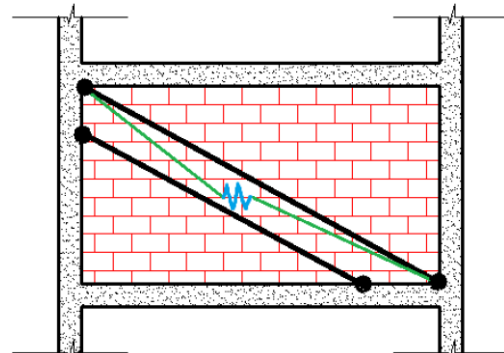


Fig. 4.3 – Double strut with shear spring  
(Crisafulli, 1997)

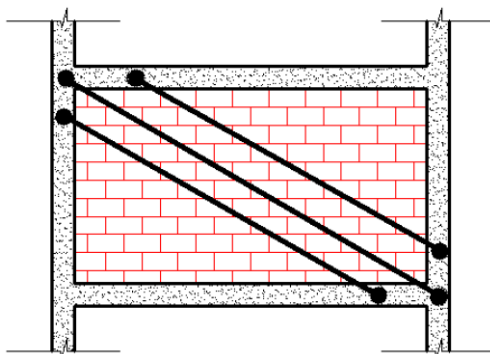


Fig. 4.4 – Triple strut approach  
(Chrysostomou et al., 2002)

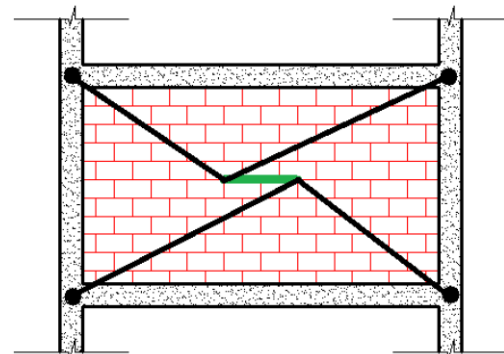


Fig. 4.5 – Rigid strut with nonlinear central element  
(Furtado et al., 2015)

#### 4.1.2.3. Meso-modelling

Meso-modeling strategies idealize the masonry infill wall as a continuous bi-dimensional element and do not discern between brick units and mortar joints (Bouarroudj and Boudaoud, 2022). The brick units, the contact between bricks and mortar joints, as well as the characteristics of the mortar, are merged into a single equivalent element, being depicted as continuous finite elements. This method relies on the selection of a periodic unit cell which contains all the component types of the wall and that can be used repeatedly to create the entire infill panel, as shown in Figure 4.6. By employing the homogenization process, the masonry infill materials are smeared out as a single equivalent element (Bouarroudj and Boudaoud, 2022). The continuum model, which treats the masonry as a continuum media, can be utilized to analyze full-scale masonry walls. Therefore, the most crucial aspect of a numerical analysis is the material homogenization, which allows for the acquisition of reliable equivalent material properties for the masonry (Ma et al., 2001). Several researchers used this modelling technique in infill walls with uniformly distributed brick units and mortar joints. Moreover, Bouarroudj and Boudaoud (2022) used the meso-modeling approach to model an equivalent homogenized diagonal strut element and assess the accuracy of equivalent diagonal strut models proposed in the literature.

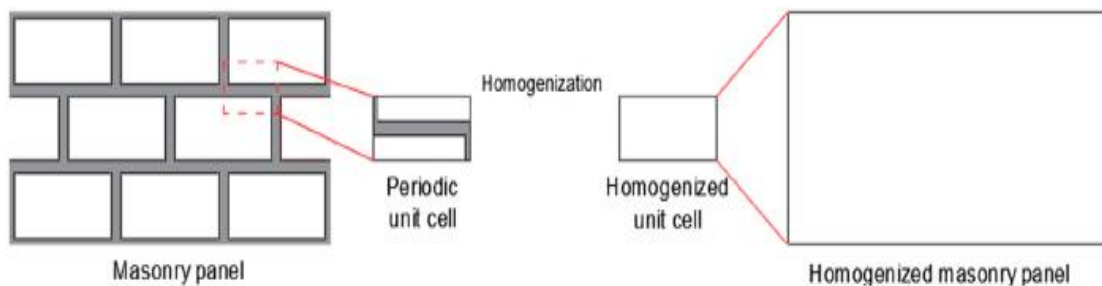


Fig. 4.6 – Homogenization process (adapted from Bouarroudj and Boudaoud, 2022)

Ma et al. (2001) have identified three main categories of homogenization techniques for masonry materials. The traditional approach, as outlined by Hendry (1990), relies on empirical approximations that consider the volume ratios, material properties, and physical characteristics of the brick and mortar joint. The second approach, proposed by Anthoine (1995), involves modelling masonry as a periodic composite continuum element using homogenization theories. This method combines the FE method with periodic media homogenization theory to calculate the overall elastic moduli for a particular type of brickwork. Further, Ma et al. (2001) report that while this homogenization method can be employed to analyze large masonry structures (without an intensively varying stress-strain field) using a small unit cell concept, it may not be adequate for detailed stress analysis and capturing different modes of failure in masonry walls.

Alternatively, the third homogenization method involves micro-structural theories and micro-mechanics. In this approach, the masonry infill is modeled using a volume element that accounts for all the constitutive and geometrical details, i.e., a representative volume element (RVE), see Figure 4.7, which contains all the component types of the wall and that can be used repeatedly to create the entire infill panel. The concept of a RVE is equivalent to a periodic unit cell. However, this method has a limited range of applications because micro-mechanics involves a variety of variables at the micro-scale, which are challenging to identify through macro-scale analysis (Petracca et al., 2017). Therefore, obtaining the equivalent masonry material properties in a continuum model through homogenization remains a difficult task (Ma et al., 2001).

Ma et al. (2001) numerically evaluated the possible failure mechanisms (failures of the brick in compression, of the mortar joint in tension, and of the brick and mortar joint in shear) and elastic constants of masonry material using the homogenization concept of an RVE. For this manner, the authors adopted Mohr-Coulomb fracturing law with degrading shear strength for the tensile failure and assumed Coulomb frictional law, in compressive-shear state, for the mortar joint interface model.

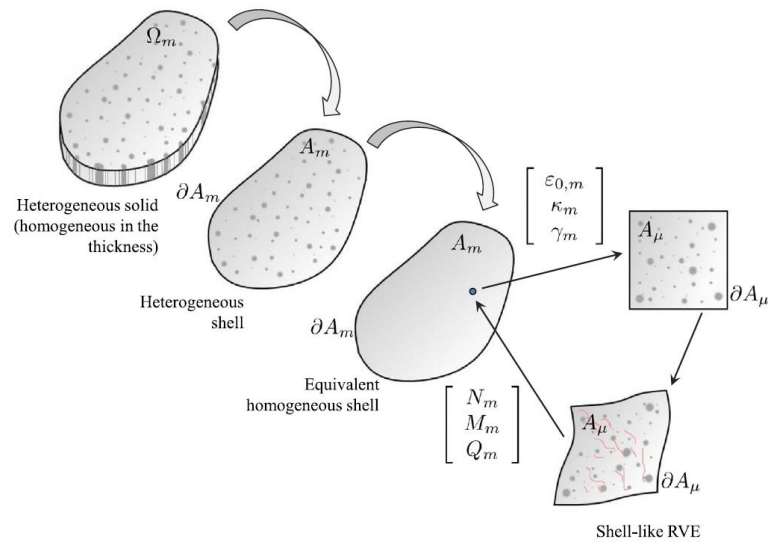


Fig. 4.7 – Homogenization for shell elements (Petracca et al., 2017)

#### 4.1.3. FRAME-INFILL MODELLING APPROACHES

Many researchers have addressed that due to the significant influence of masonry infills to the dynamic response of RC structures, in the linear and nonlinear range, the interaction between the infill and the bounding RC frame should not be disregarded.

The type of mortar used to bond brick layers is often the same type employed to fill the space between the RC frame and the infills. According to Mosalam et al. (1997), this connection between the two elements creates a vulnerable and weak area around the infill panel. In their study, Liauw and Kwan (1984) modeled the frame-infill interaction using simplified bar-type elements that could simulate both separation and slip. Dhanasekar and Page (1986), on the other hand, utilized one-dimensional interface elements to represent the frame-infill contact section. They demonstrated that the behavior of the composite frame depends on several factors, such as the geometry of the frame, the frame-infill relative stiffness, and on the strength properties of the masonry, particularly the strengths of the connection in shear and tension in relation to the compressive strength. Alternatively, to model the frame-infill interaction, Stavridis and Shing (2009) utilized a four-node, isoparametric, zero-thickness line element, illustrated in Figure 4.8.

In conventional methods, the frame-infill interface is represented by contact elements. However, recent studies have employed inelastic interface components to model this interaction more accurately. Asteris (2003) has proposed a step-by-step approach that takes into account the evolving contact length between the infill panel and the RC frame under cyclic lateral loading. This method employs a separation criteria without the need for any interface elements. Later, Asteris (2008) noted that variations in the vertical load cause the contact length to decrease during earthquake events. Therefore, in numerical simulations, the contact length should be taken into account as a crucial component of the solution rather than being assumed to remain constant throughout the earthquake.

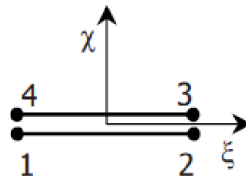


Fig. 4.8 – Frame-infill interaction model (Stavridis and Shing 2009)

#### 4.1.4. DISCRETIZATION METHODS FOR RC MEMBERS

There are several constitutive modeling approaches for brittle and quasi-brittle materials, among which continuum damage modeling stands as a commonly employed method. In the context of modeling the nonlinear behavior of RC members, beam or plane elements are usually utilized. Mosalam et al. (1997) employed a smeared-crack model with a homogeneous material for the case of plane elements. RC members are frequently discretized using a rectangular grid of nodes interconnected by quadrilateral smeared-crack components (Stavridis and Shing, 2009). When the mesh of RC components are fine enough, allowing for the representation of steel rebars, discrete truss elements are preferred over a smeared overlay.

In RC structures, smeared-crack models are often utilized due to their diffusion characteristics upon cracking. However, owing to kinematic constraints, these models have an inherent deficiency in describing the shear sliding of concrete upon cracking and the diagonal shear cracks, producing unconservative results (Lotfi and Shing, 1991). Therefore, Lotfi and Shing (1994) developed continuous-interface models, i.e., smeared-crack along with interface elements, to better account for weak planes in infill walls introduced by the mortar. Moreover, these deficiencies can be mitigated by using cohesive interface models (Stavridis and Shing, 2009).

In the study by Lotfi and Shing (1991), a modeling approach utilizing beam elements with four DOF per node was employed by the authors to model the RC members. The linear elastic behavior of the RC elements was assumed until the ultimate load was reached, at which point a perfect plasticity model was applied. The authors also incorporated the confinement effect of the RC members by modeling transverse reinforcement using additional beam elements with axial stiffness. Similarly, Mehrabi et al. (1996) adopted a methodology where the shear reinforcement was smeared out across the concrete components. Furthermore, two-node bar elements were utilized to accurately model the longitudinal rebars within the framed structure. Finally, for the representation of the RC frame, nine-node quadrilateral smeared-crack elements were employed.

## 4.2. DESCRIPTION OF THE ADOPTED NUMERICAL MODEL

### 4.2.1. INTRODUCTION

In this section, it is presented the finite element model adopted for the seismic assessment and monitoring of the RC structure in the context of this master's thesis. The development of an accurate and reliable numerical model is essential for comprehensively assessing the behavior of the structure under seismic loading conditions. This chapter aims to provide a detailed description of the FE model, including the materials model. Nevertheless, it is important to acknowledge that certain assumptions and simplifications were necessary during the development of the numerical model. These were made to strike a balance between computational efficiency and accuracy. Furthermore, it is noteworthy that the results are inherently sensitive to the selected model parameters due to the complexity of the model.

A structure might experience nonlinear deformation before reaching its ultimate limit state, which would result in inaccurate numerical results if the problem were to be solved using linear elastic theory. Therefore, the numerical model adopted for the analysis of the case study building takes into account the nonlinear behavior of the comprising materials, which can be critical when predicting how the structure will behave under a seismic event. Nonlinear behavior refers to the fact that the relationship between stress and strain in a material is not linear, meaning that the material's response to stress changes as the stress level increases.

Two distinct sources of non-linearities can be distinguished: geometric non-linearity and material non-linearity. Geometric non-linearity arises from finite deformations coupled with changes in stiffness under loading, leading to second-order effects. On the other hand, material non-linearity results from changes in the physical response of a material to stress or deformation, and takes the form of path-dependent and non-unique constitutive laws (Varum, 2003).

Geometric non-linearity occurs when the deformation of a structure becomes large enough that the structure's stiffness changes, leading to second-order effects that are not accounted for in linear analysis. For example, if a building is subjected to a strong wind or earthquake, the deformation of the structure can be large enough to cause changes in its stiffness, resulting in nonlinear behavior.

It might be challenging to collect information on the real properties of the structure, especially if previously damaged by an earthquake. Nonlinear analysis, therefore, may be problematic since it requires a thorough comprehension of the material characteristics as well as the manner in which the structure behaves under different loading and boundary conditions. For this manner, the full-scale infilled RC structure experimental dynamic tests, which were presented in Chapter 3, produced a vast amount of acceleration records that were utilized to support the numerical model that was adopted and enhanced in this master's thesis. Furthermore, the model's ability to simulate the nonlinear behavior of materials can also help identify potential weaknesses in the structure and guide the design of safer and more efficient structure. It can also provide insights into the performance of existing structures under extreme loading conditions, which is especially relevant in areas prone to earthquake events.

Overall, the use of a complex numerical model in this master's thesis can provide a more realistic and accurate representation of the behavior of structures under extreme loading conditions. The latter calibrated analytical model might be extensively applied to precisely simulate the behavior of existing RC framed structures and can be valuable in a variety of civil engineering fields.

#### 4.2.2. RC FRAME MODELING

In the STKO software, the model adopted for the representation of the RC frame and its components is a result of associating different material and element models available in the OpenSees library, or created by the Petracca et al. (2022) and added to the library. The RC frame model is described by three elements: (i) BeamColumn element, in which the element is based on the iterative forced-based formulation, is used to model the columns by adopting the Gauss-Lobatto integration scheme with three points of integration and linear coordinate transformation; (ii) Truss element, which is used to model the cylindrical rods that ensure the bracing of the frame in the  $x$  direction; and (iii) ASDShellQ4 shell element is used to model the slabs.

The ASDShellQ4 element is a four-node thick shell element that uses a two-by-two Gauss quadrature, leading to a total of 4 integration points, as illustrated in Figure 4.9. This shell element incorporates the advancements presented in the formulation by Chen et al. (2004). This formulation enhances the membrane behavior of the element, making it significantly less sensitive to geometric distortion

compared to standard iso-parametric elements. To accurately capture the rotation about the normal axis, the formulation by Hughes and Brezzi (1989) is employed, ensuring that membrane locking is avoided. Additionally, the bending behavior of the shell is addressed using the formulation proposed by Dvorkin and Bathe (1984), effectively mitigating the transverse shear locking issues typically associated with thick plate elements.

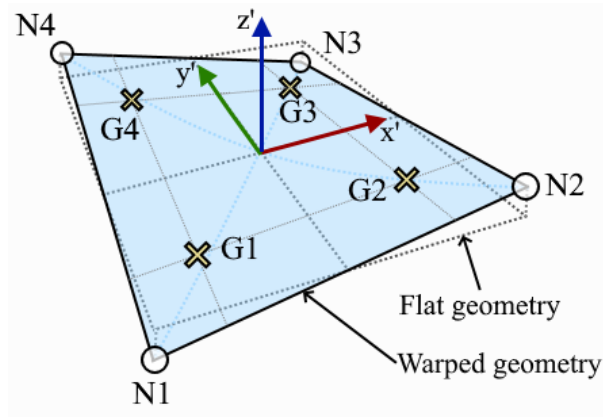


Fig. 4.9 – ASDShellQ4 representation (ASDShellQ4 user manual)

#### 4.2.2.1. Columns

In the analysis of the concrete material, the Concrete02 uniaxial material model was employed, which was developed by Mander et al. (1988), and is available in the OpenSees library. The material is based on the uniaxial model developed by Madas et al. (1992) and characterize the nonlinear behavior of concrete by using the confined-unconfined model introduced by Martinez-Rueda and Elnashai (1997).

Two-dimensional, two-node FEs with multiple-fiber control sections (as exemplified in Figure 4.10) along its length and with three integration points using Lobatto’s integration scheme were used for modeling the fiber beam-column element for the columns in the RC frame. FEs based on flexibility or stiffness have differing approaches in relation to the application of distributed element loads. To the fiber cross-section it was assigned a high torsional stiffness equal to  $3.315 \times 10^{12}$  Mpa in order to eliminate any torsional effect on the columns.

The classical formulation method (stiffness-based) for geometrically nonlinear analysis of structures derives the geometric stiffness directly from the governing differential equation. While stiffness-based elements discretely apply these loads as equivalent nodal loads, the elements based on flexibility take these forces into account internally through superposition of forces at the control sections. At the control sections the resulting internal forces are regarded as deviations from the forces obtained with the force interpolation functions.

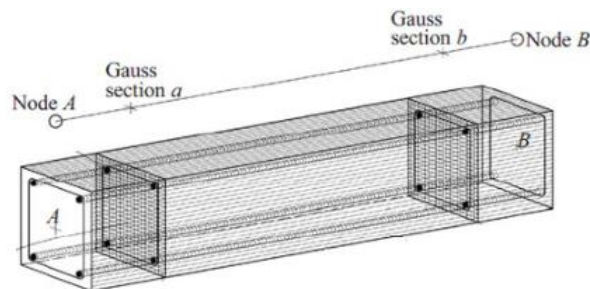


Fig. 4.10 – Example of a fiber beam-column section (Morteza Razi)

The uniaxial Concrete02 material reproduces the characteristics and constitutive laws of the employed type of concrete. At least six parameters are required to completely define the uniaxial material properties: the value of the compressive and tensile strength after 28 days; the strain value at maximum strength; the concrete material crushing strength and respectively strain; the ratio between the unloading and initial slope of loading; and tension softening stiffness. Therefore, in Table 4.1, the values of the various parameters adopted is presented in summary and Figure 4.11 illustrate the corresponding stress-strain envelope.

Table 4.1 – Concrete model mechanical parameters

Parameter	Value
$f_c$	50 [Mpa]
$f_t$	1 [Mpa]
$f_{cu}$	10 [Mpa]
$\varepsilon_c$	0.002
$\varepsilon_{cu}$	0.045
$\lambda$	0.1
$E_{ts}$	2250 [Mpa]

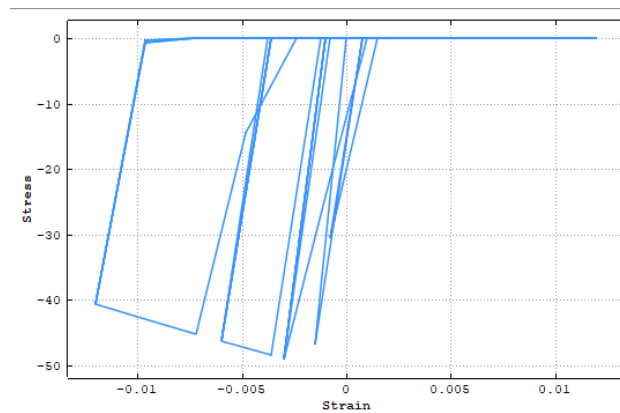


Fig. 4.11 – Concrete material stress-strain relationship

#### 4.2.2.2. Beam-Slabs

As previous demonstrated in Chapter 3, the slabs have enough reinforcement in both horizontal directions to work as rigid diaphragms in the RC frame, thus there was no need to assign a any material and raise the complexities and computational effort of the model. Therefore, the slab was modeled in a simplified two-dimensional way using an ElasticMembranePlate section, available in the OpenSees library, which is an isotropic section appropriate for shell analysis. The section properties adopted are shown in Table 4.2. Note that owing to the fact that they are really stiff members, no deformation is expected, it was assumed a high modulus of elasticity. The simplification made is best illustrated in Figures 4.12 and 4.13.

Table 4.2 – Slab plate section parameters

Parameter	Value
E	30000 [Mpa]
$\nu$	0.3
$h$	400 [mm]
$E_{pm}$	0.25

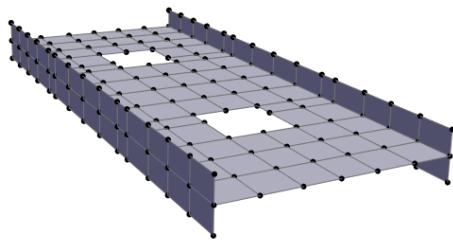


Fig. 4.12 – 1<sup>st</sup> floor slab model

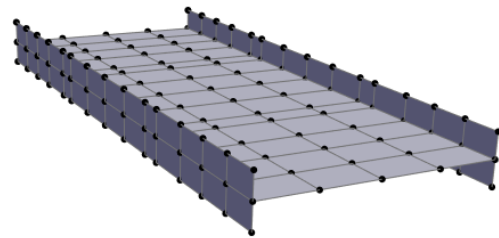


Fig. 4.13 – 2<sup>nd</sup> floor slab model

#### 4.2.3. REINFORCEMENT MODELING

For the steel reinforcement the Steel 01 uniaxial material model, which is available in the OpenSees Library, was used to construct the longitudinal steel bars. This material model has kinematic hardening and is described by a nonlinear evolution equation. The material hysteretic behavior is shown in Figure 4.14. On the other hand, Figure 4.15 shows the stress-strain relationship for the steel material model based on the adopted parameters. All the adopted values for the steel mechanical parameters are in accordance with EC2 and are summarized in Table 4.3.

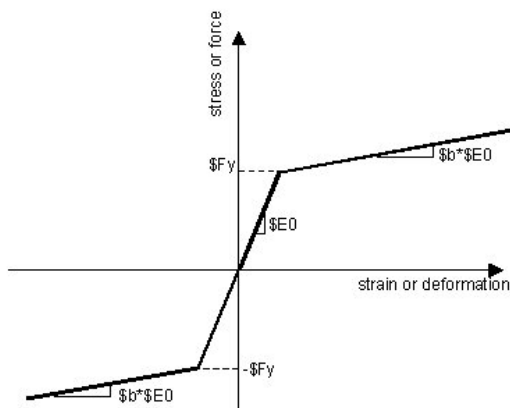


Fig. 4.14 – Hysteretic behavior with kinematic hardening

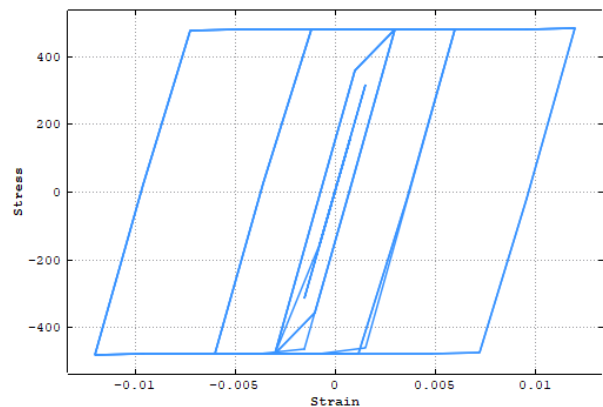


Fig. 4.15 – Steel material stress-strain envelope

Table 4.3 – Steel model mechanical parameters

Parameter	Value
-----------	-------

$F_y$	480 [Mpa]
$b$	0.001
$E_0$	210000 [Mpa]

#### 4.2.4. MASONRY INFILLS MODELING

The proposed modelling approach for the infill panels is purely based on Continuum-Damage theory and an IMPL-EX integration scheme formulated by Oliver et al. (2008), which is a mix of implicit and explicit integration algorithms that improves convergence and stability of the numerical model. Furthermore, the masonry material properties are of particular difficult to define precisely, and therefore, might be one of the main reasons that explain why infill walls have been considered as ‘non-structural’ elements.

In this project the ASDConcrete3D material along with the ASDShellQ4 element are used for modeling the simplified macro-model adopted for the infill walls, which is based on a constitutive model that lumps the brick units and mortar joints into a single element, and for the contact surface between the infill panel and the bounding RC frame. The adopted material object is a plastic-damage model, developed by Petracca et al. (2022), suitable for concrete and masonry materials that derives from an extension of the previously developed model by Petracca et al. (2017), keeping the simplicity of continuum-damage models. The original formulation by Petracca et al. (2017) is based on the classical framework of continuum-damage mechanics, in which the stress tensor is explicitly assessed from the strain tensor without the need of internal iterations at the constitutive level, making the constitutive model fast and robust for the simulation of large-scale structures. However, as it is a continuum-damage model it does not take into account inelastic permanent deformations. Therefore, the new plastic-damage model has to introduce plastic deformations in the original model in a simplified fashion and allows the user to opt for an IMPL-EX integration scheme (Oliver et al., 2008) in order to improve the computability of the constitutive models that exhibit strain-softening.

Figure 4.16 illustrate the two-dimensional plane-stress failure criteria of the ASDConcrete3D material model, whereas Figures 4.17 and 4.18 depict the tensile and compressive uniaxial laws of the shell element.

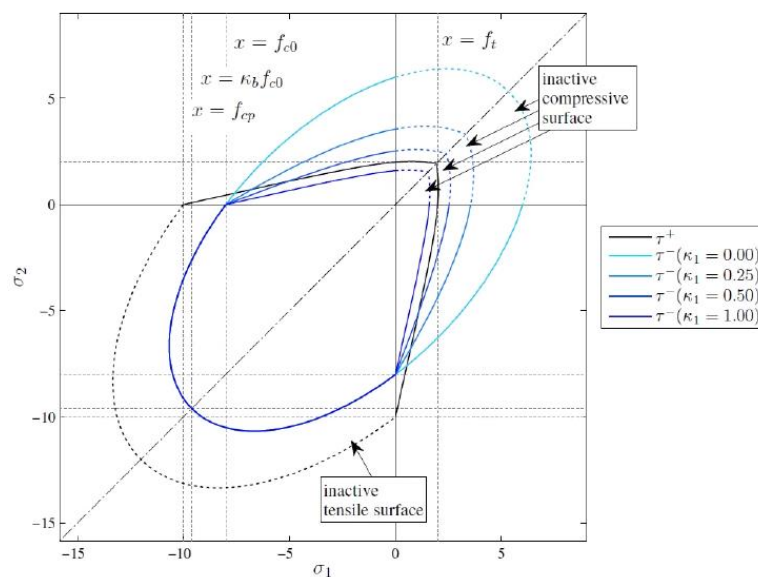


Fig. 4.16 – Damage surfaces (Petracca et al., 2017)

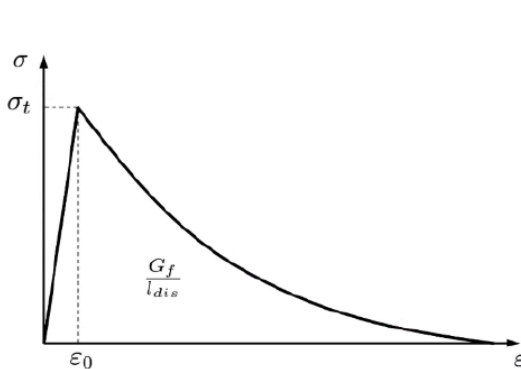


Fig. 4.17 – Tensile hardening  
(Petracca et al., 2017)

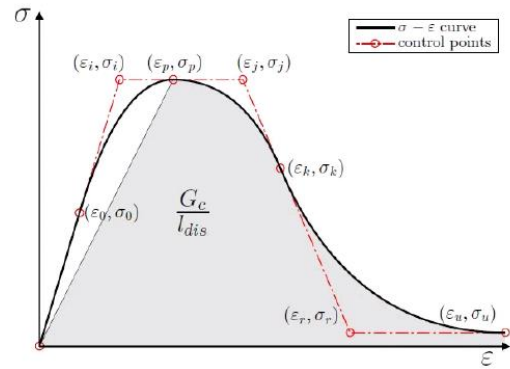


Fig. 4.18 – Compressive hardening  
(Petracca et al., 2017)

#### 4.2.4.1. Infill Panel

In order to model the behavior of the infill panel, a combination of the plastic-damage material model, described previously, and the Orthotropic material wrapper (Oller et al., 2003) is employed. This coupling enables the material’s inherent isotropic formulations to be reconstructed as implicit orthotropic formulations.

When considering the masonry behavior under plane stress, a key assumption is made regarding the homogeneity of the material. This assumption implies that the properties of the material remain consistent throughout. Specifically, the material exhibits varying moduli of elasticity in different directions. The  $x$  direction represents the direction parallel to the bed joints of the brick masonry, the  $y$  direction is perpendicular to the bed joints, and the  $z$  direction is perpendicular to the plane of the infill panel.

To provide a comprehensive understanding of the material properties used in the plastic-damage model for the infills, Table 4.4 offers a complete description of these properties.

Table 4.4 – Material parameters for the infill panels

$E_x$ [Mpa]	$E_y$ [Mpa]	$E_z$ [Mpa]	$f_{mc}$ [Mpa]	$f_{mt}$ [Mpa]	$G_c$ [Mpa]	$G_t$ [Mpa]
2381	2000	2000	2	0.2	1	0.02
$G_{xy}$ [Mpa]	$G_{yz}$ [Mpa]	$G_{zx}$ [Mpa]	$\nu_{xy}$	$\nu_{yz}$	$\nu_{zx}$	
922	833	896	0.2	0.2	0.2	

#### 4.2.4.2. Frame-Infill Contact Surface

To represent the frame-infill interface, the material model described above is coupled with a PlaneStress material wrapper, which converts the three-dimensional material to a two-dimensional one. Finally, the

resulting plane-stress material is assigned to every layer of the multi-layered shell section. This shell section is based on the studies conducted by Lu et al. (2015) and it is used with four layer that in total have the same thickness of the infill panel (80 mm).

The contact surface material, which has a Poisson's ratio of 0.1, is characterized by a shear modulus of 1500 Mpa. The contact region has a small width of 20 mm and the same thickness as the infill panel (80 mm). As a result, it acts essentially as an interface element between the RC frame and the masonry panel. To the contact surface is assigned a high modulus of elasticity, equal to 3000 Mpa, which makes it act similarly to a rigid contact in compression, meaning no crushing failure. However, it allows for easy separation in tension.



# 5

## METHODOLOGY AND VALIDATION OF THE NUMERICAL SIMULATION RESULTS

### 5.1. INTRODUCTION

In this chapter, it is presented the numerical simulation results obtained from the FE model developed in the STKO software for the assessment of the structural behavior of the masonry-infilled RC frame. The primary objective of this chapter is to provide a comprehensive analysis of the simulation results and subsequently validate them against the experimental results. The analytical time-dependent response of the structure is obtained through direct numerical integration of its differential equations of motion. By comparing the numerical predictions with real-world observations, the accuracy and reliability of the adopted simulation methodology can be evaluated.

The numerical simulation results offer valuable insights into the structural behavior and response under seismic loading conditions. Through the application of the numerical model, it can be evaluated various performance parameters such as displacements, stresses, strains, and damage distribution within the structure. These results play a crucial role in enhancing our understanding of the structural response and identification of potential vulnerabilities that may arise during seismic events.

To ensure the reliability of the numerical simulations, it is imperative to validate the obtained results against experimental results. Experimental data serve as a benchmark for assessing the accuracy and credibility of the simulation results. By comparing the numerical predictions with experimental measurements, it is possible to assess the level of agreement and identify any discrepancies or limitations within the numerical model.

It is important to recognize that certain variations between the numerical and experimental results may arise due to inherent uncertainties and limitations of the adopted numerical model. Factors such as material heterogeneity, modeling assumptions, and measurement errors can contribute to these discrepancies.

The final numerical model can be extensively used to assess the seismic performance of buildings using the same materials and structural configuration type. It enhances the understanding of the seismic response of infilled RC structures and improves the reliability of subsequent findings and recommendations. Ultimately, this chapter aims to advance in the field of seismic vulnerability assessment and to support the development of more robust and resilient structural design practices.

## 5.2. EIGEN ANALYSIS

Before proceeding to the complex time-history analysis, it was crucial to ensure the accuracy and reliability of the numerical model in the elastic domain. One way to achieve this is by conducting an eigen (modal) analysis.

The modal analysis serves as a preliminary step in the overall analysis process and plays a fundamental role in obtaining reasonable and trustworthy results in subsequent analyses. The identification of the eigenvalues and corresponding eigenvectors of the numerical model allows for insights into its dynamic behavior and identifies the natural frequencies and mode shapes of the system.

The comparison between the experimental and analytical frequencies obtained from the modal analysis serves as a means of validating the analytical model. By assessing the consistency between the frequencies predicted by the numerical model and the observed frequencies in the experimental campaign, it is possible to determine the accuracy and validity of the analytical model within the linear range.

This validation process is crucial because it ensures that the numerical model captures the essential dynamic properties of the specimen structure under investigation. Therefore, an iterative approach was adopted, which consisted of adjusting the material model parameters until the modes of vibration adequately reproduced the modes and frequencies identified during the experimental campaign.

During this iterative process, it was found that certain parameters had a significant influence on the determination of the elastic characteristics of the numerical model, namely the infill wall modulus of elasticity ( $E_x$ ,  $E_y$  and  $E_z$ ), the infill wall shear modulus ( $G_{xy}$ ,  $G_{yz}$  and  $G_{zx}$ ), the concrete compressive strength ( $f_c$ ), and the concrete maximum compressive strain ( $\epsilon_c$ ).

The modal properties were identified using the EigenCommand and the default Arpack solver, with a total of 30 eigenvalues being recorded. The results obtained show two types of mode shapes, local and global. If a mode of the specimen structure is deformed as a continuum system, the mode shape is assumed as global, which means that the whole structure deformation is higher than of the members. On the other hand, if the deformation of a member dominates the mode shape the mode is assumed as local. The need for a high amount of eigenvalues is due to the fact that the masonry infill panels introduced several local modes of vibration that are not discussed here.

The first six elastic natural frequencies of the undamaged masonry-infilled RC structure were numerically evaluated, and the resulting values are summarized in Table 5.1. It is important to note that the modes of vibration are labelled as: ( $x$ ) – translational mode along  $x$ ; ( $y$ ) - translational mode along  $y$ ; and ( $T$ ) – torsional mode. In Table 5.2 the cumulative modal participation mass ratios are presented. Next, the computed modal parameters are compared with the experimentally obtained values. The natural modes of vibration are presented in Figure 5.1. It is important to note that the natural frequencies from the 4<sup>th</sup> and 6<sup>th</sup> mode shapes (along the  $y$ -direction) are the ones of special attention for this study, as the input ground motions were applied in this direction.

Table 5.1 – Natural frequencies numerically and experimentally obtained

Mode	Direction	Numerical natural frequency [Hz]	Experimental natural frequency [Hz]	Natural frequency error [%]
1 <sup>st</sup> Mode	$x$	1.77	1.84	3.88
2 <sup>nd</sup> Mode	$x$	5.73	5.84	1.90

3 <sup>rd</sup> Mode	<i>T</i>	5.92	6.68	12.06
4 <sup>th</sup> Mode	<i>y</i>	8.49	8.39	1.18
5 <sup>th</sup> Mode	<i>x</i>	9.52	9.09	4.62
6 <sup>th</sup> Mode	<i>y</i>	26.19	29.91	13.26

Table 5.2 – Cumulative modal participation mass ratios numerically evaluated

Mode	Cumulative modal participation mass ratio along x [%]	Cumulative modal participation mass ratio along y [%]	Cumulative modal participation torsional mass ratio along z [%]
1 <sup>st</sup> Mode	83.27	0	0
2 <sup>nd</sup> Mode	94.11	0	0
3 <sup>rd</sup> Mode	94.11	0	86.25
4 <sup>th</sup> Mode	94.11	87.14	86.25
5 <sup>th</sup> Mode	98.04	87.14	86.25
6 <sup>th</sup> Mode	98.33	96.46	86.25

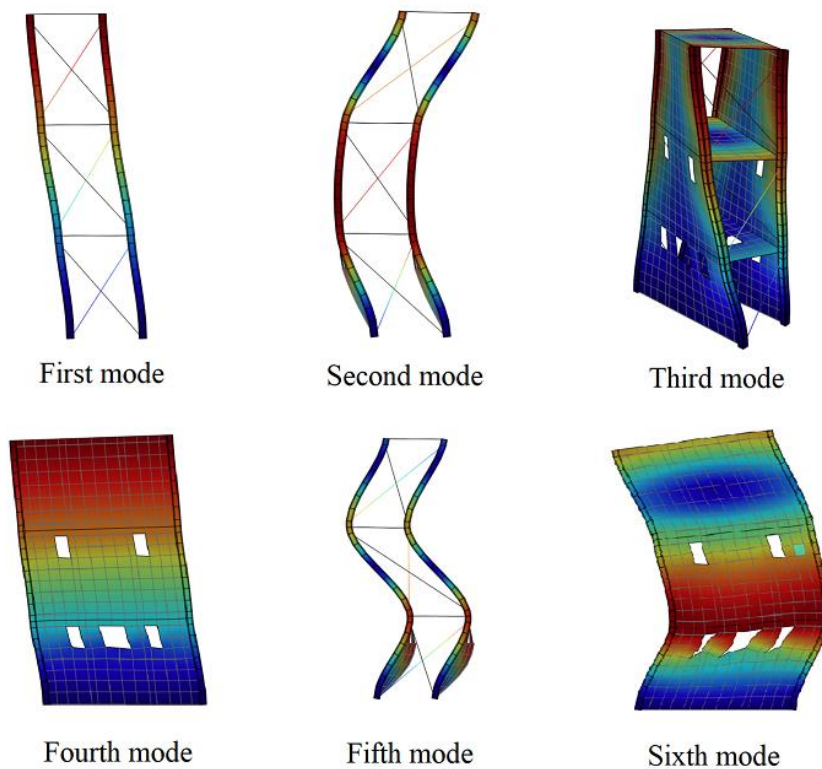


Fig. 5.1 – Computed natural modes of vibration

From the comparison of the natural frequencies and modes of vibrations a very good agreement can be observed. From the results, it can be concluded that:

- From the analysis of the modal participation mass for each mode shape, it can be observed that due to the symmetric distribution of masonry infill walls, the fourth mode (first along  $y$ ) mobilises almost the totality of the corresponding modal mass (90%), whereas the first mode mobilises circa of 80% of the modal mass along  $x$ ;
- In the fourth mode (the most important due to the high modal participation mass along  $y$ ), the difference between the numerically and experimentally evaluated natural frequencies is really low (1.18%);
- In the sixth mode (the second mode along  $y$ ), the natural frequency error is 13.26%, which is a good value taking into account that this mode mobilises only 10% of the total modal mass;
- The natural frequencies of the mode shapes along the  $x$ -direction of the experimental test are slightly higher than those numerically evaluated, with the exception of the fifth mode. In the first mode the error is 3.88%, in the second mode is 1.90% and in the fifth mode is 4.62%;
- It can be observed that the computed frequencies for the second and third modes are very similar, with the second mode being translational and the third mode being torsional, both with a cumulative modal participation mass between 85% and 95%;
- The first and fourth modes suggest a relatively constant distribution of displacements along the storey levels, while the second and sixth modes indicate more displacements at the first storey, which suggests potential for the development of soft-storey mechanisms;
- The ratio between natural frequencies for the only torsional mode (third mode) is 12.06%;
- Overall, the error for each mode of vibration is lower than 15%. Therefore, this constitutes a first confirmation of the FE model validity in the terms of stiffness.

### **5.3. TIME-HISTORY ANALYSES**

The present section of this master's thesis highlights the numerical time-history analyses carried out, which are based on a nonlinear numerical model. The analysis approach is designed to take into account the specific material properties and their nonlinear behavior. Although linear elastic analysis is widely used in the design profession for calculating forces and stresses and for proportioning structural members, its limitations in reflecting the real behavior of structures under extreme or abnormal loading conditions have been recognized (Varum, 2003). This is because almost all structures exhibit some nonlinear behavior prior to reaching their ultimate strength.

As pointed out by Varum (2003), linear elastic analysis fails to capture this nonlinear behavior. Therefore, the nonlinear numerical model used in this study can provide more realistic predictions of the structural response to extreme loading scenarios, such as in an earthquake scenario. The model's capability to account for the nonlinear behavior of the structure and the material properties makes it a powerful tool in structural analysis and design.

The nonlinear response of the infilled RC framed structure was computed for each earthquake input motion. The input ground motions were applied along the  $y$ -direction. The time-history analyses conducted on the numerical model of the masonry-infilled RC frame, which was created in STKO pre-post-processor, are performed using the Newmark numerical integration scheme, with the gamma and beta factors being equal to 0.6 and 0.3025 respectively, and using the Krylov-Newton algorithm with a maximum number of 60 iterations to improve the convergence of the model. The purpose of these

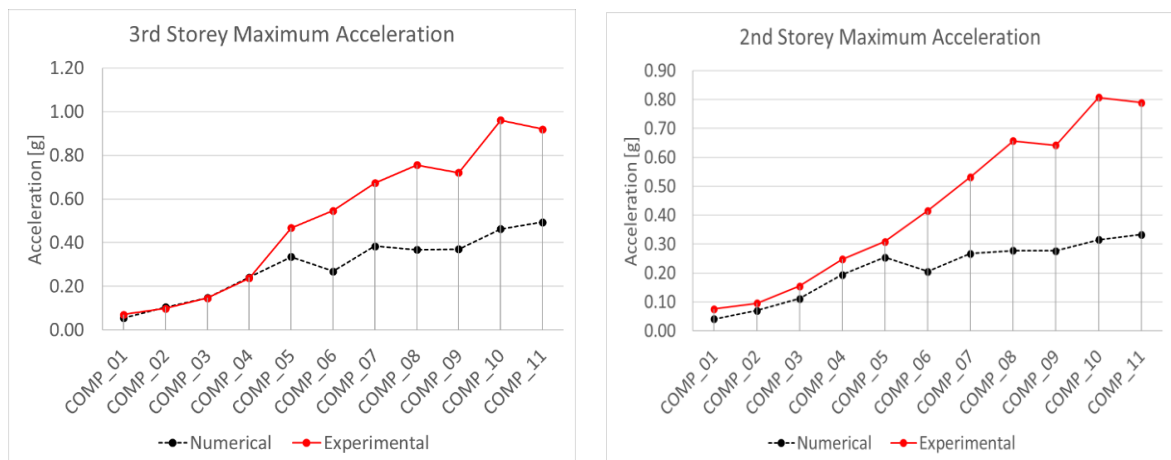
analyses is to determine displacements and accelerations of the specimen structure under different intensities of seismic action. An average time step ( $\Delta t$ ) equal to 0.01 s is used. The analyses require the use of OpenSeesMP parallel solver because of the large dimension of the model.

Dynamic time-history analyses were carried out on the specimen structure FE model with the aim to simulate the structural behavior observed on the shaking table tests conducted at EUCENTRE laboratory in Pavia, Italy. The accuracy of the numerical model is further evaluated by comparing the numerically evaluated acceleration results with the experimentally obtained accelerograms. The comparison was done in terms of temporal evolution (time-history) of accelerations on three different locations of the structure (at the geometrical center of each storey). Thus, the accelerations in the  $y$ -direction measured by accelerometers at the first storey (Acc(7)), second storey (Acc(13)) and third storey (Acc(19)) are compared with the correspondent experimental results.

This section reports the structural response of the nonlinear time-history analyses carried out using twelve ground motion records, scaled according to the reference earthquake (Irpinia). Only the horizontal component along the  $y$ -direction of the seismic event is applied in the numerical model. The nonlinear model uses a 2% Rayleigh damping. The following sections highlight the most significant results of the dynamic analysis per time series, i.e., for each earthquake's intensity record. The numerical results are composed of: (i) time histories of storey accelerations; (ii) displacement-acceleration hysteresis diagrams; (iii) inter-storey drift versus acceleration; and (iv) displacement and storey drift profiles. Additionally, Fourier transform were performed on the computed and experimentally evaluated acceleration results in order to identify the frequency band of the output signals.

In this section the discussion of the numerically evaluated results will be limited to the time-history analysis for the COMP\_05 input motion, due to the fact that for higher intensities of input motion the accuracy of the model in reproducing the expected structural behavior decreases. This can be observed in Figure 5.2, where the computed and experimentally measured maximum acceleration at storeys through the different intensities of earthquake are shown side by side. Particularly, the storey acceleration error for the COMP\_06 input motion is equal to 68%, 68% and 79% for the 3<sup>rd</sup>, 2<sup>nd</sup> and 1<sup>st</sup> storey respectively.

In the next, the most significant nonlinear numerical dynamic analyses of the three-storey masonry-infilled RC frame are presented. The reader can refer to Appendix A2 for more information about the results from higher earthquake input motions.



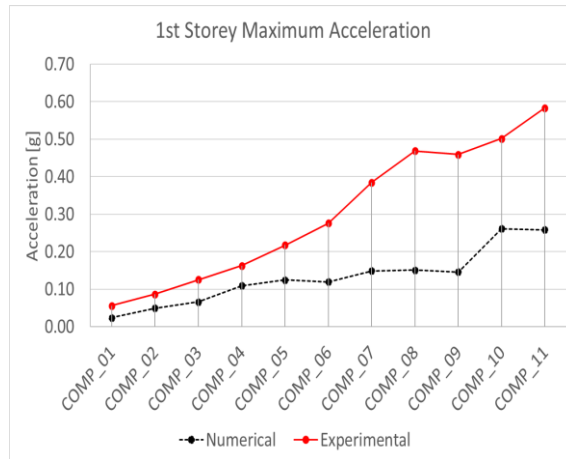
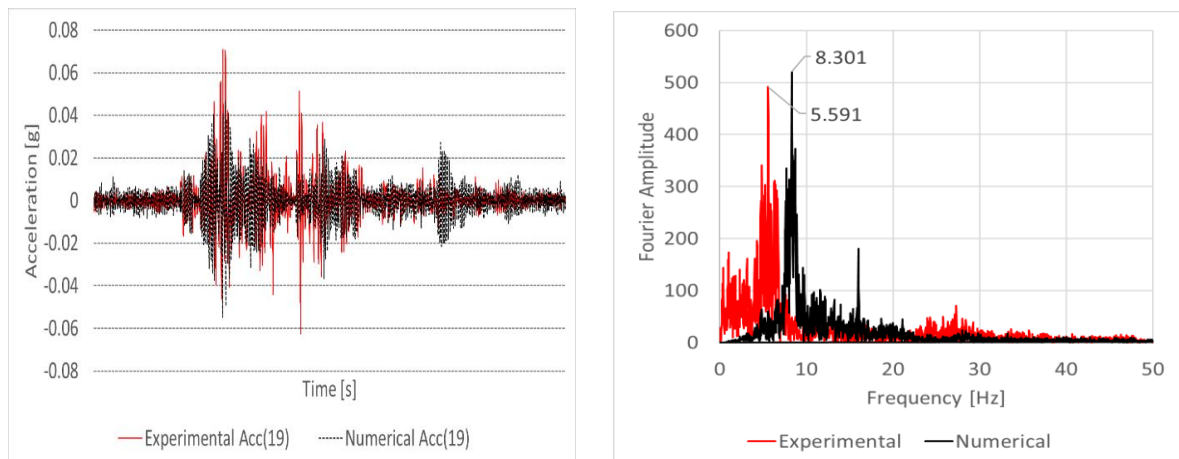


Fig. 5.2 – Maximum acceleration at storey levels

### 5.3.1. RESULTS OF THE COMP\_01 TRANSIENT ANALYSIS

Figure 5.3 shows the computed and the experimentally measured time histories accelerations at storey levels along with their corresponding Fourier transforms. In Figure 5.4, the computed relation between displacement and acceleration at storey level is depicted through displacement-acceleration hysteresis diagrams. Figure 5.5 provides the inter-storey drift versus acceleration at storey levels for the masonry-infilled RC structure when subjected to the COMP\_01 input ground motion.

From the analysis of Figure 5.6 it is evident that the structure exhibits displacement uniformly distributed along the storeys. This uniform behavior is further confirmed in the inter-storey drift profile presented in Figure 5.7.



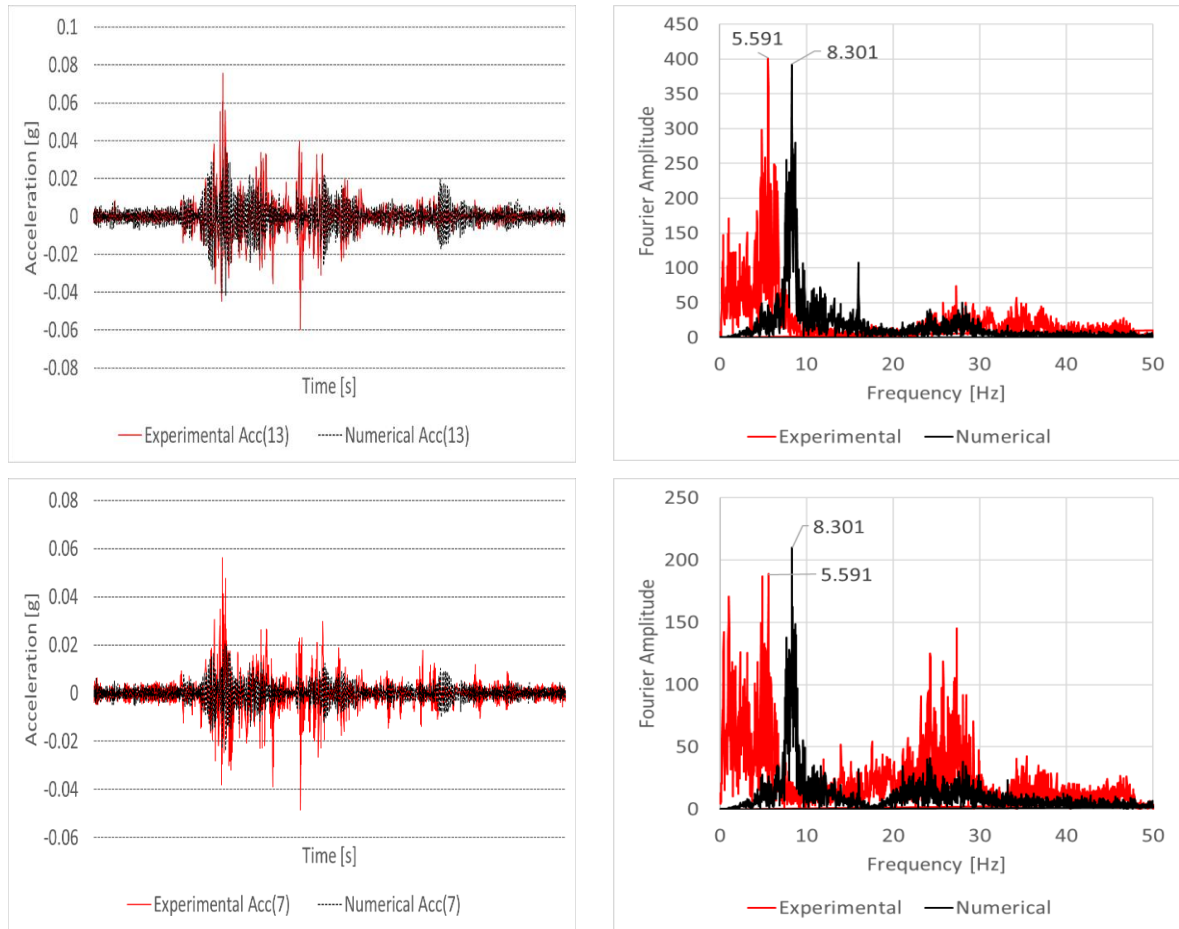
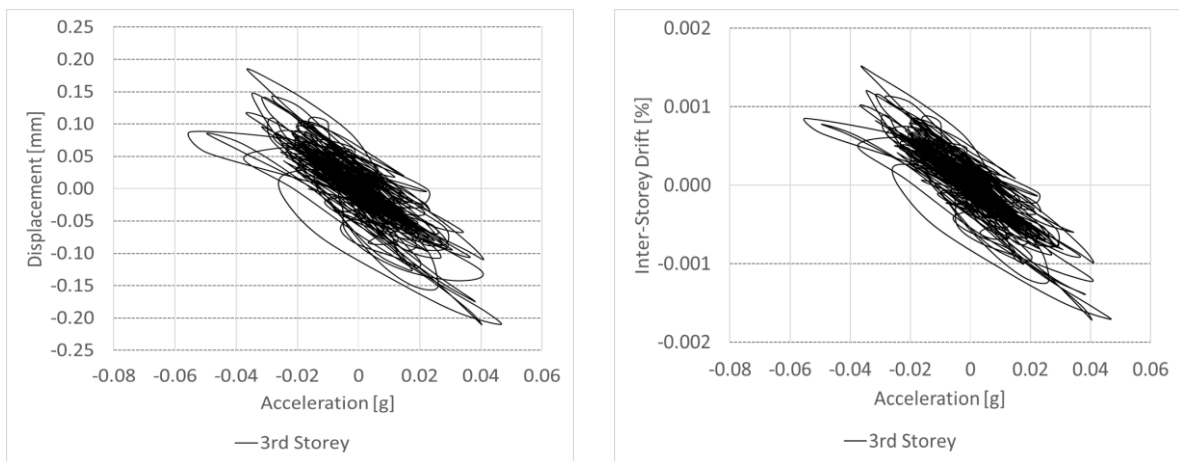


Fig. 5.3 – COMP\_01 storey acceleration time histories and Fourier transform (3<sup>rd</sup>, 2<sup>nd</sup> and 1<sup>st</sup> storeys)



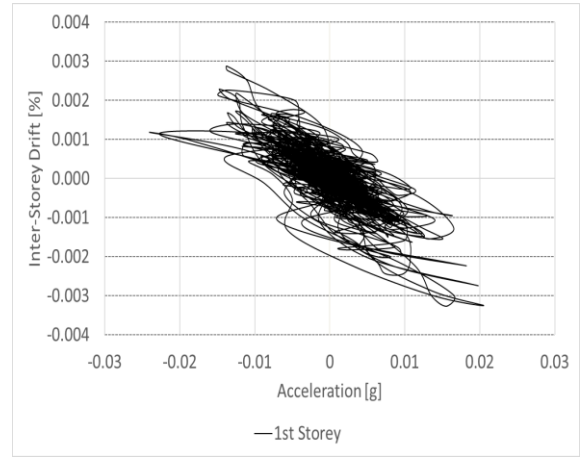
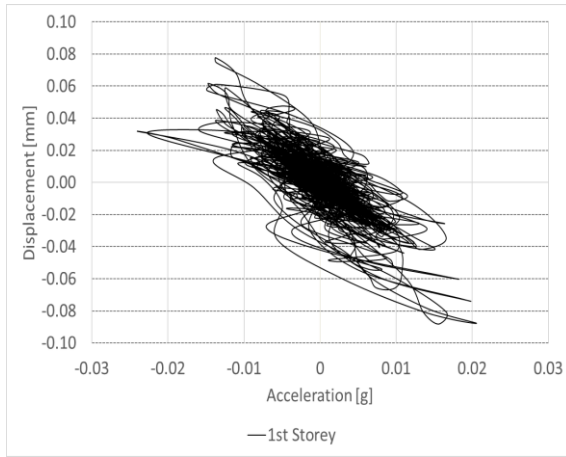
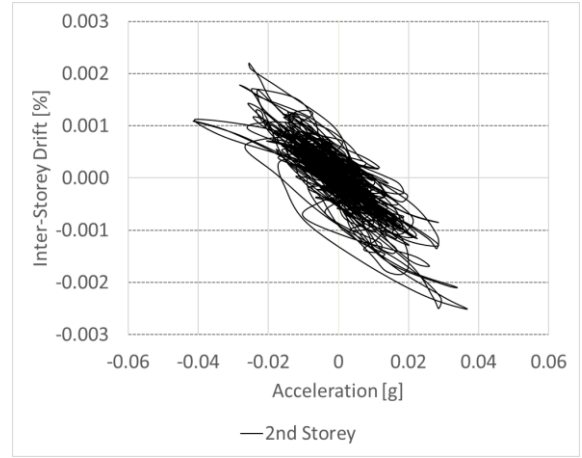
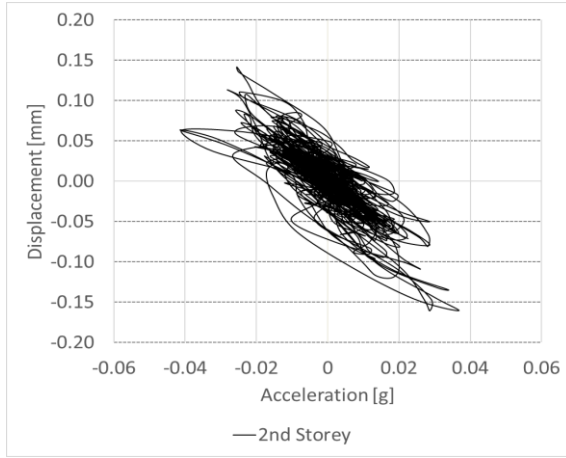


Fig. 5.4 - COMP\_01 displacement vs acceleration envelope (3<sup>rd</sup>, 2<sup>nd</sup> and 1<sup>st</sup> storeys)

Fig. 5.5 - COMP\_01 drift vs acceleration envelope (3<sup>rd</sup>, 2<sup>nd</sup> and 1<sup>st</sup> storeys)

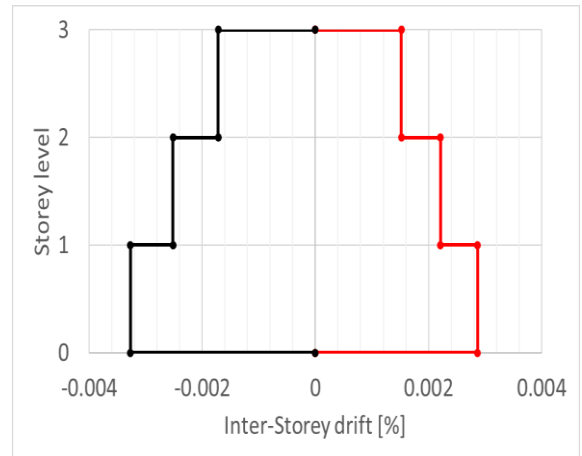
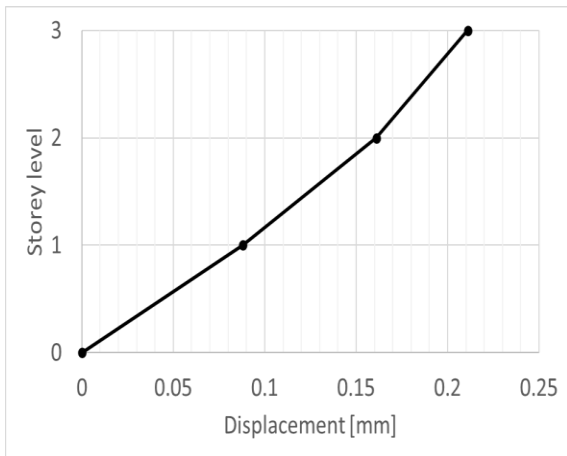


Fig. 5.6 - COMP\_01 maximum displacement profile

Fig. 5.7 - COMP\_01 maximum drift profile

### 5.3.2. RESULTS OF THE COMP\_02 TRANSIENT ANALYSIS

Figure 5.8 shows the computed and the experimentally measured time histories accelerations at storey levels along with their corresponding Fourier transforms. In Figure 5.9, the computed relation between displacement and acceleration at storey level is depicted through displacement-acceleration hysteresis diagrams. Figure 5.10 provides the inter-storey drift versus acceleration at storey levels for the masonry-infilled RC structure when subjected to the COMP\_02 input ground motion.

From the analysis of Figure 5.11 it can be observed that the first and second storey displacements are 53% and 33% lower than the displacement measured at the third storey. This relatively uniform behavior is further confirmed in the inter-storey drift profile presented in Figure 5.12.

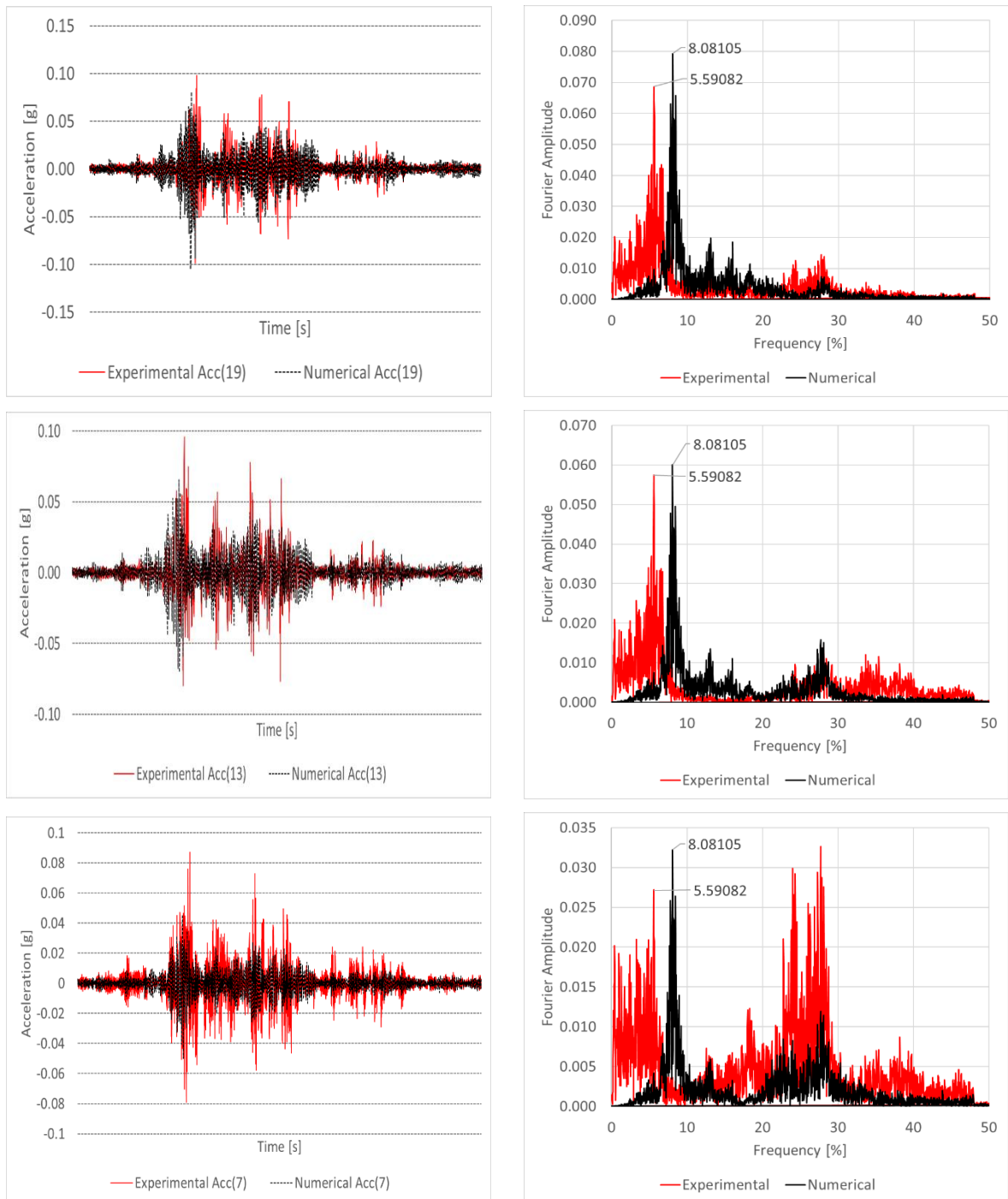


Fig. 5.8 – COMP\_02 storey acceleration time histories and Fourier transform (3<sup>rd</sup>, 2<sup>nd</sup> and 1<sup>st</sup> storeys)

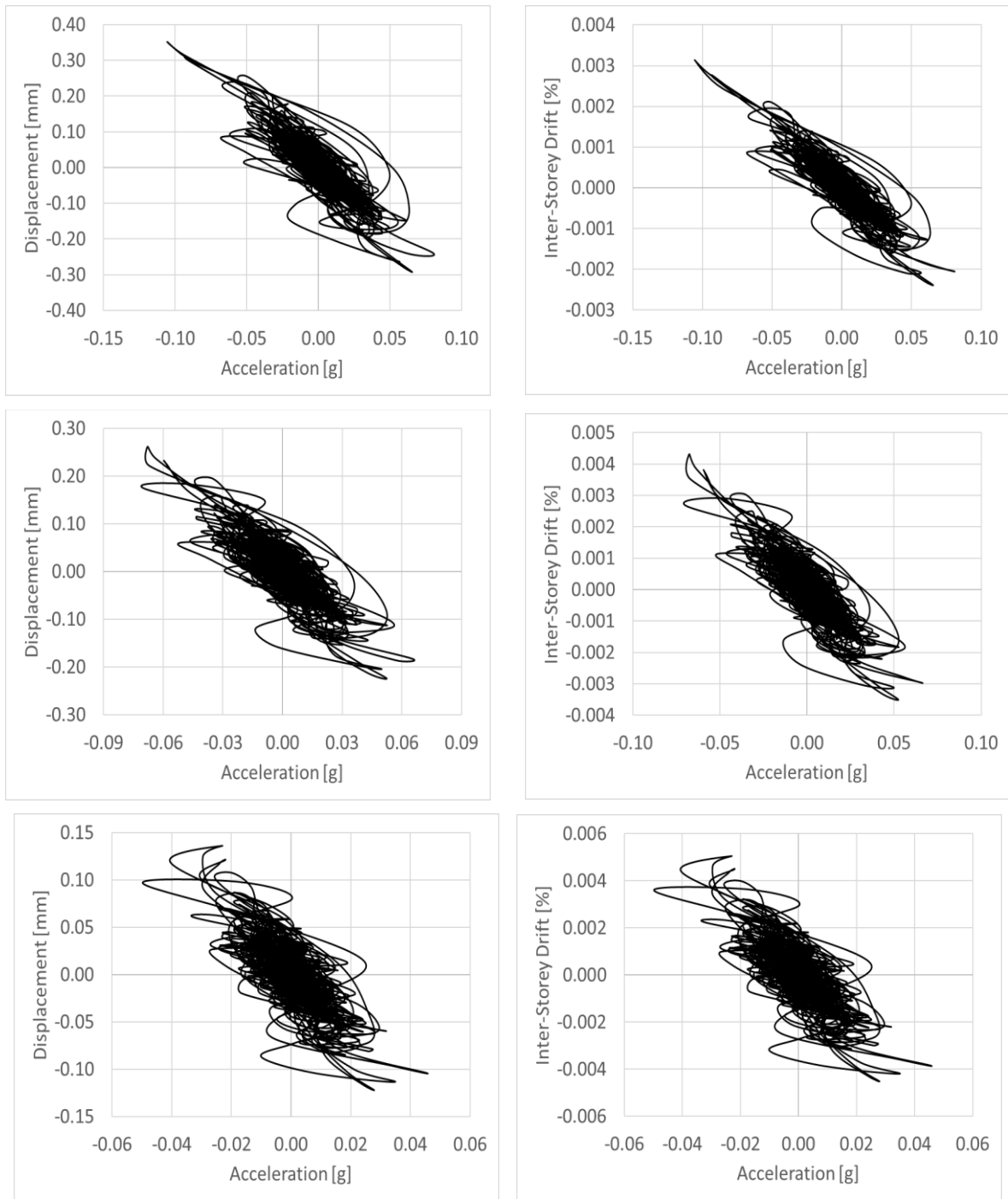


Fig. 5.9 - COMP\_02 displacement vs acceleration envelope (3<sup>rd</sup>, 2<sup>nd</sup> and 1<sup>st</sup> storeys)

Fig. 5.10 - COMP\_02 drift vs acceleration envelope (3<sup>rd</sup>, 2<sup>nd</sup> and 1<sup>st</sup> storeys)

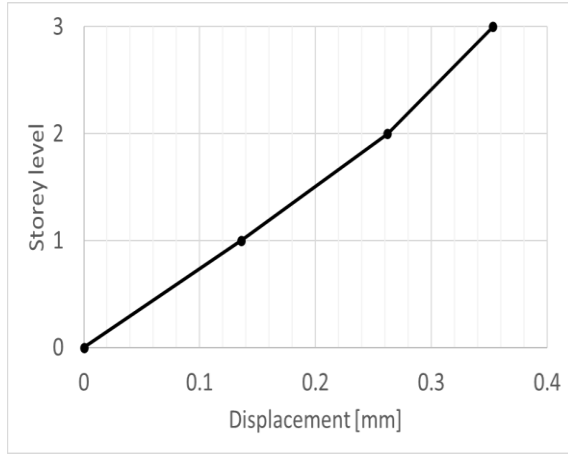


Fig. 5.11 - COMP\_02 maximum displacement profile

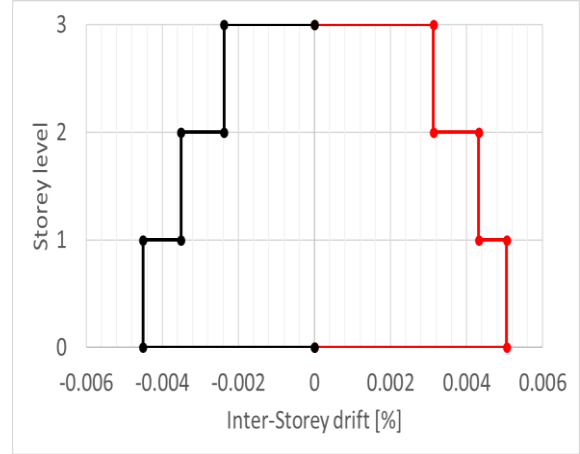
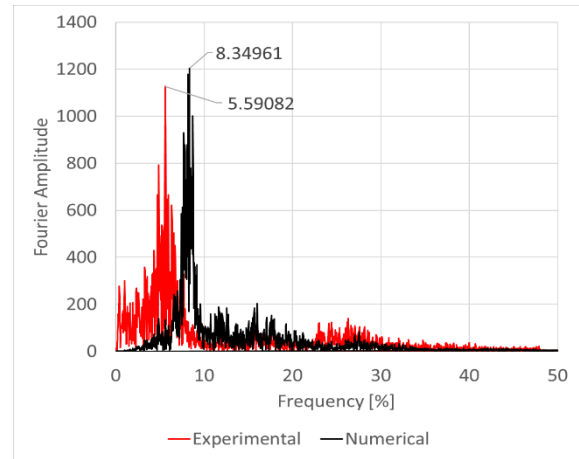
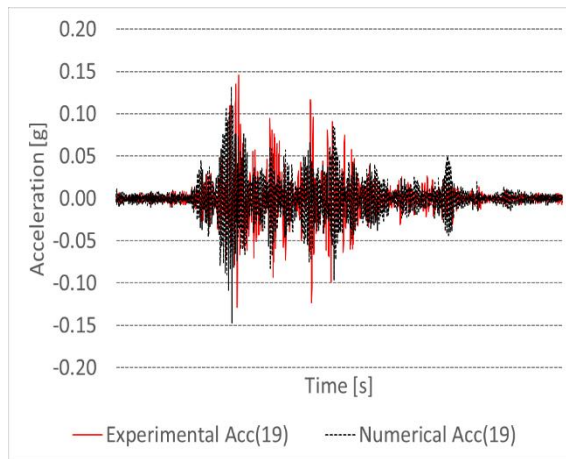


Fig. 5.12 - COMP\_02 maximum drift profile

### 5.3.3. RESULTS OF THE COMP\_03 TRANSIENT ANALYSIS

Figure 5.13 shows the computed and the experimentally measured time histories accelerations at storey levels along with their corresponding Fourier transforms. In Figure 5.14, the computed relation between displacement and acceleration at storey level is depicted through displacement-acceleration hysteresis diagrams. Figure 5.15 provides the inter-storey drift versus acceleration at storey levels for the masonry-infilled RC structure when subjected to the COMP\_03 input ground motion.

Figure 5.16 suggests a linear distribution of displacement along the storeys. This uniform behavior is further confirmed in the inter-storey drift profile presented in Figure 5.17.



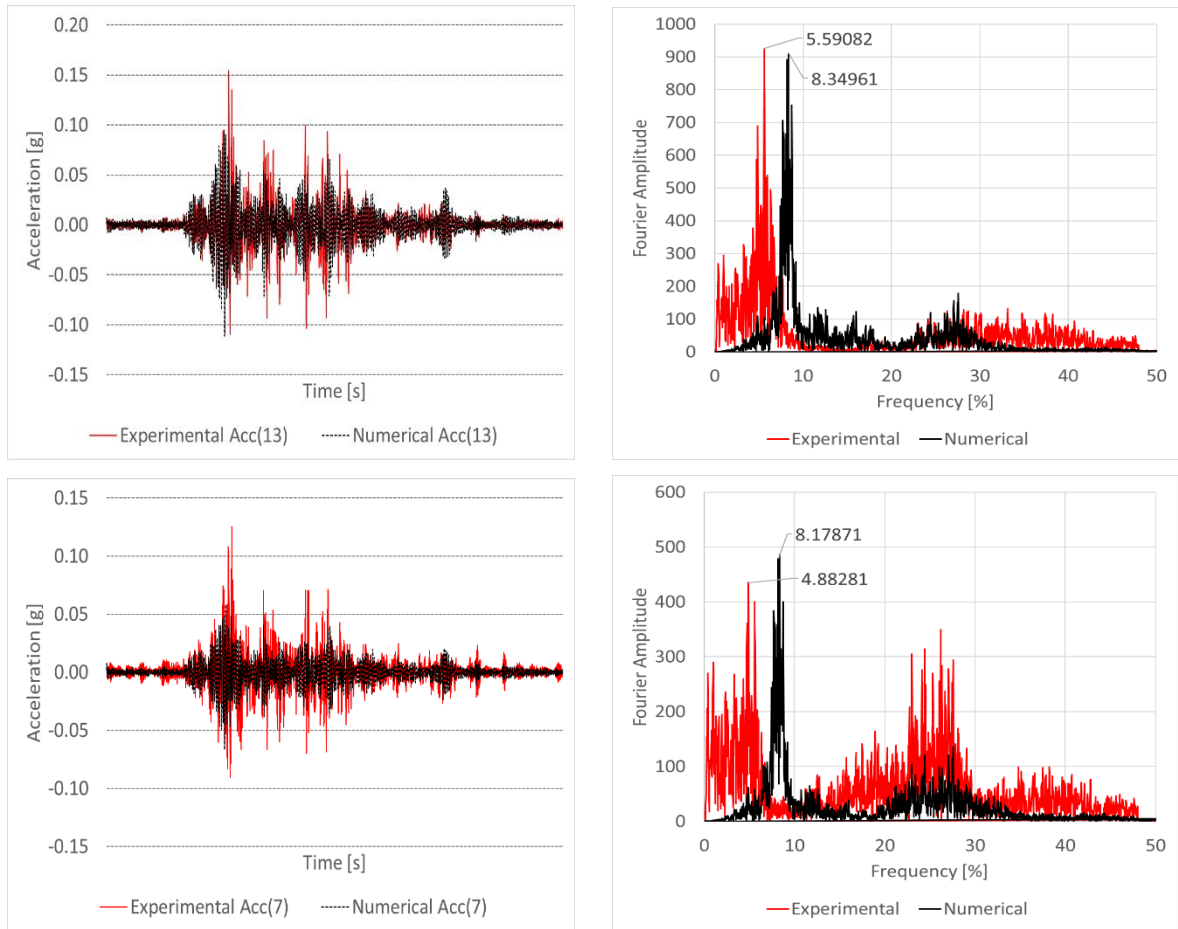
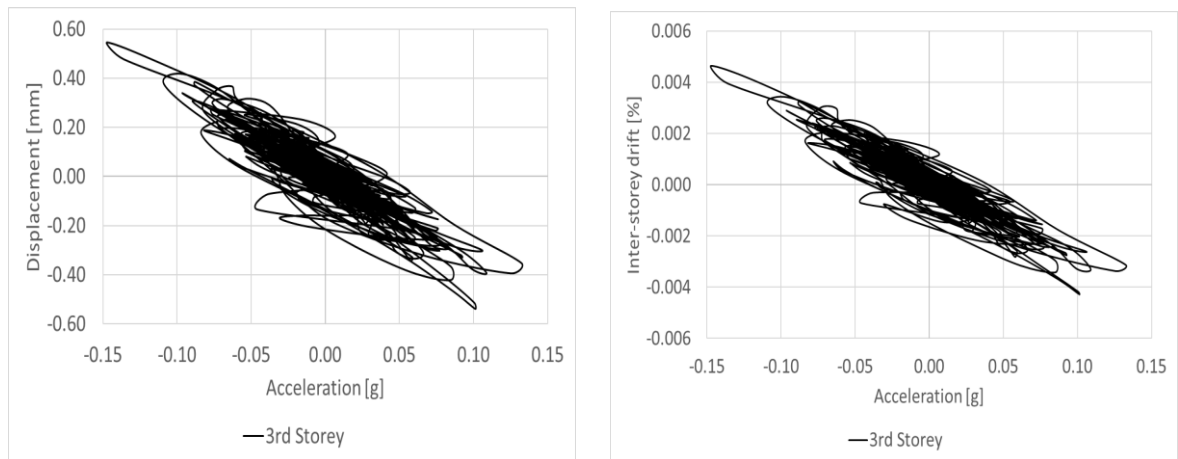


Fig. 5.13 – COMP\_03 storey acceleration time histories and Fourier transform (3<sup>rd</sup>, 2<sup>nd</sup> and 1<sup>st</sup> storeys)



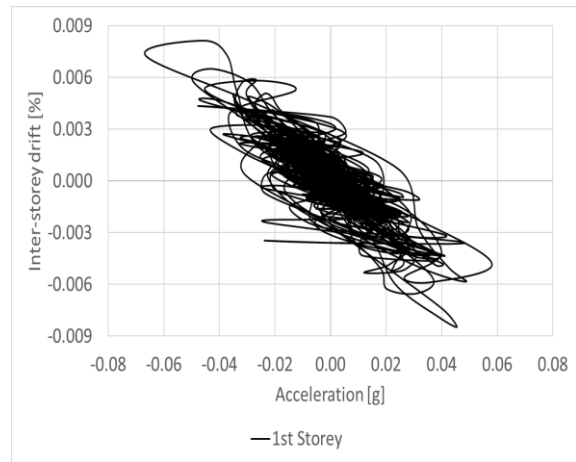
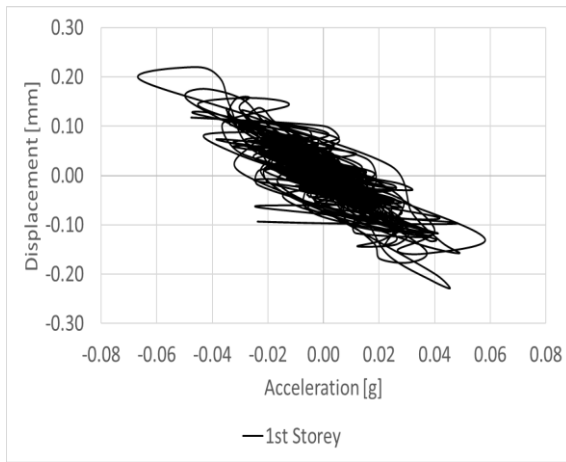
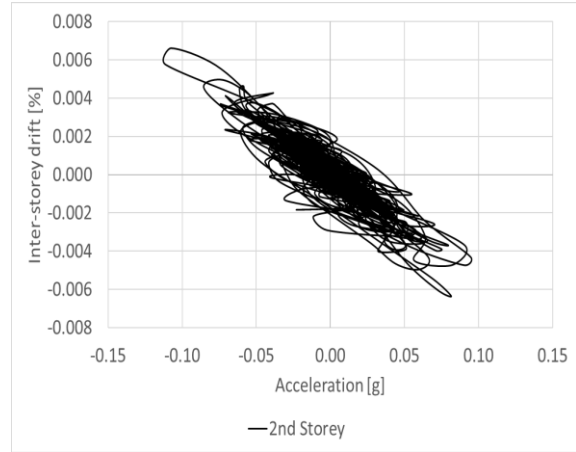
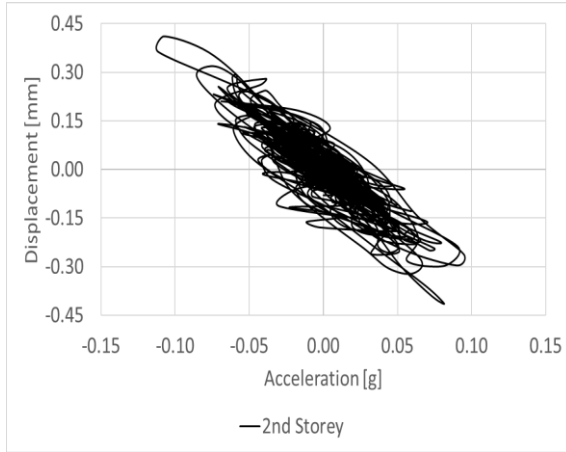


Fig. 5.14 - COMP\_03 displacement vs acceleration envelope (3<sup>rd</sup>, 2<sup>nd</sup> and 1<sup>st</sup> storeys)

Fig. 5.15 - COMP\_03 drift vs acceleration envelope (3<sup>rd</sup>, 2<sup>nd</sup> and 1<sup>st</sup> storeys)

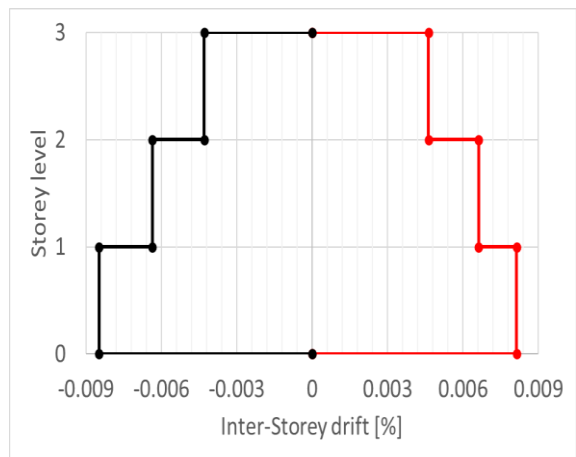
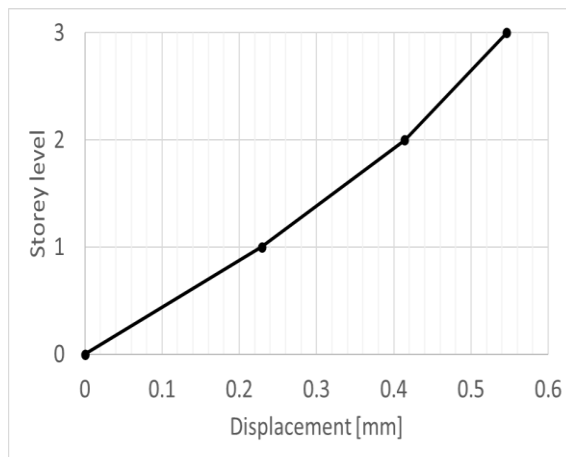


Fig. 5.16 - COMP\_03 maximum displacement profile

Fig. 5.17 - COMP\_03 maximum drift profile

### 5.3.4. RESULTS OF THE COMP\_04 TRANSIENT ANALYSIS

Figure 5.18 shows the computed and the experimentally measured time histories accelerations at storey levels along with their corresponding Fourier transforms. In Figure 5.19, the computed relation between displacement and acceleration at storey level is depicted through displacement-acceleration hysteresis diagrams. Figure 5.20 provides the inter-storey drift versus acceleration at storey levels for the masonry-infilled RC structure when subjected to the COMP\_04 input ground motion.

From the analysis of Figure 5.21 it is evident that the structure exhibits displacement uniformly distributed along the storeys. This uniform behavior is further confirmed in the inter-storey drift profile presented in Figure 5.22.

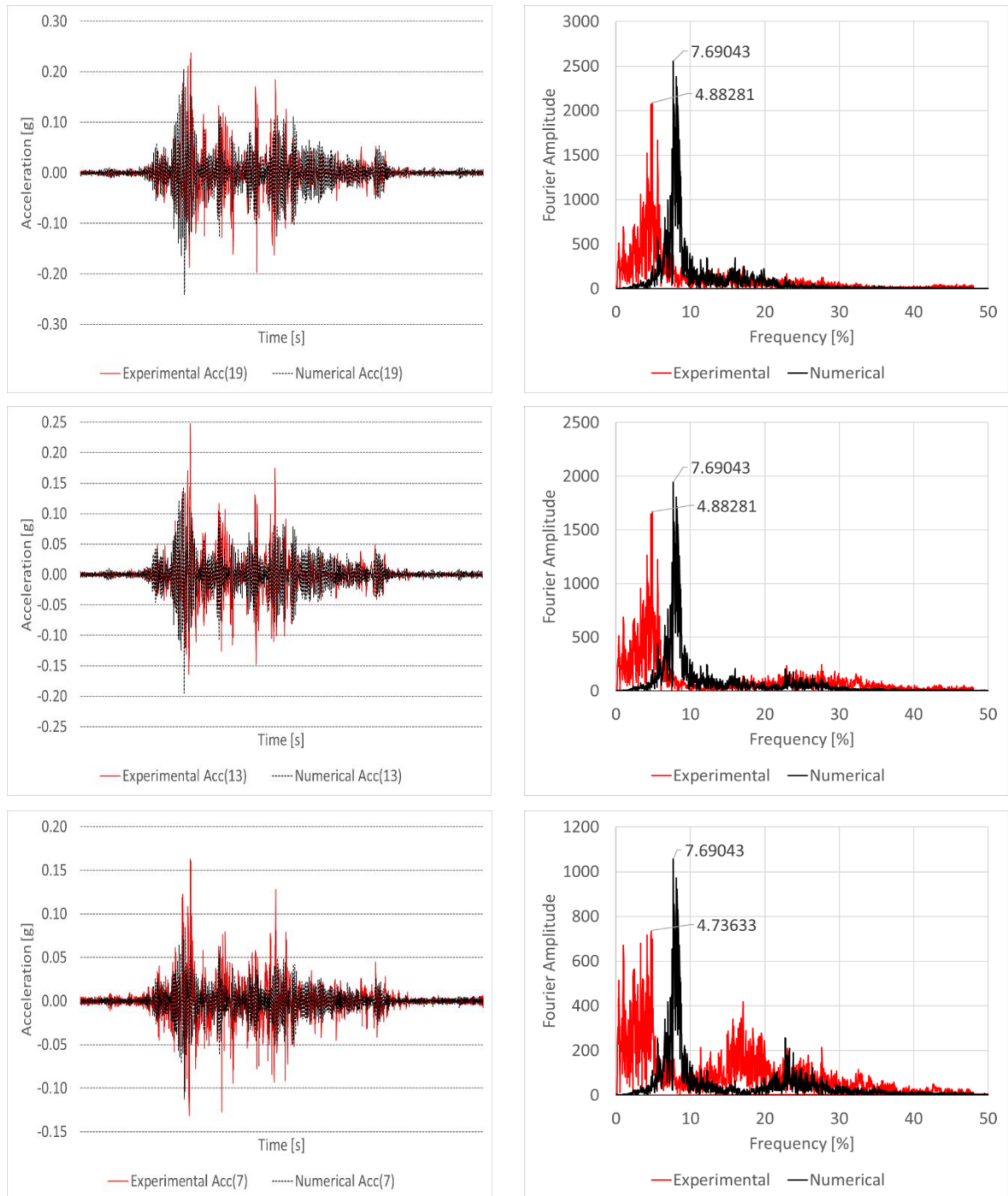


Fig. 5.18 – COMP\_04 storey acceleration time histories and Fourier transform (3<sup>rd</sup>, 2<sup>nd</sup> and 1<sup>st</sup> storeys)

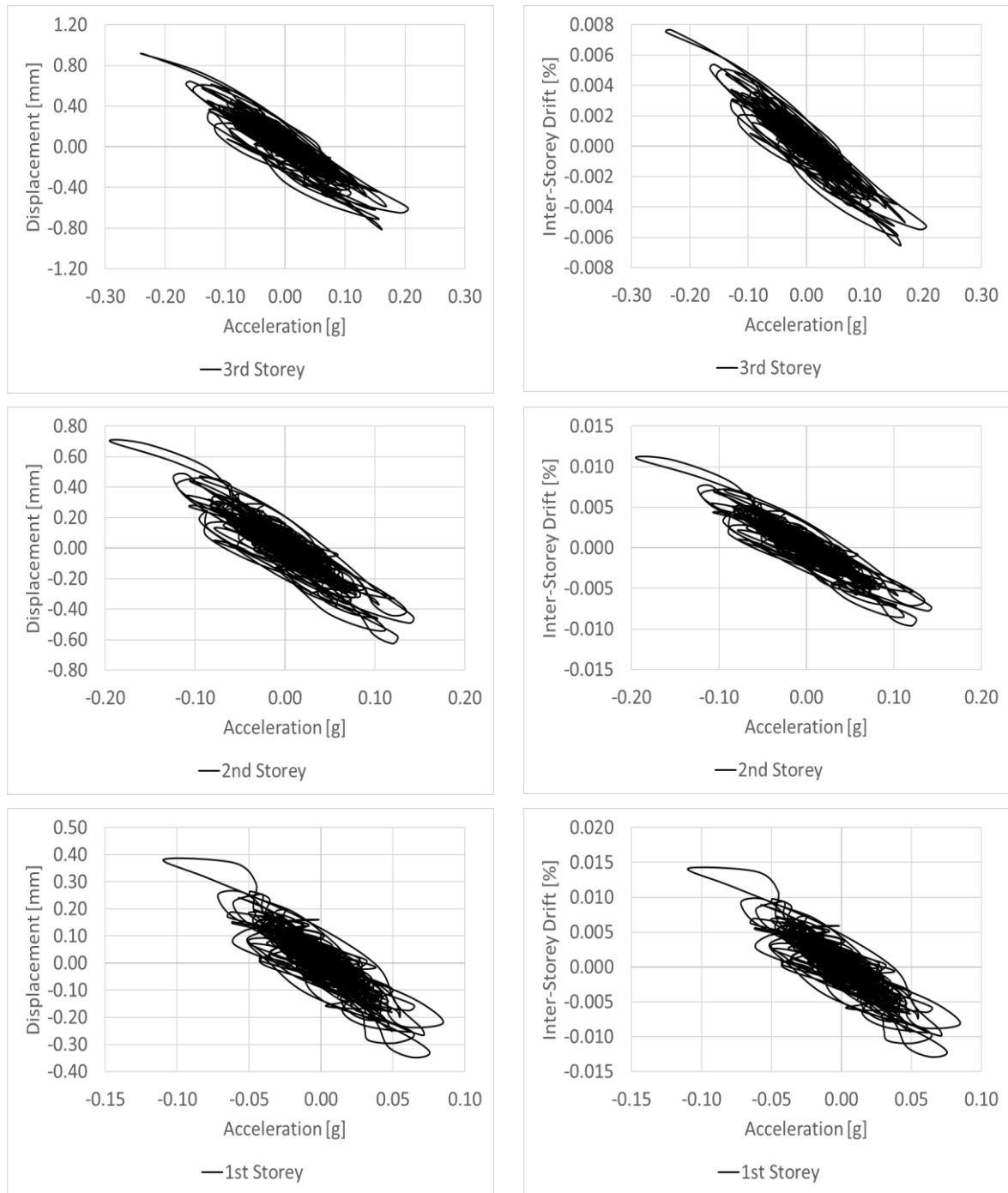


Fig. 5.19 - COMP\_04 displacement vs acceleration envelope (3<sup>rd</sup>, 2<sup>nd</sup> and 1<sup>st</sup> storeys)

Fig. 5.20 - COMP\_04 drift vs acceleration envelope (3<sup>rd</sup>, 2<sup>nd</sup> and 1<sup>st</sup> storeys)

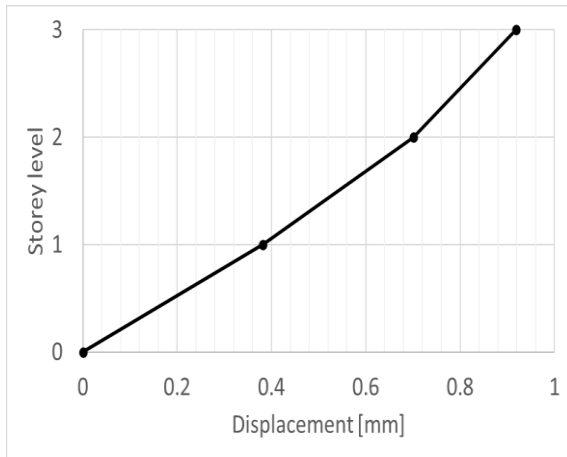


Fig. 5.21 - COMP\_04 maximum displacement profile

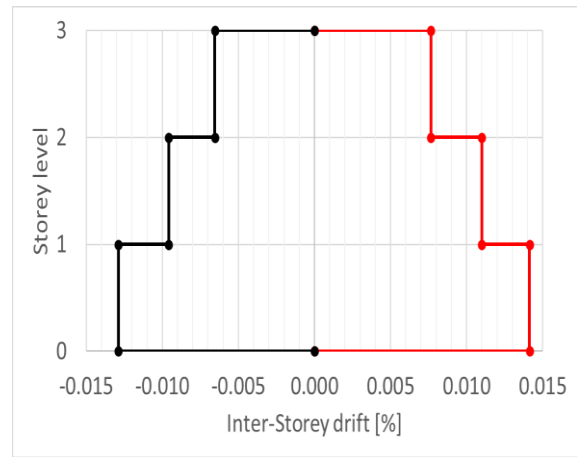
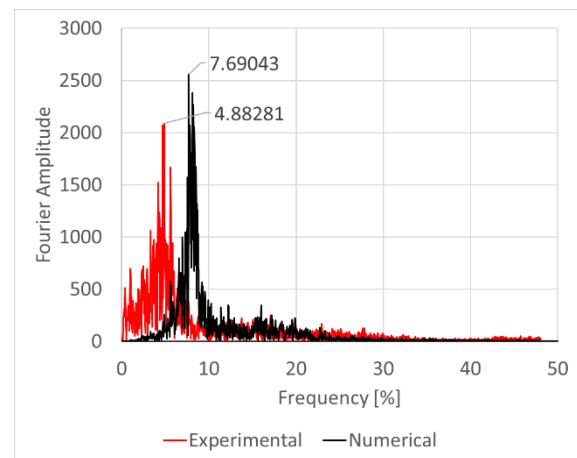
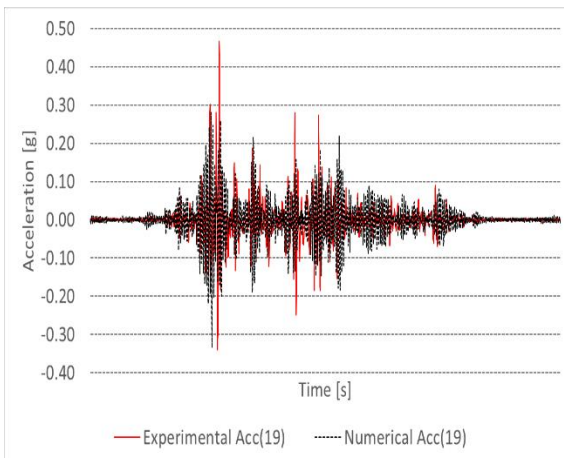


Fig. 5.22 - COMP\_04 maximum drift profile

### 5.3.5. RESULTS OF THE COMP\_05 TRANSIENT ANALYSIS

Figure 5.23 shows the computed and the experimentally measured time histories accelerations at storey levels along with their corresponding Fourier transforms. In Figure 5.24, the computed relation between displacement and acceleration at storey level is depicted through displacement-acceleration hysteresis diagrams. Figure 5.25 provides the inter-storey drift versus acceleration at storey levels for the masonry-infilled RC structure when subjected to the COMP\_05 input ground motion.

From the analysis of Figure 5.26 it can be observed that the first and second storey displacements are 63% and 24% lower than the displacement measured at the third storey. A similar behavior is suggested from the inter-storey drift profile presented in Figure 5.27.



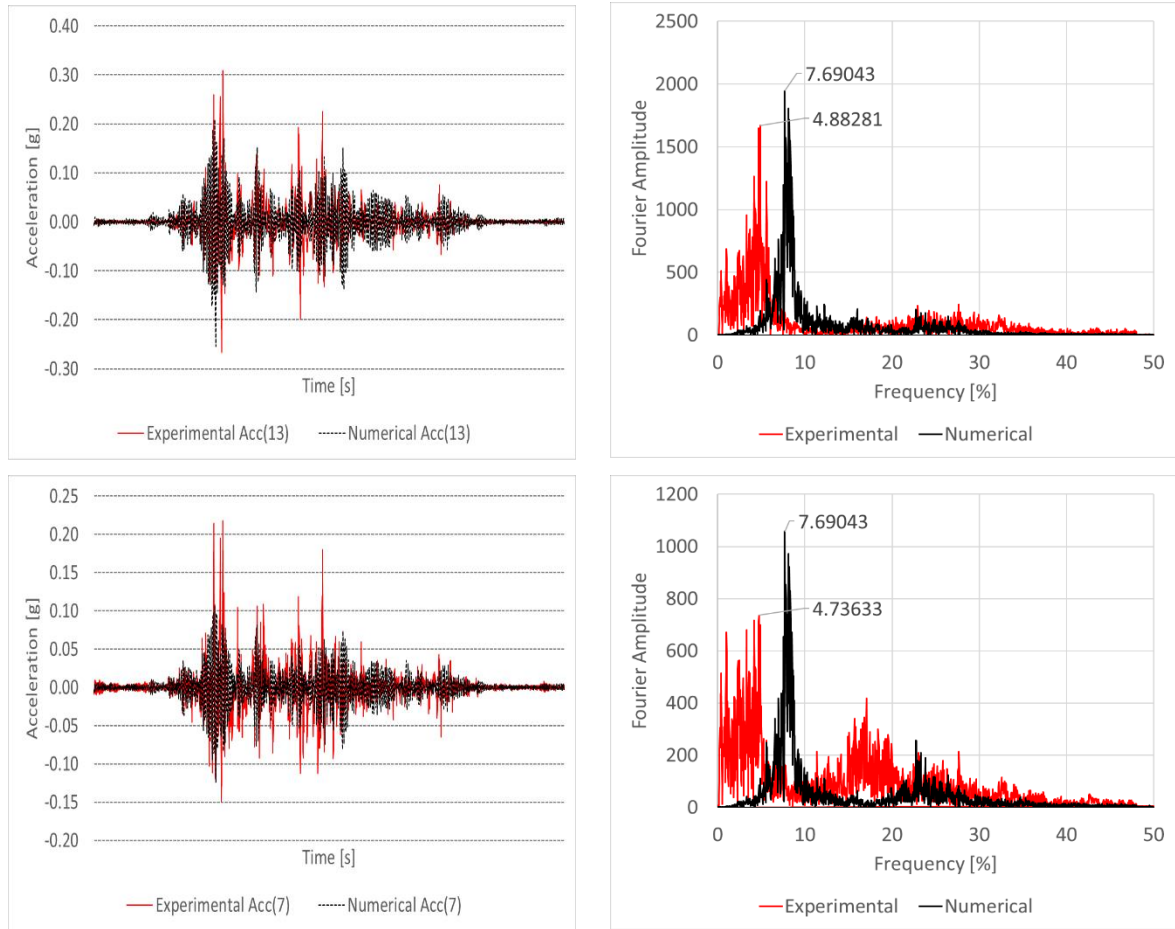
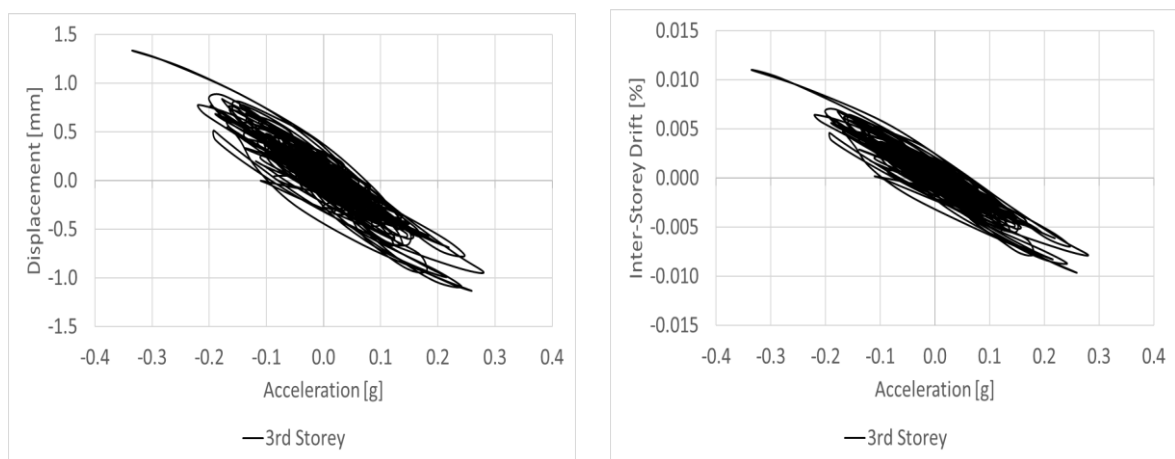


Fig. 5.23 – COMP\_05 storey acceleration time histories and Fourier transform (3<sup>rd</sup>, 2<sup>nd</sup> and 1<sup>st</sup> storeys)



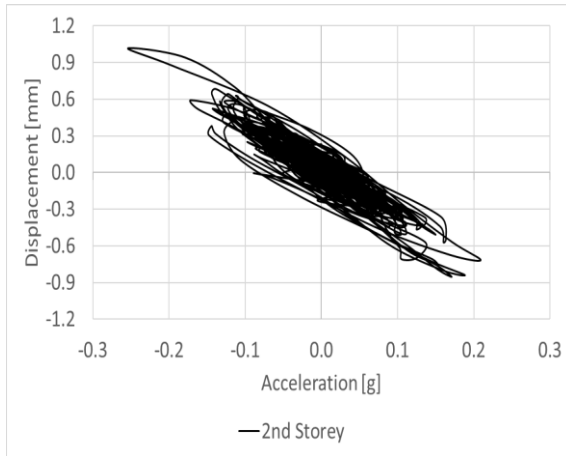


Fig. 5.24 - COMP\_05 displacement vs acceleration envelope (3<sup>rd</sup>, 2<sup>nd</sup> and 1<sup>st</sup> storeys)

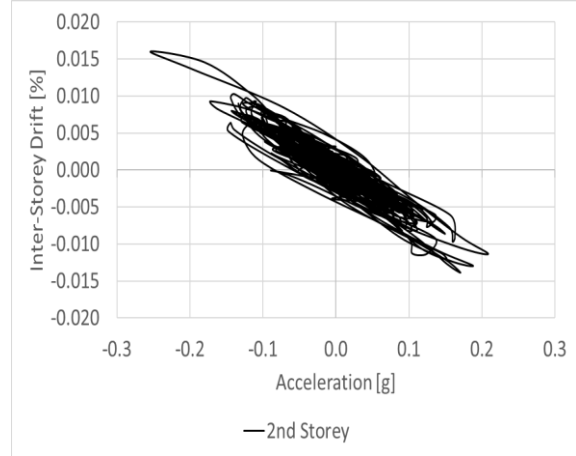


Fig. 5.25 - COMP\_05 drift vs acceleration envelope (3<sup>rd</sup>, 2<sup>nd</sup> and 1<sup>st</sup> storeys)

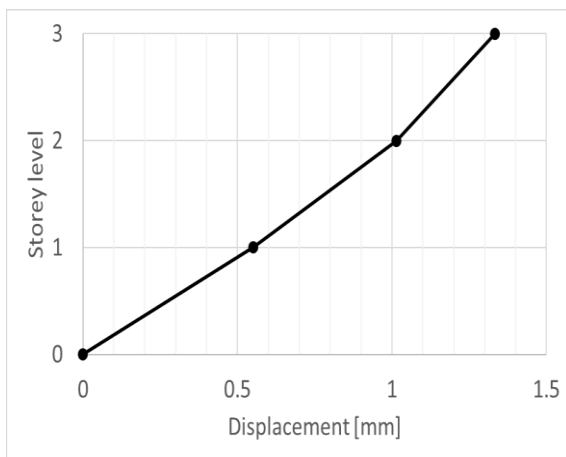
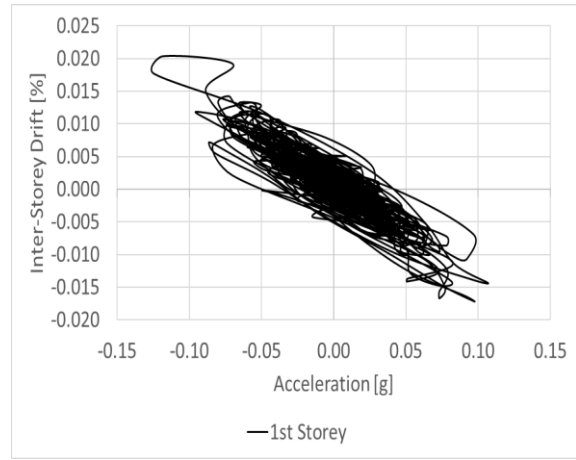
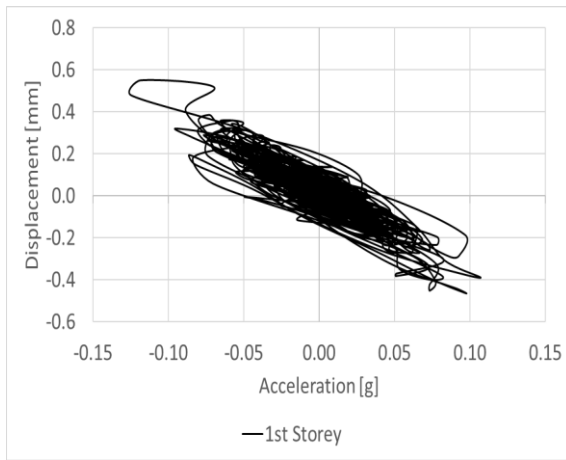


Fig. 5.26 - COMP\_05 maximum displacement profile

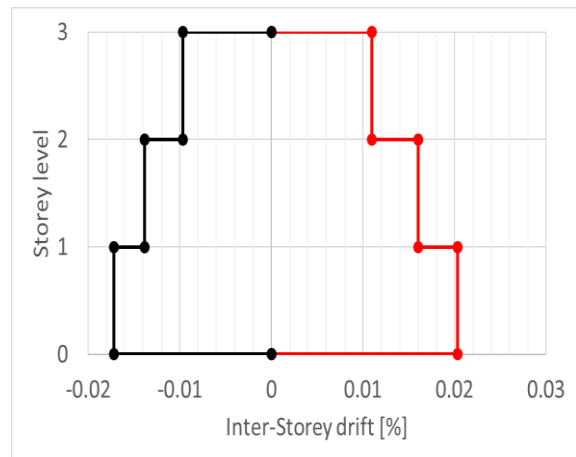


Fig. 5.27 - COMP\_05 maximum drift profile

#### 5.4. DISCUSSION OF THE NUMERICAL RESULTS

In this section, an evaluation is conducted on the seismic vulnerability of the numerical model of the specimen structure that was introduced in Chapter 3. A precise assessment of the structure's vulnerability

to seismic activities enables the identification of potential areas requiring reinforcement at either a global or local (element) level. This study plays a vital role in ensuring that, in the event of future seismic events, the resulting consequences are considerably less severe. Moreover, it primarily aims to enhance the protection of both the structure's occupants and the surrounding areas.

From the comparison between the numerically evaluated results with the experimental ones, the following conclusions can be reached:

- In terms of storey acceleration time histories, it is possible to observe that the accelerations of the 2<sup>nd</sup> and 3<sup>rd</sup> storeys are reproduced reasonably well for low intensity earthquake input motions;
- The acceleration time history for the 1<sup>st</sup> storey cannot be reproduced so well. This might be due to masonry non-linearities that were not triggered in the numerical model. Thus, through the time history analyses, the first storey always has the highest acceleration error;
- From the Fourier transform of acceleration signals, it can be observed that the computed frequency band of the storeys acceleration is in quite good agreement with the experimentally evaluated ones. Overall, the error between frequencies band ranges from 30% to 40%;
- The best match of the model is accomplished in the COMP\_03 transient analysis, where the errors from the computed accelerations in the 3<sup>rd</sup>, 2<sup>nd</sup> and 1<sup>st</sup> storey are equal to 7%, 31% and 55% respectively;
- After the COMP\_05 input ground motion, a substantial increase in the disparity between the numerically evaluated acceleration results and the experimental ones can be noticed;
- Overall, the numerical model reproduces quite well the damage and respective changes in the structural response induced during previous earthquake input motion analyses;
- The closer the measurement point to the top of the structure, the greater the horizontal acceleration during the dynamic tests (Figures 5.3, 5.8, 5.13, 5.18 and 5.23);
- The acceleration measured by the Acc(19) accelerometer is significantly greater, in comparison to the accelerations at (7) and (13) measurement points. In fact, thorough the dynamic analyses the accelerations at measuring points (7) and (13) are consistently 50-65% and 20-30%, respectively, lower than the values recorded at measuring point (19);
- Due to the symmetric characteristics of the specimen structure, as expected, the displacements and corresponding storey drifts are observed to be well distributed through the storeys;
- The horizontal displacement response of measurement point (19) is the largest, (13) is the second largest and (7) is the smallest (as shown by Figures 5.4, 5.9, 5.14, 5.19 and 5.24), which is consistent with the time history acceleration results;
- The maximum inter-storey drift profiles obtained from the time-history analyses (illustrated in Figures 5.6, 5.11, 5.16, 5.21 and 5.26) confirm the tendency of soft-storey mechanisms occurring typically at the first storey of structures. In the can be seen that for the specimen structure the most vulnerable storey is the first one, where the resulting seismic stresses concentrate and, therefore, the storey experiences a higher drift level than the adjacent storeys;
- The increasing inter-storey drift of the specimen structure due to the mainshock shaking and corresponding damages, indicates that the structure might present extreme vulnerabilities to aftershock shakings of low PGA intensity;
- The drift profiles also indicate that the damages resulting from the deformation of masonry infills in one direction does not affect the behavior of the infilled frame in the opposite direction.

- Due to high seismic demands being concentrated at the first storey, retrofitting techniques for the specimen structure should be focused in increasing the load-bearing capacities of the elements present at this storey, guaranteeing an adequate earthquake resisting mechanism. In fact, the strengthening against the brittle behavior of the first storey masonry infill walls is crucial, as it was demonstrated in Chapter 3 that this storey is the first to exhibit damage.

Throughout the time histories analyses, the drift of the top floor is approximately 50% lower than of the first storey, this can be observed in Table 5.3. Therefore, as demonstrated in the experimental tests described in Chapter 3, damage on the first floor develops at an earlier stage than on adjacent storeys. As the intensity of the earthquake input motion increases from a PGA of 0.04 g (COMP\_01) to a three times greater PGA of 0.12 g (COMP\_05), at the first storey the structure experiences a drift six times greater than the one when the structure is subjected to the lowest input ground motion, as illustrated in Figure 5.28. This demonstrates that the demands for slightly higher earthquake input motions results in much larger inter-storey drifts.

Table 5.3 – Numerical results of maximum displacement and maximum storey drift

	COMP_01	COMP_02	COMP_03	COMP_04	COMP_05
1st storey displacement [mm]	0.088	0.136	0.229	0.382	0.55
2nd storey displacement [mm]	0.161	0.262	0.414	0.701	1.015
3rd storey displacement [mm]	0.211	0.353	0.546	0.918	1.333
1st storey drift [%]	0.0033	0.0051	0.0085	0.0142	0.0204
2nd storey drift [%]	0.0025	0.0043	0.0066	0.0110	0.0160
3rd storey drift [%]	0.0017	0.0031	0.0046	0.0077	0.0110

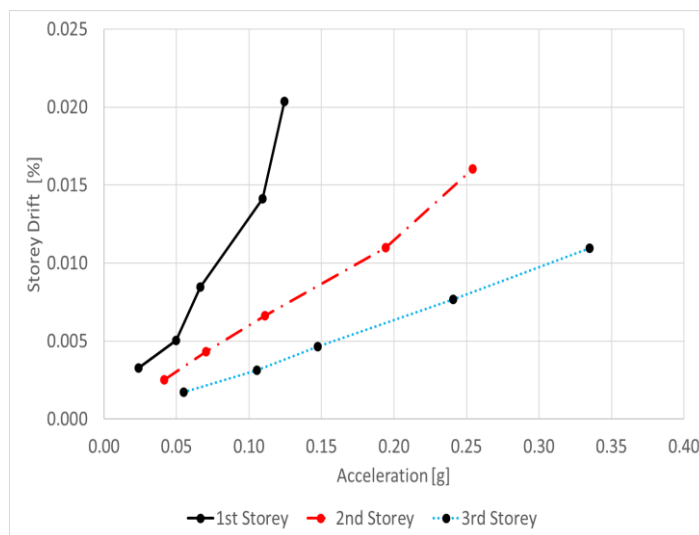


Fig. 5.28 - Evolution of the maximum drift along the y-direction at storey levels

## 5.5. CONTRIBUTION OF MASONRY INFILL WALLS

### 5.5.1. INTRODUCTION

In order to evaluate the seismic vulnerability of buildings, it is imperative to study existing buildings to determine their behavior under seismic actions. However, this process is time-consuming, which, associated to the absence of mandatory legislation, results in a limited understanding of the potential consequences that may arise from medium/high intensity earthquakes.

Throughout this section, a brief investigation will be carried out to evaluate the influence of masonry infill walls on the seismic response of the specimen structure, which was characterized in Chapter 3 of this thesis. This evaluation involves a comparative analysis of results obtained from two different numerical models. The first model, labelled as (IN), incorporates masonry infill walls and is equivalent to the original model of the specimen structure discussed in previous sections, with the results and calibration process presented accordingly. The second model represents the three-story RC bare frame (BF) without any infills. Both original IN and bare frame BF configurations are modeled independently. A brief discussion of the results, for the BF and IN frames, is also performed.

The impact of masonry infills will be assessed through eigen and time-history analyses conducted on the two models. The first analysis allows the verification of how the presence of masonry infills modifies the dynamic characteristics of the structure. The summary results of the time-history analyses of both numerical models (with and without masonry infills) will be presented. Following this analysis, maximum drift and displacement curves for each storey will be evaluated.

### 5.5.2. MODAL PROPERTIES

From the modal analyses performed, the natural frequencies for each model were obtained, as well as the mode shape configurations. In order to provide a good representation of the modes of vibration, the modes characterized by longitudinal translation (along the  $x$ -direction), transversal translation (along the  $y$ -direction), or torsion were denoted as  $x$ ,  $y$ , and  $T$ , respectively.

From the analysis of Table 5.4 and the corresponding configurations for the mode shapes, it is evident that, in comparison with the BF model, the presence of masonry infill walls in the full height of the structure changed the direction of the first mode shape. Particularly, it shifted from a translational mode along the  $y$  direction, to a translational mode along the  $x$  direction.

Furthermore, it is worth noting that the presence of masonry infill walls leads to a considerable increase in the natural frequencies relatively to the values obtained from the BF model, circa of 1.1 times for the 1<sup>st</sup> mode, 3.26 times for the 2<sup>nd</sup> mode, 2.15 times for the 3<sup>rd</sup> mode, circa of 1.65 times for the 4<sup>th</sup> and 5<sup>th</sup> modes, and 2.65 times for the 6<sup>th</sup> mode. This confirms the significant increment of the system stiffness due to masonry infill walls, resulting in higher natural oscillation periods, specially if positioned on the first storey.

Table 5.4 – Computed modal properties for the IN and BF models

Mode	IN Model		BF Model	
	Direction	Natural frequency [Hz]	Direction	Natural frequency [Hz]
1 <sup>st</sup> Mode	$x$	1.77	$y$	1.63
2 <sup>nd</sup> Mode	$x$	5.73	$x$	1.76

3 <sup>rd</sup> Mode	T	5.92	T	2.75
4 <sup>th</sup> Mode	y	8.49	y	5.16
5 <sup>th</sup> Mode	x	9.52	x	5.82
6 <sup>th</sup> Mode	y	26.19	x	9.85

5.5.3. DYNAMIC ANALYSIS

Figures 5.29 and 5.30 depict the evolution of displacement versus acceleration at different storey levels for the IN and BF models, respectively. The relation between inter-storey drift and acceleration at storey levels, represented by drift-acceleration hysteresis diagrams, are shown in Figures 5.31 and 5.32 for both configurations.

From the analysis of the inter-storey drift profiles, it becomes evident that the BF model exhibits a significant concentration of drift on the second storey, indicating the development of the soft-storey mechanism at this particular level. On the contrary, in the IN model, the inter-storey drift is concentrated on the first storey. Significant differences can be observed in the storey drift values between the two models. Specifically, at the first storey, the BF model exhibits inter-storey drift values that are 13 to 20 times greater than those obtained from the IN model. However, in the remaining storeys (2<sup>nd</sup> and 3<sup>rd</sup>), this difference almost doubles and, consequently, the BF model experiences inter-storey drifts that are 23 to 40 times higher.

Both models exhibit linear distribution of displacements at storey levels. Furthermore, the displacement results for the IN model are more conservative compared to the values obtained from the BF model. Overall, the IN model experiences displacements approximately 90% lower in comparison to those experienced by the BF model.

In Figures 5.29 and 5.30, it is evident that the presence of masonry infill walls restricts the accelerations experienced by the structure, particularly at the first storey, where the infills led to a reduction in acceleration ranging from 25% to 47%. This reduction is comparatively less significant for the storeys above, with the second storey experiencing a reduction in acceleration ranging from 10% to 25%, and the third storey ranging from 3% to 18%. Therefore, the numerical analysis confirms that the presence of masonry infill walls provides protection to the RC structure against low-intensity earthquake inputs.

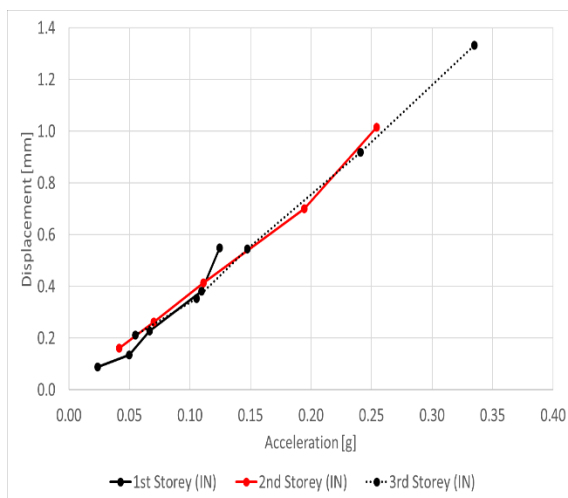


Fig. 5.29 – Displacement versus acceleration at storey levels for the IN model

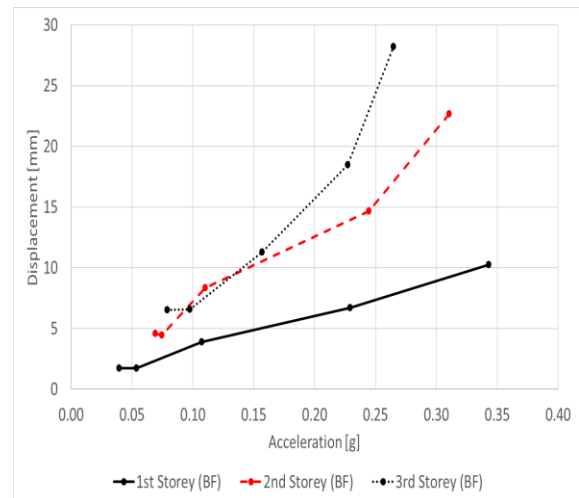


Fig. 5.30 – Displacement versus acceleration at storey levels for the BF model

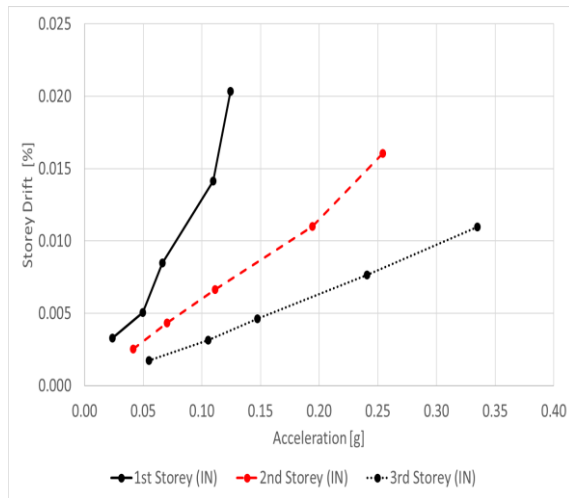


Fig. 5.31 – Drift-acceleration hysteresis diagram at storey levels for the IN model

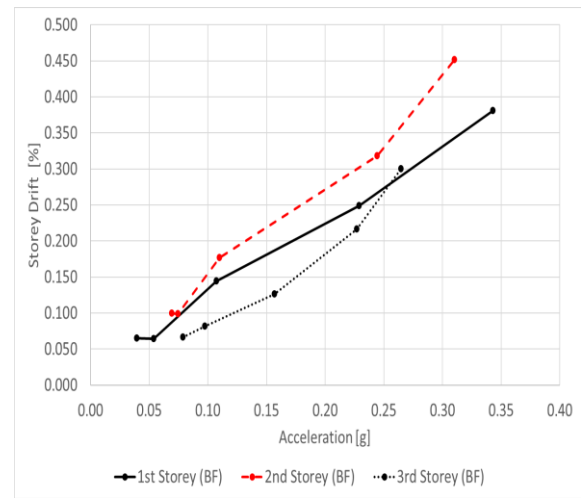


Fig. 5.32 – Drift-acceleration hysteresis diagram at storey levels for the BF model



# 6

## CONCLUSION AND FUTURE WORKS

### 6.1. INTRODUCTION

In this chapter it will be presented the most important aspects to highlight of the work carried out, as well as some conclusions that have been drawn. Additionally, some suggestions for possible future works will be provided in the final section in order to further expand and build upon the findings derived from this study.

### 6.2. CONCLUDING REMARKS

The theoretical and analytical works subject of this master's thesis were carried out with the aim of monitoring the structural behavior of an infilled RC frame when subjected to increasing intensity earthquake input motions and evaluating its seismic vulnerabilities.

For this manner, it was reviewed in Chapter 2 the possible damages that seismic actions might cause in structures, specially the damage and corresponding structural behavior changes in masonry-infilled RC frames. The recent post-earthquake field reports presented in the second chapter highlight that by far the major damages and collapses of structures and human losses are due to detailing deficiencies and the non-ductility of existing RC buildings. Frame type RC structures were the primary structural system in many southern European regions, commonly adopted until the 1970's. The majority of these structures were designed following old design codes, resulting in inadequate earthquake resistance systems. Most of them were constructed with ground storeys with big openings. Moreover, the most commonly reported failures mechanisms (soft-storey and short-column) in earthquake-prone areas were described. It was discussed the primarily influencing aspects that trigger these mechanisms, namely structural and non-structural elements with different lengths at the same storey level and their irregular distribution in elevation. Despite the strict earthquake-resistant requirements from modern seismic codes, the well-known mistakes of the past were observed to still occur in the construction and design of most current structures.

A brief description is also presented in Chapter 2 for the development and implementation of seismic retrofitting solutions in existing buildings. As stated in the chapter, in order to correctly rehabilitate buildings, the intervention strategy should be guided by results of detailed evaluation of the structure's seismic performance. These retrofitting approaches are focused on the strengthening of the structural system (global intervention) or of members (local intervention). In the majority of the cases, these two interventions are combined.

The study carried out in this master's thesis focus on a three-storey masonry-infilled RC structure designed by the ISAAC in order to investigate the efficiency of an active control seismic damping system. The complex experimental campaign was conducted in the EUCENTRE laboratory facility. The extensive campaign consisted of twelve dynamic tests of increasing earthquake intensity, using as reference the Irpinia earthquake record. The obtained results from the shaking table tests on the full-scale structure produced a vast amount of data, useful to calibrate the methodologies and assumptions of the nonlinear numerical model that is used for the assessment of the seismic fragility of the specimen structure.

It is known the significant impact caused by infills on the structural behavior and on the natural frequencies of buildings. The understanding of the impact of masonry model parameters on the structural behavior was achieved through manual calibration of the material models' parameters, coupled with an investigation into prior analytical research on masonry-infilled frames with similar characteristics.

Comparing the natural frequencies experimentally measured before the dynamic earthquake tests to the frequencies obtained with the numerical model, a very good agreement was observed. Thus, the eigen analysis results served as an initial confirmation of the numerical model capacities in predicting the real stiffness of the specimen structure. In fact, the numerical model reproduces quite well the expected dynamic properties of the specimen structure, the errors for the computed natural frequencies from the first six modes of vibration are below 15%.

The seismic vulnerability assessment of this specimen structure was performed thorough nonlinear time-history analyses of increasing PGA in a numerical model based on FEs. This evaluation was mainly accomplished by comparing the different numerical results, as the maximum displacement and maximum inter-storey drift profiles, the time-history accelerations, natural frequencies and mode shapes.

The numerical results from time-history analyses were observed to be extremally sensitive to the material parameters as the intensity of the earthquake input motion increased. Uncertainties related to the modeling approach and material parameters, especially in heterogeneous materials as masonry, significantly increased the complexity of the model. Particularly, in order to accurately reproduce the structural behavior of the specimen structure for shaking-table tests of higher PGA, a more extensive investigation of the impact of each model parameter on the global response would be necessary. Therefore, owing to some limitations of this master's thesis, it was expected that for higher input motions, PGA above 0.12 g, the validity of the model would decrease dramatically.

The numerically evaluated results have shown the susceptibility of RC structures typically developing soft-storey mechanisms at the first storey, owing to the high seismic demands and, consequently, inter-storey drift levels that are concentrated at this storey. Therefore, in structures with big openings at a specific storey, mitigation policies for this mechanism and corresponding modes of failure (column failure in shear or bending) are of crucial importance, as these elements have insufficient strength to support the totality of the lateral loads. The results also confirm the importance of adequate detailing and shear reinforcement at the base of the columns in order to avoid the development of premature shear cracks on these elements.

Regarding the important impact of masonry infill walls in the structural behavior of buildings under seismic actions. It was observed through a brief analysis the development of soft-storey mechanisms in both original (IN) and bare frame (BF) models. While in the BF model this mechanism was observed to occur on the second storey, the presence of masonry infills in the IN model shifted the mechanism to the first storey. Moreover, the stiffness increment introduced by masonry infills is reflected in the natural frequencies. Specially, the natural frequencies from the IN model were 2 to 3 times greater than the

values from the BF model. This is also observed in the drift profiles, as the presence of infill walls reduced the inter-storey drifts of the structure up to 40 times, depending on the storey.

The results of the time-history analyses confirm the reduction of the structure's ductility and the stiffness increase due to the presence of masonry infills, as indicated in the literature. No significant differences in the distribution of displacements through the storeys were observed between the two models. This is particularly due to the fact that for the IN model the masonry infill walls were uniformly distributed (in plan and in elevation).

### **6.3. FUTURE WORKS**

Following the conclusion of this study, it is presented the most relevant suggestions for being developed in the future:

- Investigation of possible retrofit approaches;
- Numerical modeling of strengthening solutions;
- Economically evaluation of a strengthening solution for the building using fiber reinforcing materials;
- Experimental campaigns in order to validate the adopted strengthened model and assess the efficiency of different retrofit techniques;
- Investigations aiming at parameter calibration for improving the structural response predicted by the numerical model.



**BIBLIOGRAPHIC REFERENCES**

- [1] Angel, R. *Behavior of Reinforced Concrete Frames with Masonry Infills*. PhD Thesis, University of Illinois at Urbana-Champaign, 1994.
- [2] Mehrabi, A., et al. *Experimental Evaluation of Masonry-Infilled RC Frames*. Journal of Structural Engineering ASCE, 1996, 122(3):228–37.
- [3] Furtado, A., De Risi, M. *Recent Findings and Open Issues Concerning the Seismic Behaviour of Masonry Infill Walls in RC Buildings*. Hindawi: Advances in Civil Engineering, 2020. <https://doi.org/10.1155/2020/9261716>.
- [4] Gesualdi, G., et al. *Seismic Performance of RC Frame Buildings Accounting for the Out-of-Plane Behavior of Masonry Infills*. Bulletin of Earthquake Engineering, 2020, 18:5343-5381.
- [5] Furtado, A., et al. *A Review of the Performance of Infilled RC Structures in Recent Earthquakes*. Applied Sciences, 2021, 11(13):5889. <https://doi.org/10.3390/app11135889>.
- [6] UN Office for the Coordination of Humanitarian Affairs (UNOCHA). *Türkiye: 2023 Earthquakes Situation Report No. 15*. UNOCHA, 2023.
- [7] Varum, H. *Seismic Assessment, Strengthening and Repair of Existing Buildings*. PhD Thesis, University of Aveiro, 2003.
- [8] Fardis, M. *Seismic Assessment and Retrofit of RC Structures*. ECEE, Paris, France, Invited lecture (ISBN 90 5809 027 2), 1998.
- [9] Petracca, M., et al. *Multiscale Computational First Order Homogenization of Thick Shells for The Analysis of Out-Of-Plane Loaded Masonry Walls*. Computer Methods in Applied Mechanics and Engineering, 2017, 315:273-301.
- [10] Benessia, A., De Marchi, B. *When The Earth Shakes ... and Science with It. The Management and Communication of Uncertainty in The L'Aquila Earthquake*. Futures, 2017, 91:35-45. <https://doi.org/10.1016/j.futures.2016.11.011>.
- [11] Pondrelli, S., et al. *Seismic Moment Tensors of The April 2009, L'Aquila (Central Italy), Earthquake Sequence*. Geophysical Journal International, 2009, 180(1):238-242.
- [12] Marazzi, F., et al. *The L'Aquila (Italy) Earthquake of 6 April 2009: Report and Analysis from A Field Mission*. Publication Office of the European Union (JRC62359), 2011. <https://dx.doi.org/10.2788/188>.

- [13] Liel, A., Lynch, K. *Vulnerability of Reinforced-Concrete-Frame Buildings and Their Occupants in The 2009 L'Aquila, Italy, Earthquake*. Natural Hazards Review, 2012, 13(1):11-23. [http://dx.doi.org/10.1061/\(ASCE\)NH.1527-6996.0000047](http://dx.doi.org/10.1061/(ASCE)NH.1527-6996.0000047).
- [14] Leti, M., Bilgin, H. *Performance of RC and Masonry Structures During 2019 Durrës Earthquake*. Civil Engineering Beyond Limits, 2021.
- [15] Andonov, A., et al. *EERI Earthquake Reconnaissance Report - M6.4 Albania Earthquake on November 26, 2019*. EERI, 2022.
- [16] International Federation of Red Cross and Red Crescent Societies (IFRC). *Albania: Earthquake – Final Report (MDRAL008)*. Reliefweb, 2021.
- [17] McKenney, C. (2019). *Reconnaissance Observation Report Albania M6.4 Earthquake on November 26, 2019*.
- [18] European Committee of Standardization (CEN). *Eurocode 8: Design of structures for earthquake resistance – Part 1: General rules, seismic actions and rules for buildings*. Brussels, EN 1998-1, 2004.
- [19] Marinkovic, M., et al. *Performance of RC Cast-in-Plane Buildings During The November 26, 2019 Albania Earthquake*. Bulletin of Earthquake Engineering, 2022, 20:5427-5480.
- [20] Koçer, M., Ünal, A. *RC Structural Damages Observed After 30.10.2020 Seferihisar-Izmir Earthquake and Analytical Evaluation Existing Sample RC Buildings*. Research Square, 2022. <https://doi.org/10.21203/rs.3.rs-1180428/v1>.
- [21] Karakale, V., İpek, C. *Damage Analysis of Structural Elements Affected by Earthquake: Case Study of Izmir Earthquake*. 6<sup>th</sup> International Conference on Earthquake Engineering and Seismology, 2020.
- [22] Emre, Ö., et al. *Active Fault Map of Turkey with and Explanatory Text*. General Directorate of Mineral Research and Exploration, Special Publication Series-30, 2013.
- [23] Mehrabi, A., et al. *Performance of Masonry-infilled R/C Frames under In-plane Lateral Loads*. Report N°: CU/SR-94-6, Department of Civil, Environmental, and Architectural Engineering, University of Colorado, Boulder, CO, U.S.A., 1994.
- [24] Cardone, D., Perrone, G. *Damage and Loss Estimation of Pre-70 Reinforced Concrete Frame Buildings with FEMA P-58: A Case Study*. Journal of Earthquake Engineering, 2016, 21:23–61. <http://dx.doi.org/10.1080/13632469.2016.1149893>.
- [25] NTC2008. *Decreto Ministeriale 14 Gennaio 2008 - Norme Tecniche per Le Costruzioni NTC2008*. Supplemento ordinario n. 30, Gazzetta Ufficiale 4 febbraio 2008, n 29.

- [26] Zahra, T., Dhanasekar, M. *A Generalised Damage Model for Masonry Under Compression*. International Journal of Damage Mechanics, 2016.
- [27] Anthoine, A. *Derivation of The In-Plane Elastic Characteristics of Masonry Through Homogenization Theory*. Journal of Solids Structures, 1995, 32(2):137–163.
- [28] Zucchini, A., Lourenço, P. *Mechanics of Masonry in Compression: Results from a Homogenisation Approach*. Computers and Structures, 2007, 85:193-204.
- [29] Basha, S., Kaushik, H. *Behavior and Failure Mechanisms of Masonry-Infilled RC Frames (in Low-Rise Buildings) Subject to Lateral Loading*. Engineering Structures, 2016, 233-245.
- [30] Asteris, P., Cotsovos, D. *Numerical Investigation of The Effect of Infill Walls on The Structural Response of RC Frames*. The Open Construction and Building Technology Journal 2012a; 6:164–81.
- [31] Asteris, P., et al. *Mathematical Micromodeling of Infilled Frames: State of The Art*. Engineering Structures, 2013a; 56:1905–21.
- [32] Murty, C., Jain, S. *Beneficial Influence of Masonry Infills on Seismic Performance of RC Frame Buildings*. 12th World Conference on Earthquake Engineering, 2000, paper n° 1790.
- [33] Panagiotakos, T., Fardis, M. *Seismic Response of Infilled RC Frames Structures*. Proceedings of the 11th world conference on earthquake engineering, Acapulco, México, 1996, Paper N° - 225.
- [34] Verderame, G., et al. *Experimental Tests on Masonry-Infilled Gravity- and Seismic-Load Designed RC Frames*. In Brick and Block Masonry: Trends, Innovations and Challenges-Proceedings of the 16th International Brick and Block Masonry Conference, IBMAC, 2016, 1349-1358.
- [35] De Risi, M., et al. *In-Plane Behaviour and Damage Assessment of Masonry Infills with Hollow Clay Bricks in RC Frames*. Engineering Structures, 2018, 168:257–275.
- [36] Fardis, M. *Seismic Design, Assessment and Retrofitting of Concrete Buildings, Based on EN-Eurocode 8*. Geotechnical, Geological and Earthquake Engineering, Springer, 2009.
- [37] Markulak, D., et al. *Cyclic Testing of Single Bay Steel Frames with Various Types of Masonry Infill*. Engineering Structures, 2016, 51:267-277.
- [38] Chiou, T.C., Hwang, S.J. *Tests on Cyclic Behavior of Reinforced Concrete Frames with Brick Infill*. Earthquake Engineering Structural and Dynamics, 2015, 44(12):1939–1958.
- [39] Christiana, A., et al. *Numerical Study of the Seismic Retrofitting of Masonry-Infilled RC Frames with Openings Using TRM*. Earthquake Engineering Structural and Dynamics, 2022.
- [40] Kakaletsis, D., Karayannis, C. *Experimental Investigation of Infilled R/C Frames with Eccentric Openings*. Structural Engineering and Mechanics, 2007.

- [41] Kakaletsis, D., Karayannis, C. *Influence of Masonry Strength and Openings on Infilled R/C Frames Under Cycling Loading*. Journal of Earthquake Engineering 2008; 12 (2):197–221.
- [42] Mansouri, A., et al. *Analytical Estimation of Lateral Resistance of Low-Shear Strength Masonry Infilled Reinforced Concrete Frames with Openings*. The Structural Design of Tall and Special Buildings, 2018.
- [43] Mallick, D., Garg, R. *Effect of Openings on the Lateral Stiffness of Infilled Frames*. Proceedings of the Institution of Civil Engineers, 1971, 49:193–209.
- [44] Asteris, P., et al. *Masonry Infilled Reinforced Concrete Frames with Openings*. 3<sup>rd</sup> International Conference on Computational Methods in Structural Dynamics and Earthquake Engineering, 2011a.
- [45] Asteris, P., et al. *Mathematical Macromodeling of Infilled Frames: State of the Art*. Journal of Structural Engineering, 2011b.
- [46] Asteris, P., et al. *Modeling of Infilled Frames with Openings*. The Open Construction and Building Technology Journal, 2012b, 6(1):81-91. <http://dx.doi.org/10.2174/1874836801206010081>.
- [47] Cardone, D., Perrone, G. *Developing Fragility Curves and Loss Functions for Masonry Infill Walls*. Earthquakes and Structures, 2015, 9(1):257–279.
- [48] Di Domenico, M. *Out-of-Plane Seismic Response and Modelling of Unreinforced Masonry Infill Walls*. Ph.D. Thesis, University of Naples Federico II, 2018.
- [49] De Risi, M., et al. *Experimental investigation on the Influence of the Aspect Ratio on the In-Plane/Out-of-Plane Interaction for Masonry Infills in RC Frames*. Engineering Structures, 2019.
- [50] Verderame, G., et al. *Experimental Assessment of the Out-of-Plane Response of Strengthened One-Way Spanning Masonry Infill Walls*. Composite Structures, 2019.
- [51] Dawe, J., Seah, C. *Out-Of-Plane Resistance of Concrete Masonry Infilled Panels*. Canadian Journal of Civil Engineering, 1989, 16(6):854–864.
- [52] Hak, S., et al. *Out-Of-Plane Experimental Response of Strong Masonry Infills*. 2nd European Conference on Earthquake Engineering and Seismology, 2014.
- [53] Ricci, P., et al. *Experimental Investigation of the Influence of Slenderness Ratio and of the In-Plane/Out-of-Plane Interaction on the Out-of-Plane Strength of URM Infill Walls*. Construction and Building Materials, 2018a.
- [54] Ricci, P., et al. *Experimental Assessment of the In-Plane/Out-of-Plane Interaction in Unreinforced Masonry Infill Walls*. Engineering Structures, 2018b.
- [55] Kaushik, H., et al. *Code Approaches to Seismic Design of Masonry Infilled Reinforced Concrete Frames: A State-Of-The-Art-Review*. Earthquake Spectra 2006; 22(4):961–83.

- [56] Pokharel, T., Goldsworthy, H. *Lessons Learned from the Nepal Earthquake 2015*. 10<sup>th</sup> Pacific Conference on Earthquake Engineering, 2015.
- [57] Bertero, V. *Earthquake Engineering*. Structural Engineering Slide Library - Godden Collection, Earthquake Engineering Library, University of California, Berkeley, 1997.
- [58] National Research Council. *Guide for the Design and Construction of Externally Bonded Fibre Reinforced Inorganic Matrix Systems for Strengthening Existing Structures*. Advisory Committee on Technical Recommendations for Construction (CNR-DT 215/2018), 2018.
- [59] Sagar, S., et al. *In-Plane and Out-of-Plane Behavior of Masonry-Infilled RC Frames Strengthened with Fabric-Reinforced Cementitious Matrix*. Journal of Composites for Construction, 2019.
- [60] Bussini, A., et al. *Prove di Laboratorio Sistema di Controllo Attivo I-Pro 1*. Technical Report from ISAAC, 2020.
- [61] European Committee of Standardization (CEN). *Eurocode 2: Design of concrete structures, Part 1-1: General rules and rules for buildings*. Brussels, EN 1992-1-1, 2004.
- [62] Del Gaudio, C., et al. *Seismic Fragility for Italian RC Buildings Based on Damage Data of The Last 50 Years*. Bulletin of Earthquake Engineering, 2020, 18:2023-2059. <https://doi.org/10.1007/s10518-019-00762-6>.
- [63] Crisafulli, F. *Seismic Behaviour of Reinforced Concrete Structures with Masonry Infills*. PhD Thesis, University of Canterbury, 1997.
- [64] Bouarroudj, M., Boudaoud, Z. *Comparison Between Numerical Modeling Approaches of infilled Frames Under In-Plane Load*. Frontiers in built Environment, 2022. <https://doi.org/10.3389/fbuil.2021.783051>.
- [65] Asteris, G., et al. *Modeling of Infilled Framed Structures*. Computational Methods in Earthquake Engineering, 2013b. [http://dx.doi.org/10.1007/978-94-007-6573-3\\_10](http://dx.doi.org/10.1007/978-94-007-6573-3_10).
- [66] Mucedero, G., et al. *Numerical Modelling and Validation of the Response of Masonry Infilled RC Frames Using Experimental Testing Results*. Buildings, 2020. <http://dx.doi.org/10.3390/buildings10100182>.
- [67] Liauw, T., Kwan, K. *Nonlinear Behaviour of Non-Integral Infilled Frames*. Computers and Structures, 1984, 18:551–560.
- [68] Asteris, P. *Lateral Stiffness of Brick Masonry Infilled Plane Frames*. Journal of Structural Engineering ASCE, 2003; 129(8):1071–9.
- [69] Stavridis, A., Shing, P. *Finite Element Modeling of Nonlinear Behavior of Masonry-Infilled RC Frames*. Journal of Structural Engineering, 2009.

- [70] Lotfi, H., Shing, P. *An Appraisal of Smeared Crack Models for Masonry Shear Wall Analysis*. Journal of Computers Structures, 1991, 120(1):63–80.
- [71] Lotfi, H., Shing, P. *An Interface Model Applied to Fracture of Masonry Structures*. Journal of Structural Engineering, 1994, 120(1):63–80.
- [72] Holmes, M. *Steel Frames with Brickwork and Concrete Filling*. In Proceedings of the Institution of Civil Engineers, London, UK, 1961, 19:473–478.
- [73] Chrysostomou, C., et al. *A Six-Strut Model for Nonlinear Dynamic Analysis of Steel Infilled Frames*. International Journal of Structural Stability and Dynamics, 2002, 2(3):335–53.
- [74] Furtado, A., et al. *Simplified Macro-Model for Infill Masonry Walls Considering the Out-Of-Plane Behaviour*. Earthquake Engineering and Structural Dynamic, 2015, 45:507–524. <https://doi.org/10.1002/eqe.2663>.
- [75] Ma, G., et al. *Homogenization of Masonry Using Numerical Simulations*. Journal of Engineering Mechanics, 2001.
- [76] Hendry, A. *Masonry Materials and the Effect of Workmanship*. In Proceeding of the 3<sup>rd</sup> International Seminar on Structural Masonry for Developing Countries, 1990.
- [77] Mosalam, K., et al. *Computational Strategies for Frames with Infill Walls: Discrete and Smeared Crack Analyses and Seismic Fragility*. Technical Report NCEER-97- 0021, 1997.
- [78] Dhanasekar, M., Page, A. *Influence of Brick Masonry Infill Properties on The Behaviour of Infilled Frames*. ICE Proc., 1986, 81(4):593–605.
- [79] Asteris, P. *Finite Element Micro-Modeling of Infilled Frames*. Electronic Journal of Structural Engineering, 2008.
- [80] Petracca, M., et al. *Efficient Constitutive Model for Continuous Micro-Modeling of Masonry Structures*. International Journal of Architectural Heritage, 2022. <http://dx.doi.org/10.1080/15583058.2022.2124133>.
- [81] Force-Based Beam-Column. [https://opensees.berkeley.edu/wiki/index.php/Force-Based\\_Beam-Column\\_Element](https://opensees.berkeley.edu/wiki/index.php/Force-Based_Beam-Column_Element).
- [82] Truss. [https://opensees.berkeley.edu/wiki/index.php/Truss\\_Element](https://opensees.berkeley.edu/wiki/index.php/Truss_Element).
- [83] ASDShellQ4 User Manual. <https://opensees.github.io/OpenSeesDocumentation/user/manual/model/elements/ASDShellQ4.html>.

- [84] Chen, X.M., et al. *Membrane Elements Insensitive to Distortion Using the Quadrilateral Area Coordinate Method*. Computers & Structures, 2004.
- [85] Hughes, et al. *On Drilling Degrees of Freedom*. Computer methods in applied mechanics and engineering, 1989.
- [86] Dvorkin, et al. *A Continuum Mechanics Based Four-Node Shell Element for General Non-Linear Analysis*. Engineering computations, 1984.
- [87] Concrete02. [https://opensees.berkeley.edu/wiki/index.php/Concrete02\\_Material\\_-\\_Linear\\_Tension\\_Softening](https://opensees.berkeley.edu/wiki/index.php/Concrete02_Material_-_Linear_Tension_Softening).
- [88] Mander, J., et al. *Theoretical Stress-Strain Model for Confined Concrete*. Journal of Structural Engineering, 1988, 114:1804-1826.
- [89] Madas, P., Elnashai, A. *A New Passive Confinement Model for Transient Analysis of Reinforced Concrete Structures*. Earthquake Engineering and Structural Dynamics, 1992, 21:409-431.
- [90] Martinez-Rueda, J., Elnashai, A. *Confined Concrete Model Under Cyclic Load*. Materials and Structures, 1997, 30:139-147.
- [91] ElasticMembranePlateSection. [https://opensees.berkeley.edu/wiki/index.php/Elastic\\_Membrane\\_Plate\\_Section](https://opensees.berkeley.edu/wiki/index.php/Elastic_Membrane_Plate_Section).
- [92] Steel01. [https://opensees.berkeley.edu/wiki/index.php/Steel01\\_Material](https://opensees.berkeley.edu/wiki/index.php/Steel01_Material).
- [93] Oliver, J., et al. *An Implicit/Explicit Integration Scheme to Increase Computability of Non-Linear Material and Contact/Friction Problems*. Computer Methods in Applied Mechanics and Engineering, 2008, 197:1865-1889.
- [94] ASDConcrete3D. <https://opensees.github.io/OpenSeesDocumentation/user/manual/material/ndMaterials/ASDConcrete3D.html>.
- [95] Oller, S., et al. *Definition of a General Implicit Orthotropic Yield Criterion*. Computer methods in applied mechanics and engineering, 2003, 192(7-8):895-912.
- [96] PlaneStress. [https://opensees.berkeley.edu/wiki/index.php/Plane\\_Stress\\_Material](https://opensees.berkeley.edu/wiki/index.php/Plane_Stress_Material).
- [97] Lu, X.Z., et al. *A Shear Wall Element for Nonlinear Seismic Analysis of Super-Tall Buildings Using Opensees*. Finite Elements in Analysis & Design, 2015, 98:14-25.







# **Appendix A1**

## **PHOTOGRAPHIC DOCUMENTATION AND REINFORCEMENT DETAILS**



Fig. A.1 – Casting of the 2nd storey (general view) at the external area of the EUCENTRE laboratory (ISAAC technical report, 2020)



Fig. A.2 – Transport of the RC frame and the security steel structure to the shaking table (ISAAC technical report, 2020)

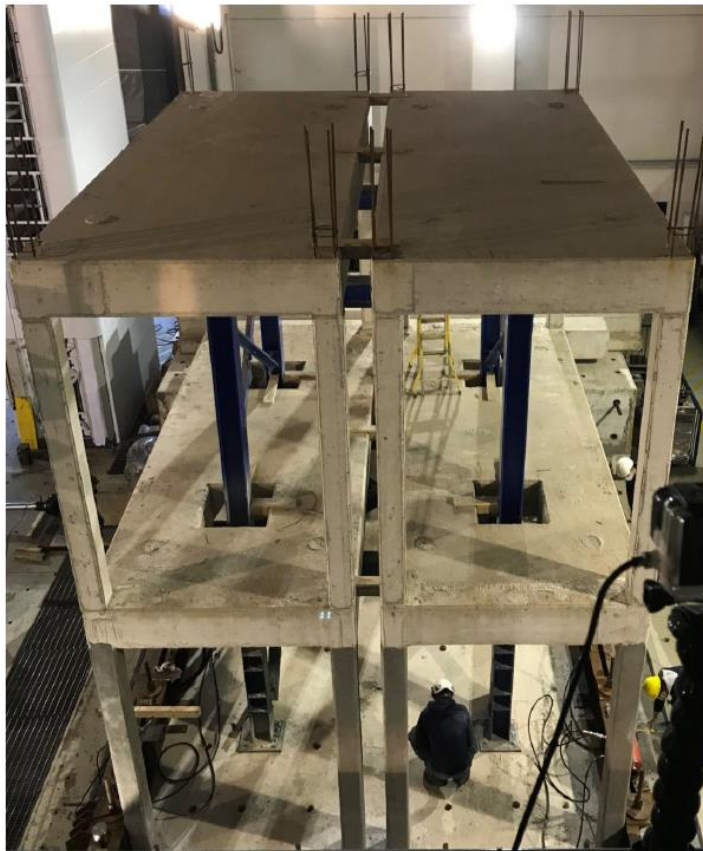


Fig. A.3 – Fastening of the structure to the shaking table (ISAAC technical report, 2020)



Fig. A.4 – Casting of the 3rd storey of the specimen structure (ISAAC technical report, 2020)



Fig. A.5 – Filling of the 1st storey bay with hollow clay brick units (ISAAC technical report, 2020)



Fig. A.6 – Final stages of the construction (ISAAC technical report, 2020)

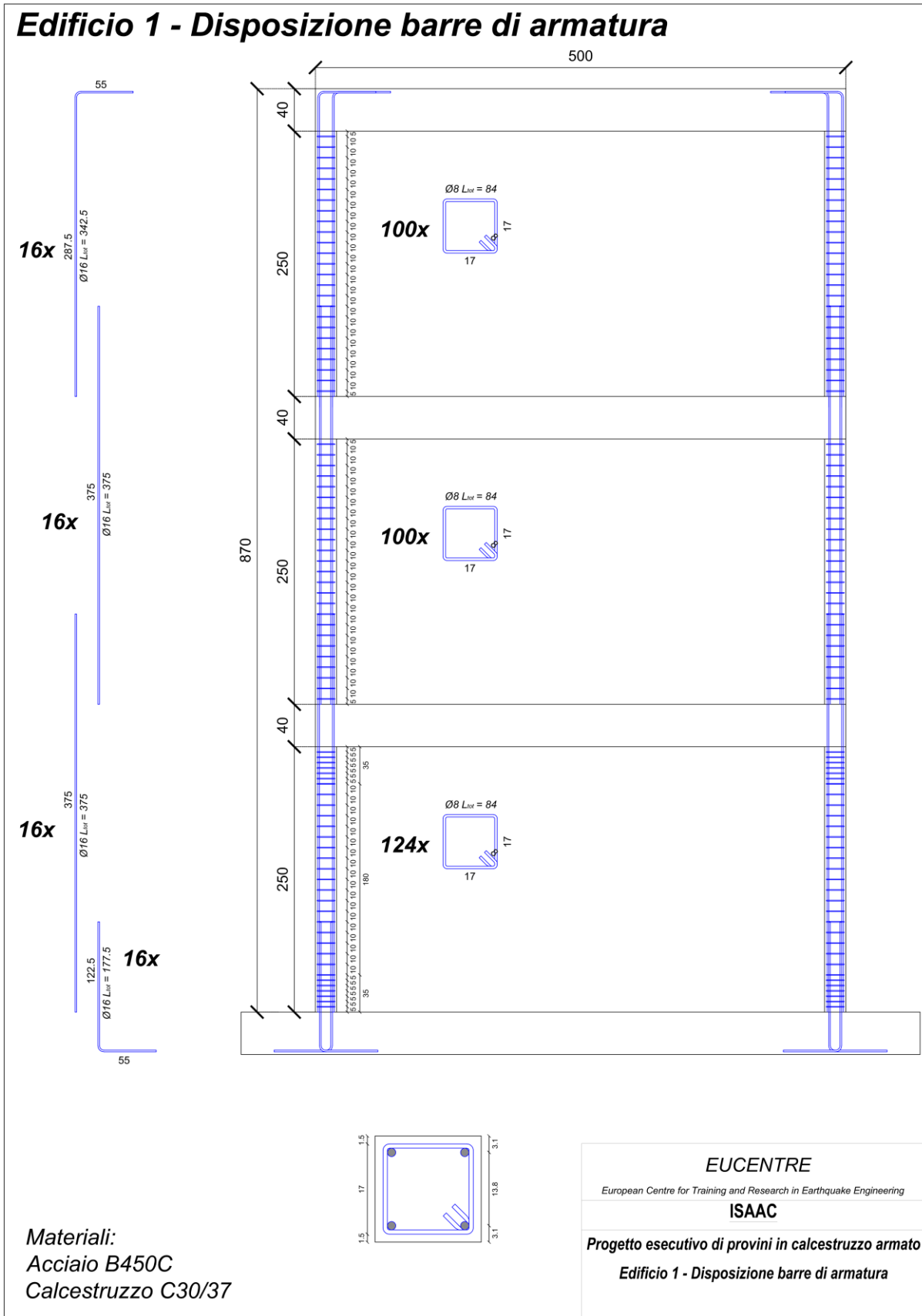


Fig. A.7 – Columns reinforcement details (ISAAC technical report, 2020)

**Plataea fondazione - Disposizione barre di armatura**

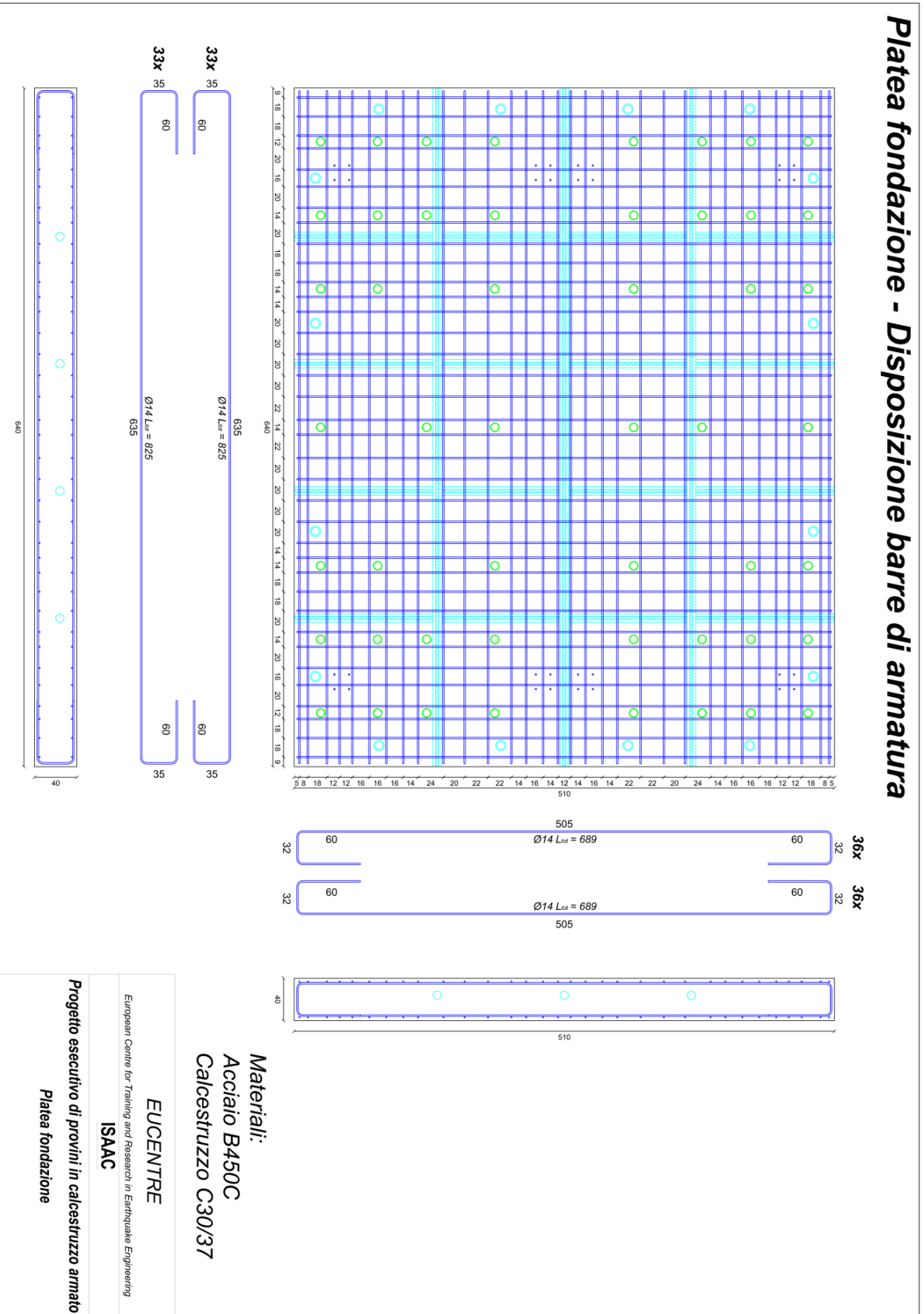


Fig. A.8 – Foundation reinforcement details (ISAAC technical report, 2020)

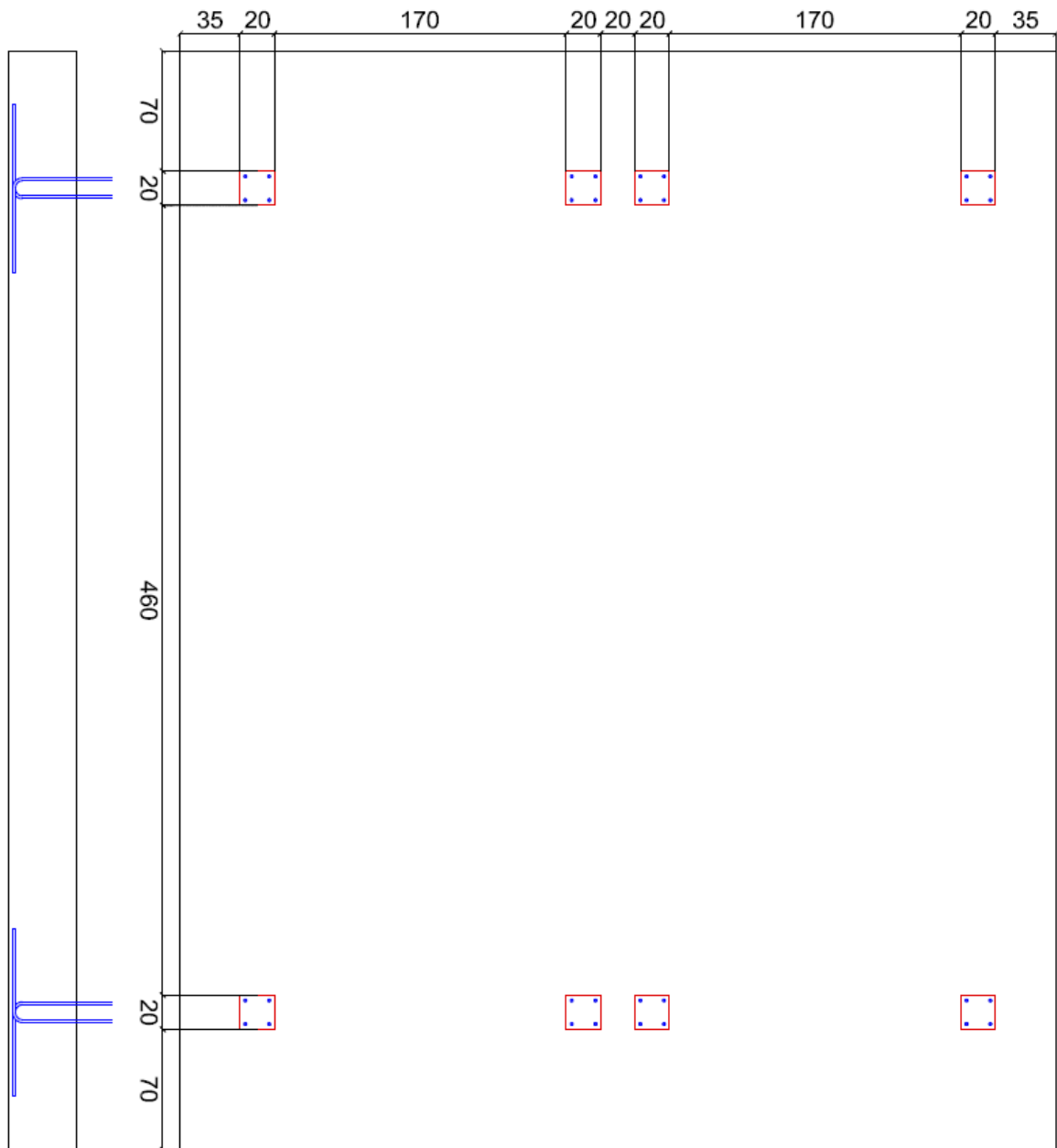


Fig. A.9 – Plan view of the columns positioning (ISAAC technical report, 2020)

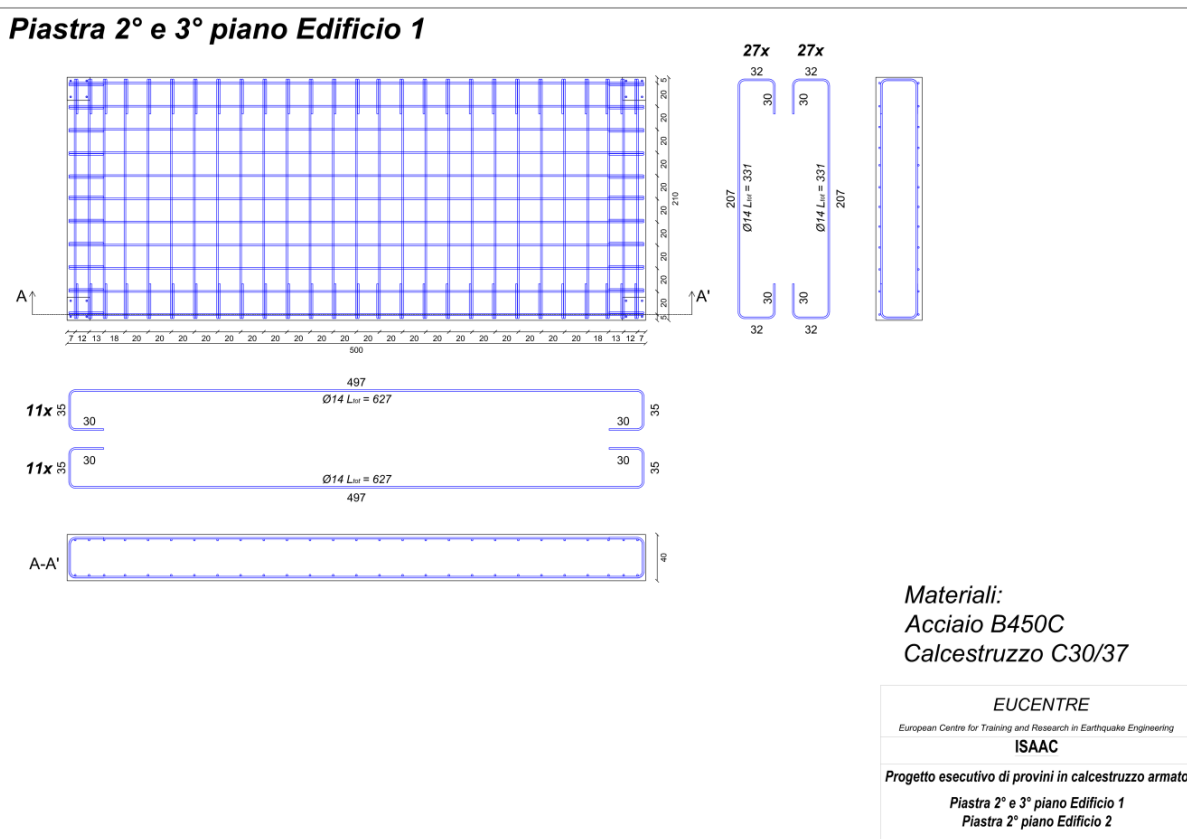
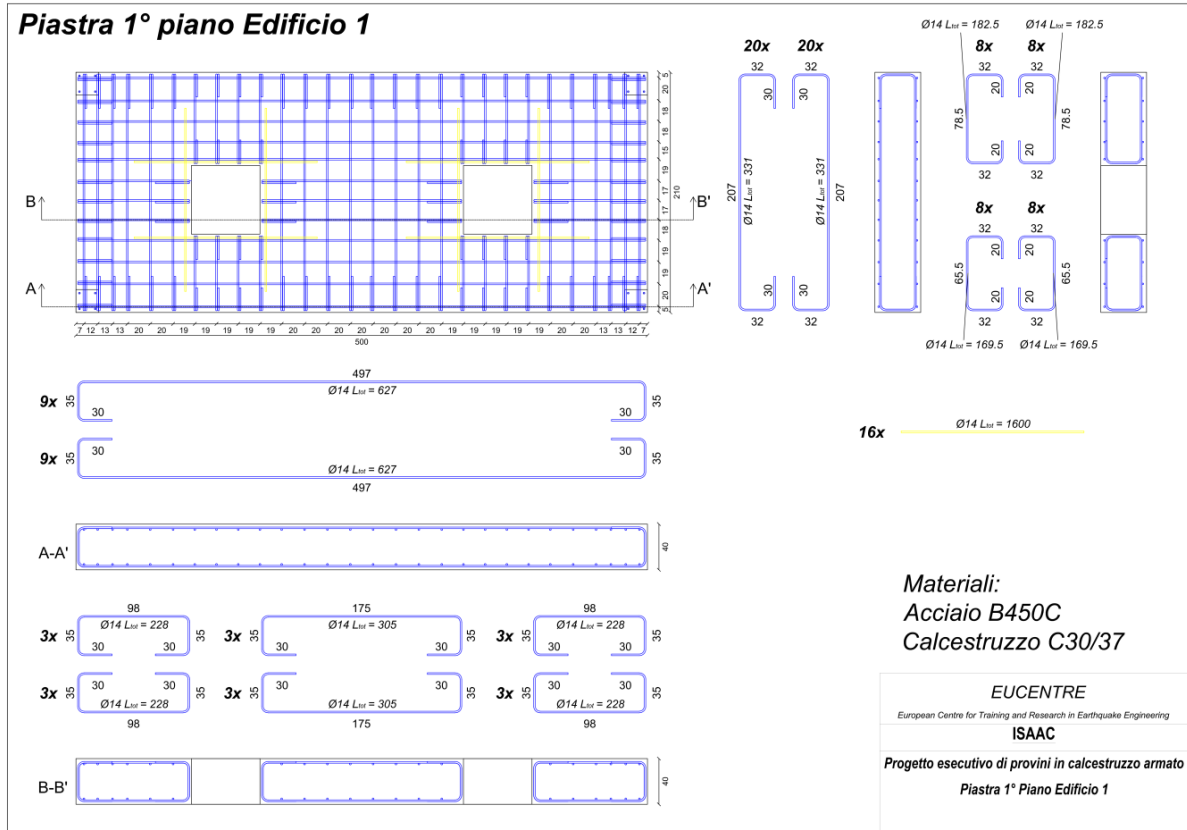


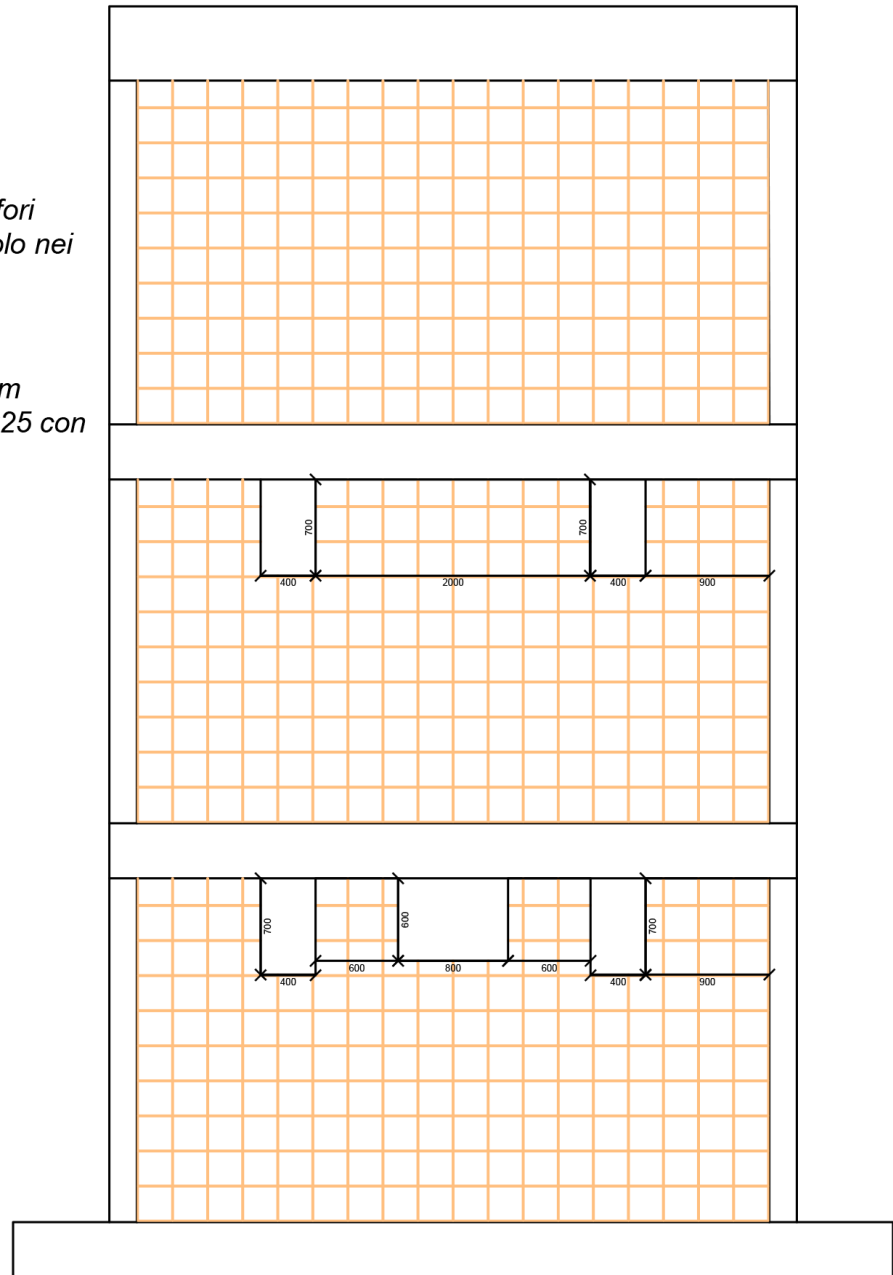
Fig. A.10 – Slab reinforcement details (1st, 2nd and 3rd storeys) (ISAAC technical report, 2020)

## Edificio 1 - Tamponamenti sui lati lunghi

Blocchi disposti con fori orizzontali e malta solo nei letti orizzontali

Materiali:

- Forati spessore 8 cm
- Dimensioni circa 25x25 con foratura circa 55%
- Malta M5



**EU CENTRE**

European Centre for Training and Research in Earthquake Engineering

**ISAAC**

**Progetto esecutivo di provini in calcestruzzo armato**

**Tamponamenti**

Fig. A.11 – Masonry infills openings dimensions (ISAAC technical report, 2020)

# **Appendix A2**

## **TIME-HISTORY ANALYSES RESULTS FOR HIGHER EARTHQUAKE INPUT MOTIONS**

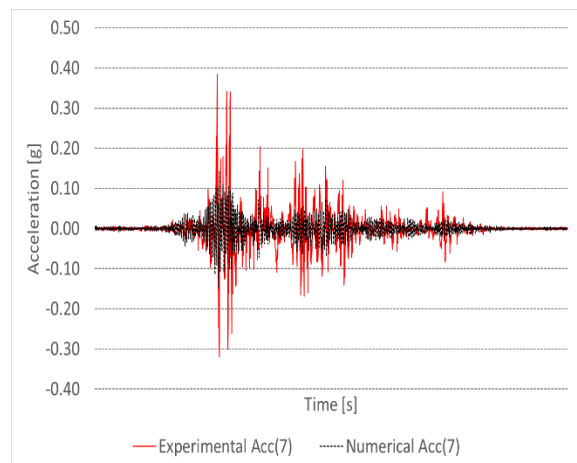
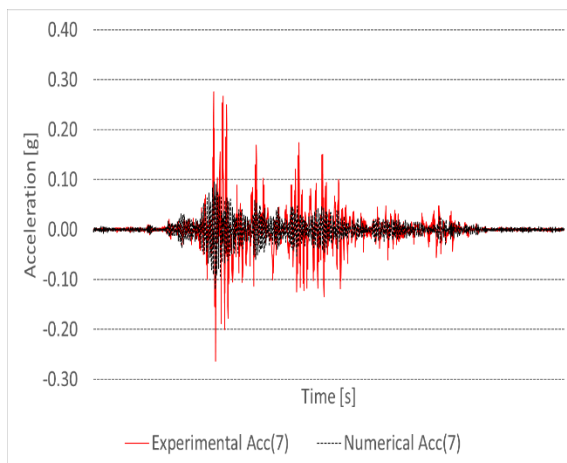
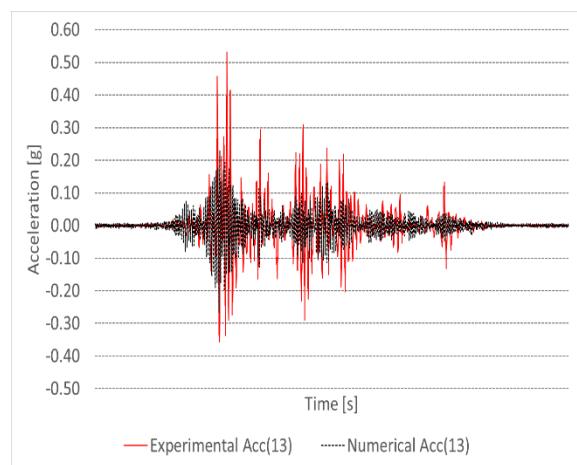
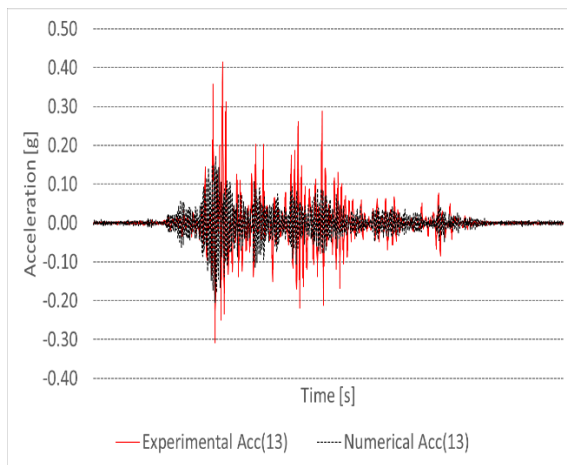
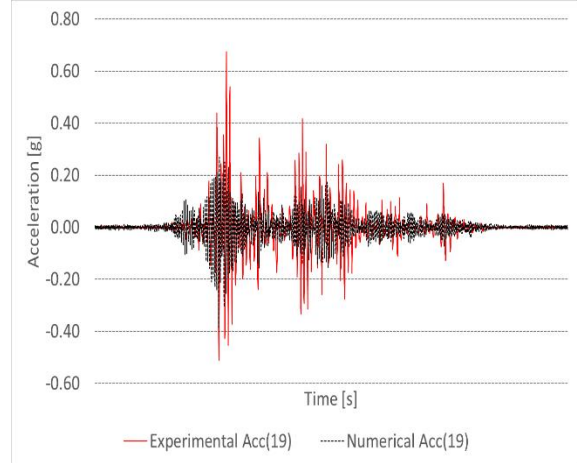
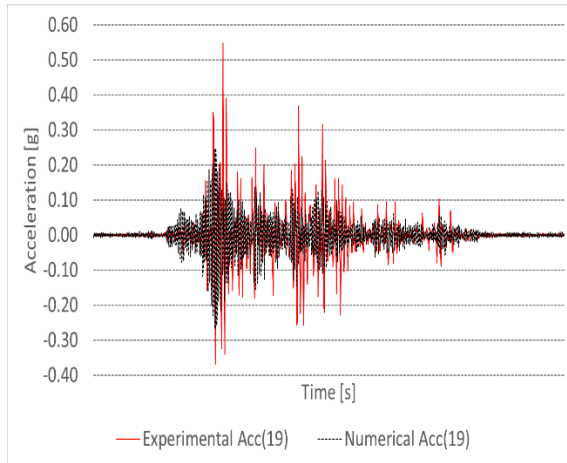


Fig. A.12 – COMP\_06 storey acceleration time histories (3<sup>rd</sup>, 2<sup>nd</sup> and 1<sup>st</sup> storeys)

Fig. A.13 – COMP\_07 storey acceleration time histories (3<sup>rd</sup>, 2<sup>nd</sup> and 1<sup>st</sup> storeys)

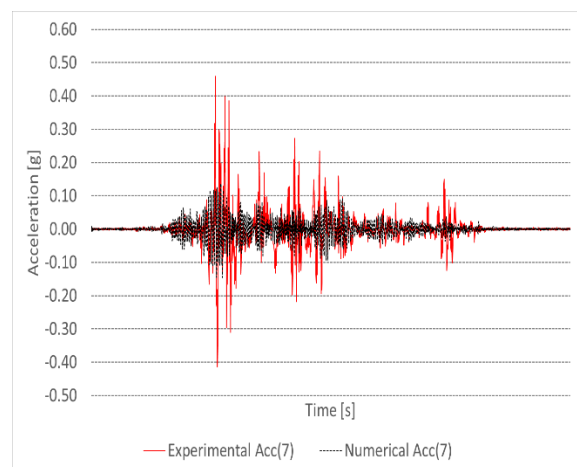
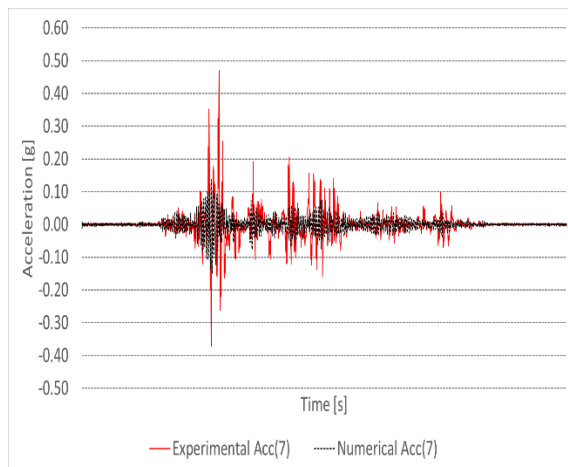
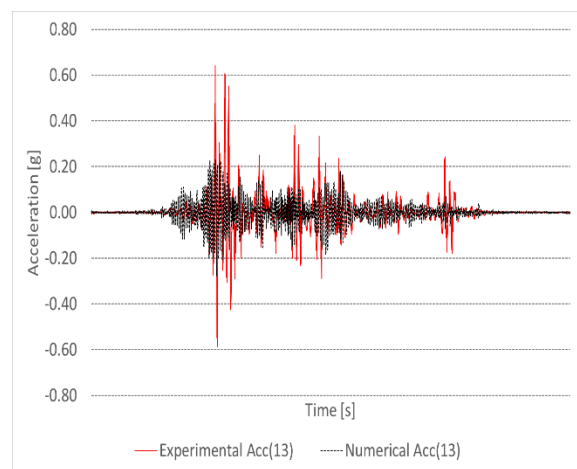
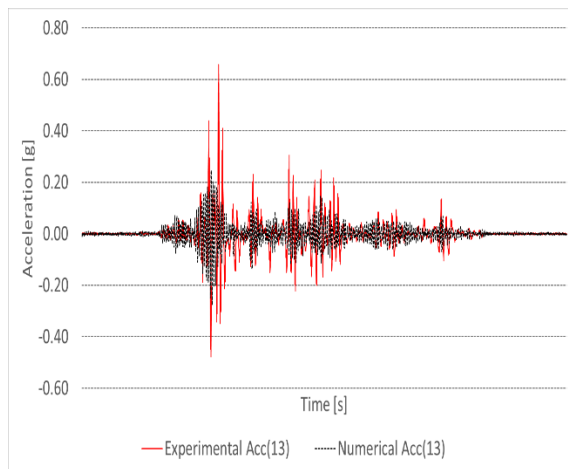
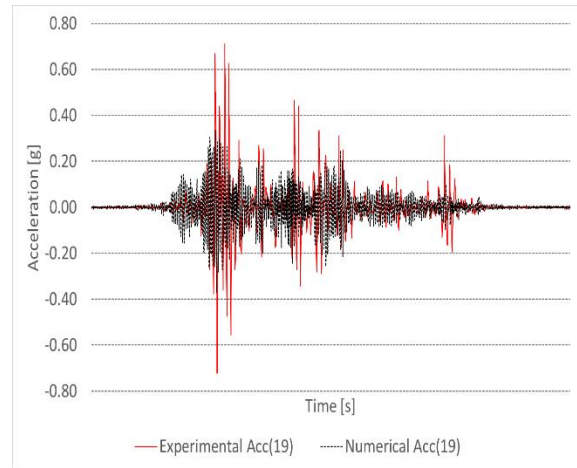
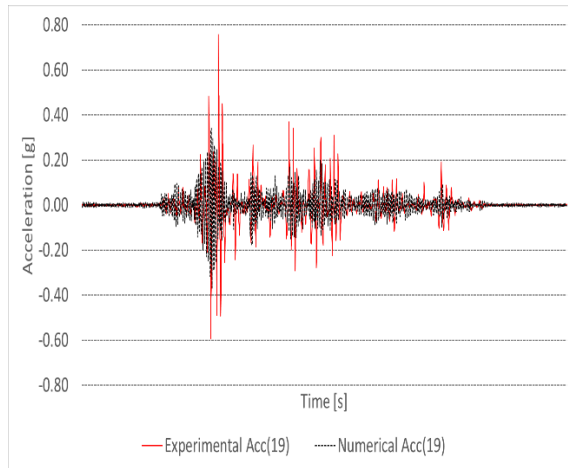


Fig. A.14 – COMP\_08 storey acceleration time histories (3<sup>rd</sup>, 2<sup>nd</sup> and 1<sup>st</sup> storeys)

Fig. A.15 – COMP\_09 storey acceleration time histories (3<sup>rd</sup>, 2<sup>nd</sup> and 1<sup>st</sup> storeys)

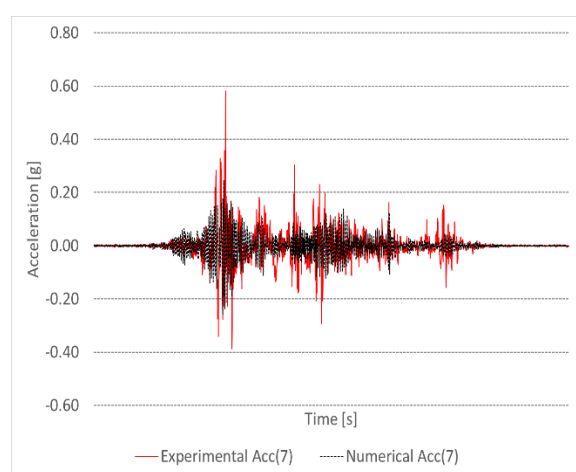
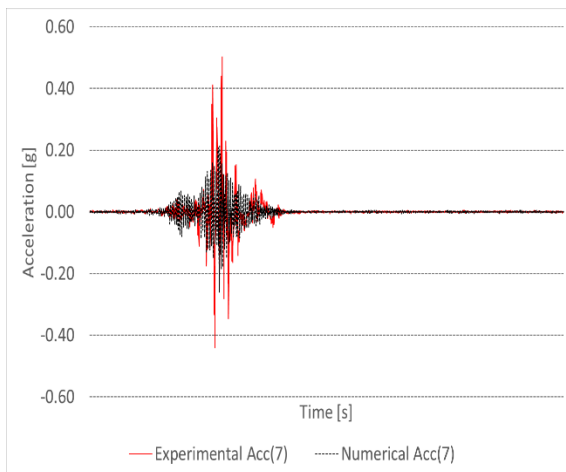
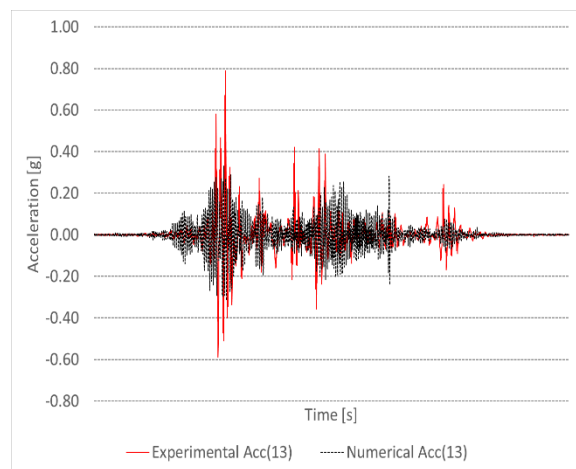
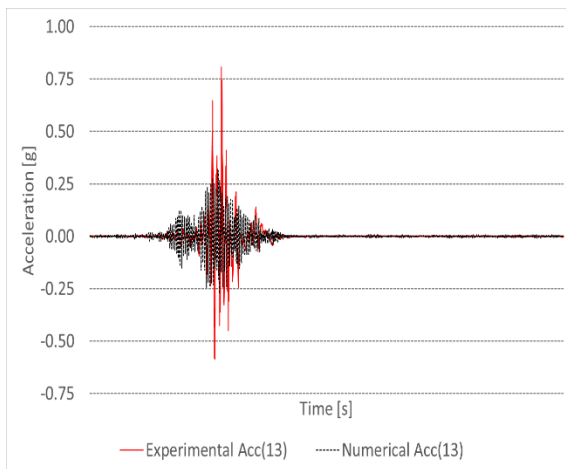
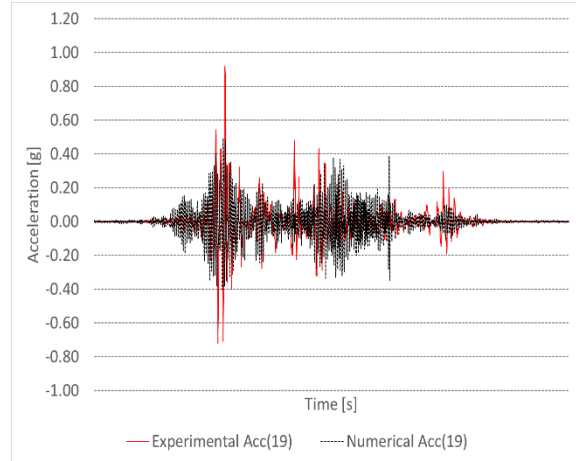
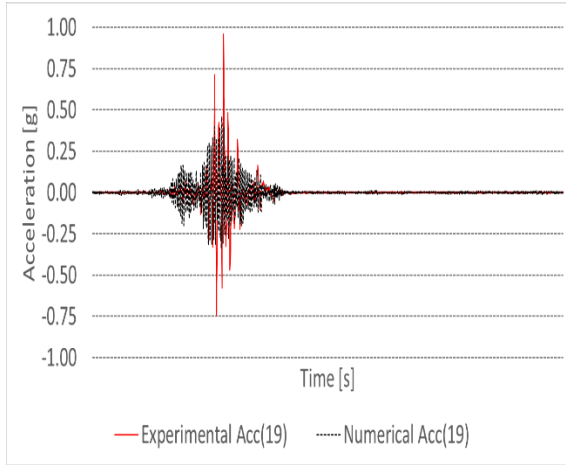


Fig. A.16 – COMP\_10 storey acceleration time histories (3<sup>rd</sup>, 2<sup>nd</sup> and 1<sup>st</sup> storeys)

Fig. A.17 – COMP\_11 storey acceleration time histories (3<sup>rd</sup>, 2<sup>nd</sup> and 1<sup>st</sup> storeys)